JGR Planets

REVIEW ARTICLE
10.1029/2020JE006655

Special Section:
Exoplanets: The Nexus of Astronomy and Geoscience

Aerosols in Exoplanet Atmospheres

Peter Gao[1,2], Hannah R. Wakeford[3], Sarah E. Moran[4], and Vivien Parmentier[5]

[1]Department of Astronomy and Astrophysics, University of California, Santa Cruz, CA, USA, [2]NHFP Sagan Fellow, [3]School of Physics, HH Wills Physics Laboratory, University of Bristol, Bristol, UK, [4]Department of Earth and Planetary Sciences, Johns Hopkins University, Baltimore, MD, USA, [5]Department of Physics (Atmospheric, Oceanic and Planetary Physics), University of Oxford, Oxford, UK

Abstract Observations of exoplanet atmospheres have shown that aerosols, like in the solar system, are common across a variety of temperatures and planet types. The formation and distribution of these aerosols are inextricably intertwined with the composition and thermal structure of the atmosphere. At the same time, these aerosols also interfere with our probes of atmospheric composition and thermal structure, and thus a better understanding of aerosols lead to a better understanding of exoplanet atmospheres as a whole. Here we review the current state of knowledge of exoplanet aerosols as determined from observations, modeling, and laboratory experiments. Measurements of the transmission spectra, dayside emission, and phase curves of transiting exoplanets, as well as the emission spectrum and light curves of directly imaged exoplanets and brown dwarfs have shown that aerosols are distributed inhomogeneously in exoplanet atmospheres, with aerosol distributions varying significantly with planet equilibrium temperature and gravity. Parameterized and microphysical models predict that these aerosols are likely composed of oxidized minerals like silicates for the hottest exoplanets, while at lower temperatures the dominant aerosols may be composed of alkali salts and sulfides. Particles originating from photochemical processes are also likely at low temperatures, though their formation process is highly complex, as revealed by laboratory work. In the years to come, new ground- and space-based observatories will have the capability to assess the composition of exoplanet aerosols, while new modeling and laboratory efforts will improve upon our picture of aerosol formation and dynamics.

Plain Language Summary For nearly 2 decades we have had the opportunity to probe the atmospheres of planets orbiting other stars ("exoplanets"). These efforts have revealed the existence of clouds and hazes in these atmospheres, which prevent us from learning more about exoplanet atmospheres as a whole by blocking us from probing parts of the atmosphere below the cloud and haze layers. Here we summarize our current understanding of these structures. Using data from telescopes on the ground and in space, we have found that exoplanet clouds are patchy and are distributed mostly according to the temperature of the local atmosphere. Using computer simulations, we have surmised that these clouds are likely made of materials that make up rocks on Earth, as the exoplanets we have probed thus far orbit their stars closely, resulting in very high temperatures in their atmospheres. At lower temperatures, but still several hundred degrees above room temperature, hazes composed of organic material are possible. These hazes are likely formed from complex chemical reactions, which are the current focus of laboratory experiments. Future efforts in data collection, computer simulations, and lab work will lead to a better understanding of exoplanet clouds and hazes.

Key Points:

- Aerosols are common in the atmospheres of exoplanets of all temperatures, masses, and compositions
- Observations and models are painting a coherent picture of the nature of exoplanet aerosols
- Advances in laboratory work are essential for unveiling how exoplanet aerosols form and evolve

Correspondence to:
P. Gao,
pgao8@ucsc.edu

Citation:
Gao, P., Wakeford, H. R., Moran, S. E., & Parmentier, V. (2021). Aerosols in exoplanet atmospheres. *Journal of Geophysical Research: Planets*, *126*, e2020JE006655. https://doi.org/10.1029/2020JE006655

Received 14 AUG 2020
Accepted 5 FEB 2021

1. Introduction

Aerosols are fundamental components of planetary atmospheres. Every perennial atmosphere in the solar system, including that of Pluto, Saturn's moon Titan, Neptune's moon Triton, and every planet except Mercury possess some form of such small suspended particulates. The composition of these aerosols is extremely diverse, including sulfuric acid on Venus (Hansen & Hovenier, 1974), water on Earth, water, mineral dust, and carbon dioxide on Mars (Montmessin et al., 2007), ammonia on Jupiter and Saturn (Baines et al., 2009; Brooke et al., 1998), and complex organics and condensed hydrocarbons and nitriles on Uranus, Neptune, Titan, Triton, and Pluto (Brown et al., 2002; Gladstone et al., 2016; Lavvas et al., 2020; Ohno et al., 2020b; Rages & Pollack, 1992; Romani & Atreya, 1988; Sagan et al., 1992; Sromovsky et al., 2011; M. L. Wong et al., 2017). In addition, these aerosols are inexorably tied to the chemistry, dynamics, and radiative

environments of their host atmospheres. Sulfuric acid clouds on Venus form a vital branch of its sulfur chemical cycle and provide the planet its high albedo (Mills et al., 2007) while water clouds on Earth and dust on Mars are strong controls of their surface climates (Martínez et al., 2017; Rosenfeld et al., 2014). In the outer solar system, moist convection on the giant planets with the condensation of ammonia, water, and methane sculpts their global atmospheric dynamics and trace gas distributions (Bolton et al., 2017; Hueso & Sánchez-Lavega, 2006; Li & Ingersoll, 2015; Lunine, 1993); organic hazes on Titan and Pluto are the products of complex chemical networks and are major contributors to heating and cooling rates in their atmospheres (McKay et al., 1989; X. Zhang et al., 2017); and latent heat release from nitrogen condensation on Triton could control its atmospheric thermal structure (Rages & Pollack, 1992). Understanding the formation and impact of aerosols on solar system objects have thus been vital for understanding their atmospheres as a whole. The same applies to exoplanets.

Aerosols were anticipated to exist in exoplanet atmospheres not long after the discovery of the first exoplanet orbiting a sun-like star (Guillot et al., 1996; Saumon et al., 1996). In the few years that followed, several works (Baraffe et al., 2003; Barman et al., 2001; Burrows et al., 1997; Hubbard et al., 2001; Marley et al., 1999; Seager & Sasselov, 1998, 2000; Seager et al., 2000; Sudarsky et al., 2000, 2003) considered the formation of mineral and metal aerosols, for example, silicates and iron, in one-dimensional (vertical), globally averaged models, as inspired by earlier and contemporary studies into equilibrium condensation and cloud formation processes in brown dwarf atmospheres (Ackerman & Marley, 2001; Allard et al., 1997, 2001; Burrows et al., 2000, 2002; Chabrier et al., 2000; Cooper et al., 2003; Helling et al., 2001; Lodders, 1999, 2002; Lunine et al., 1989; Marley et al., 1996, 2002; Tsuji, 2002; Tsuji et al., 1999; Woitke & Helling, 2003), which possess similar temperatures (≥1,000 K) to those of the first exoplanets found. These early studies clearly demonstrated the importance of high temperature aerosol formation on the composition of the atmosphere and the planets' albedo, optical phase curve, polarization, and transmission, reflected light, and emission spectra.

Observational evidence for aerosols in exoplanet atmospheres arrived with the measurement of the first exoplanet transmission spectrum - light from the host star filtered through the atmosphere of the planet during transit captured at a range of wavelengths. With this, Charbonneau et al. (2002) showed that absorption by atomic sodium in the atmosphere of the hot Jupiter HD 209458b was less than predicted in clear atmosphere models, suggesting the existence of a layer of aerosols at high altitudes that obscured the wings of the sodium doublet (Fortney et al., 2003). Subsequent transmission spectroscopy of another hot Jupiter, HD 189733b at optical (Pont et al., 2008) and infrared wavelengths (Tinetti et al., 2007) showed a non-detection of alkali metal absorption lines and a significant offset in the transit radius between the two wavelength ranges; this again suggested the existence of high altitude aerosols that became optically thin at wavelengths ≥1 μm (Lecavelier Des Etangs et al., 2008). Aerosols were also inferred in the atmospheres of some of the first directly imaged young giant exoplanets due to their red infrared colors (Marois et al., 2008). These initial observations were the first hints that aerosols were just as ubiquitous in exoplanet atmospheres as in the atmospheres of our solar system worlds.

In this review, we will summarize our current understanding of exoplanet aerosols, focusing primarily on advancements in knowledge made in the 2010s. These advancements include (1) the proliferation of exoplanet transmission spectroscopy, reflected light and emission photometry, and observations of exoplanet phase curves, which can all be used to probe exoplanet aerosols, (2) greater synergy between exoplanet and brown dwarf science with a focus on photometry and spectroscopy of directly imaged exoplanets, (3) development of more rigorous aerosol models in 1D and the extension to 3D, and (4) the application of laboratory experiments to investigate exoplanet aerosol formation and corresponding impact on observations. We refer the reader to Helling et al. (2008a) and Marley et al. (2013) for comprehensive reviews of pre-2010 studies.

We begin by defining specific types of aerosols based on their formation processes and describing their possible compositions in §2 to facilitate our discussions. In §3 we will provide an overview of the insights into exoplanet aerosols we have gained through observing exoplanet atmospheres in transmission, emission, and reflection. We will then focus on the usage of and predictions made by various aerosol models in §4 and the complexities in aerosol formation revealed by laboratory work in §5. Finally, in §6 we describe an emerging picture of how aerosol properties vary among different exoplanets and discuss how our understanding of exoplanet aerosols can progress in the years to come.

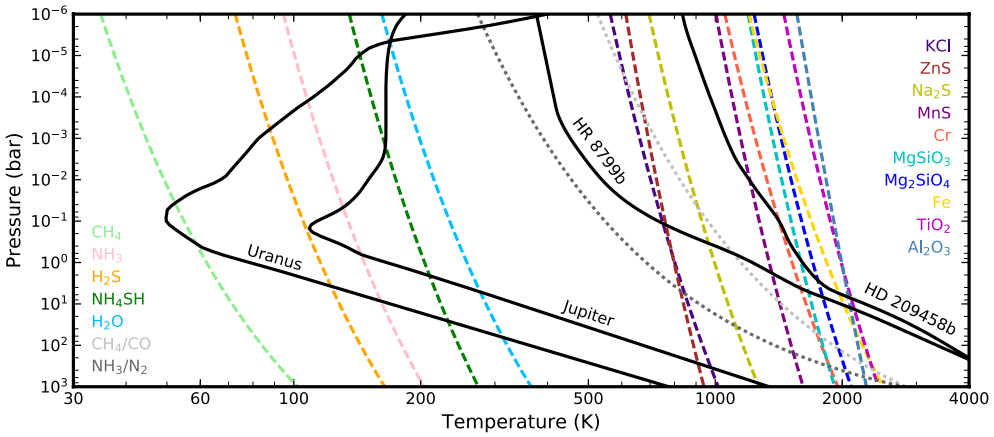

Figure 1. Condensation temperatures of various cloud species as a function of atmospheric pressure, assuming solar metallicity, compared to temperature-pressure (TP) profiles of several objects. Condensation of a given species can occur when the planet TP profile becomes lower than its condensation temperature profile. TP profiles for Jupiter and Uranus are taken from Moses and Poppe (2017) while those of HR 8799b and HD 209458b are generated by a thermal structure model (Saumon & Marley, 2008) assuming appropriate planetary parameters. The condensation curve for CH_4 is computed by combining the CH_4 saturation vapor pressure (Lodders & Fegley, 1998) with its mixing ratio in a solar metallicity gas (Lodders, 2010), assuming that all carbon is in the form of CH_4. The condensation curves for NH_3, NH_4SH, and H_2O are taken from Lodders and Fegley (2002); that of H_2S is from Visscher et al. (2006); those of KCl, ZnS, Na_2S, MnS, and Cr are from Morley et al. (2012); those of $MgSiO_3$, Mg_2SiO_4, and Fe are from Visscher et al. (2010); that of TiO_2 is from Helling et al. (2001); and that of Al_2O_3 is from Wakeford et al. (2017b). The CH_4/CO and NH_3/CO transition curves are from Lodders and Fegley (2002).

2. Aerosol Definitions, Composition, and Provenance

A number of terms have been used to refer to aerosols in planetary and exoplanet atmospheres in the literature, including clouds, hazes, and dust. For clarity, we will assign to them specific definitions based on their provenance in this review, inspired by Hörst (2016). Where provenance is unclear, we will use the catch-all term, "aerosols."

Dust: We define dust as particles lifted into the atmosphere from a planetary surface, such as sand and sea salt on Earth, fine regolith particles on Mars, and organic dune particles and ices on Titan and Pluto.

Clouds: We define clouds as collections of particles forming in the atmosphere under thermochemical equilibrium. This definition includes both first order phase changes, such as

$$H_2O(g) \rightleftarrows H_2O(s,l) \qquad ((R1))$$

as well as thermochemical reactions like

$$2Mg(g) + 3H_2O(g) + SiO(g) \rightleftarrows Mg_2SiO_4(s,l) + 3H_2(g) \qquad ((R2))$$

Thermochemical equilibrium arises from the minimization of Gibbs free energy given the local temperature, pressure, and elemental abundances. Because of this, cloud formation is locally reversible, such that the loss of clouds through evaporation or chemical decomposition is in balance with condensation and synthesis. In the solar system, clouds tend to form via condensation, a first order phase change, such as those of water, carbon dioxide, ammonia, methane, and nitrogen. Meanwhile, ammonium hydrosulfide (NH_4SH) clouds, for which we have indirect evidence for in the atmospheres of the giant planets, form through chemical reactions between gaseous ammonia and hydrogen sulfide (e.g., Bjoraker et al., 2018; Carlson et al., 1988; de Pater et al., 2014; J. S. Lewis, 1969; M. H. Wong et al., 2015b).

Thermochemical equilibrium models have predicted a myriad of cloud compositions in exoplanet atmospheres under the assumption that the atmospheric gas composition is one to only several times more enriched in metals than a solar composition gas. "Metals" in this case refers to all elements heavier than hydrogen and helium (Figure 1; see e.g., Burrows & Sharp, 1999; Lodders, 1999, 2002; Visscher et al., 2006, 2010;

Wakeford et al., 2017b). Some of the proposed clouds form via phase changes, for example, iron, chromium, potassium chloride, while others form via chemical reactions, for example, forsterite, enstatite, corundum, and various sulfides. These compositions can vary significantly at higher metallicities and/or different carbon-to-oxygen ratios, such as the formation of clouds of graphite and carbides at high C/O (Helling et al., 2017; Mbarek & Kempton, 2016; Moses et al., 2013). Additional cloud compositions can arise from the condensation of gases produced from photochemistry, such as sulfuric acid on Venus, hydrocarbons and nitriles on Titan and Pluto, and elemental sulfur in reducing atmospheres (e.g., Hu et al., 2013; Zahnle et al., 2016).

Hazes: Clouds derived from gases originating from photochemistry are distinct from hazes, which we define as collections of particles formed *directly* from energy input via photochemistry and energetic particle bombardment. Hazes form through these processes via the breakdown of simple molecules like methane, nitrogen, carbon monoxide, hydrogen sulfide, etc. at low pressures to create radicals and ions, which then react to build more complex species, eventually forming small particles through successive reactions (Lavvas et al., 2013; Trainer et al., 2013; Yoon et al., 2014). As a result, the exact compositions of hazes are highly uncertain, though their elemental make-up reflects the major gases in the atmosphere. Unlike clouds, haze formation is locally irreversible, tending toward complexity due to the external input of energy. Examples of hazes in the solar system include those of Titan, Pluto, and the giant planets, as well as smog in Earth cities. Hazes in exoplanet atmospheres, particularly at high temperatures, could be more complex since they can incorporate elements that would otherwise be hidden in deep clouds on cooler worlds, including sodium, potassium, chlorine, magnesium, and iron.

Our definitions of clouds, hazes, and dust are different from some of the previous and current usages of these terms in the exoplanet literature. For example, dust has been used to refer to high temperature condensates like iron and silicates as they likely condense to solid particles (Ebel, 2006; Pont et al., 2013; Seager & Sasselov, 1998), but as they form via condensation and thermochemical reactions of atmospheric gasses these would be referred to as clouds under our definition regardless of their phase. By specifying dust as originating from a planetary surface due to mechanical processes like weathering, we relegate them to only thin atmospheres, such as those of rocky exoplanets. In addition, when interpreting observations, clouds and hazes have been used to refer to particles of different sizes and/or structures of different optical depths, independent of their formation processes. In transmission spectroscopy in the optical and near-infrared, large particles that act as gray absorbers/scatterers are often labeled as clouds, while small particles that preferentially scatter short wavelength visible light are labeled as hazes (Barstow et al., 2017; Goyal et al., 2018; Pont et al., 2008; Sing et al., 2016). Hazes have also been used to describe low optical depth aerosol layers above more optically thick "cloud" layers (H. Yang et al., 2015). These uses are convenient for differentiating between the effects different aerosols have on observations when aerosol provenance is unknown. However, as we probe exoplanet atmospheres with more advanced instruments and more sophisticated techniques (Kempton et al., 2017; Powell et al., 2019; Wakeford & Sing, 2015), aerosol definitions that are more connected to their formation mechanisms and underlying atmospheric processes will become increasingly informative.

3. Insights from Observations

Aerosols impact every method of exoplanet atmosphere characterization (Figure 2). Aerosol opacity controls the pressure levels probed in transmission through the atmosphere, emission from the atmosphere, and reflection by the atmosphere, suppressing the spectral signatures of molecular species at higher pressures. Heating and cooling by aerosols change the atmospheric temperature profile, regulating the planet's emitted flux. The reflectivity of aerosols, controlled by their optical constants, size, and shape, determines the albedo of a planet and thus the reflected light spectrum. Aerosol scattering and absorption also generate their own features in exoplanet spectra. In this section, we describe what observations of exoplanet atmospheres have revealed about exoplanet aerosols.

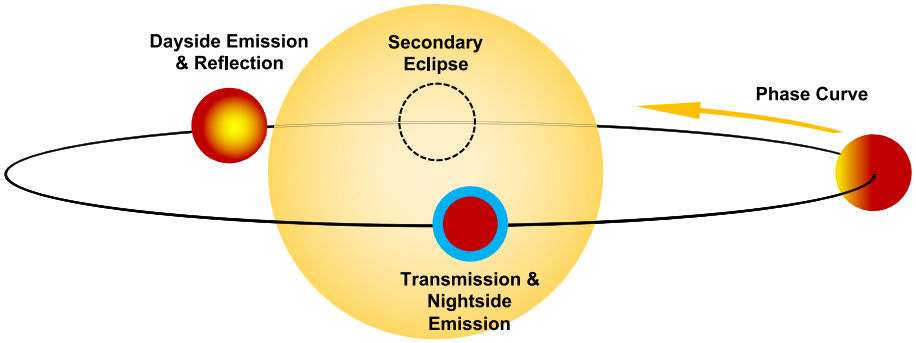

Figure 2. The geometry of a transiting exoplanet as seen from Earth. When the exoplanet passes in front of its star with respect to us, we can measure the transmission spectrum of the limb of its atmosphere thanks to light from the host star filtering through the atmosphere on its way to us, as well as thermal emission from the nightside. When the exoplanet passes behind its star during secondary eclipse, its dayside is blocked; comparison between the total brightness of the exoplanet-star system before/after and during the secondary eclipse then allows for the measurement of the dayside flux, which is a combination of reflected star light and thermal emission. During the rest of the exoplanet's orbit, reflected star light and thermal emission as a function of longitude can be measured by observing the exoplanet's phase curve. The figure is not to scale.

3.1. Aerosols in Transmission

Transmission spectroscopy probes the day-to-night terminator of planetary atmospheres. Although it has become the most prolific method by which we probe exoplanet atmospheres (Kreidberg, 2018), it also leads to the most complex results to interpret, due to the large thermal and wind gradients across the atmospheric limb. The slant optical path through the atmosphere tangential to the target planet afforded by the observational geometry allows for probes of minute abundances of both molecular species (~1–100 ppm) and aerosol particles (Fortney, 2005). Transmission spectra of a variety of exoplanets ranging from hot Jupiters to cool rocky worlds have been observed from the near-UV to the mid-infrared by ground- and space-based instruments (e.g., Bean et al., 2010; Benneke et al., 2019b; Bruno et al., 2018; Chachan et al., 2019; Charbonneau et al., 2002; Crossfield et al., 2013; Deming et al., 2013; Désert et al., 2011; de Wit et al., 2016; Gibson et al., 2012; Kilpatrick et al., 2018; Knutson et al., 2014a; Kreidberg et al., 2014a, 2018b; Libby-Roberts et al., 2020; Sing et al., 2015; Swain et al., 2013; Thao et al., 2020; Wakeford et al., 2017a, 2020; Wood et al., 2011), all of which have been shown to be impacted by aerosols. The effect of aerosols span a continuum, from increased scattering slopes and reduced molecular features to completely featureless spectra (Figure 3).

The relatively large number (~50) of published transmission spectra have allowed for population studies of exoplanet atmospheres. Several studies have focused on the amplitude of the 1.4 μm water absorption feature above its adjacent low opacity regions at ~1.2 and 1.6 μm (equivalent to the J and H bands), modulated by the atmospheric scale height, as a measure of the vertical extent of the aerosols in the atmospheres of these planets (Figure 4; Crossfield & Kreidberg, 2017; Fu et al., 2017; Iyer et al., 2016; Sing et al., 2016; Stevenson, 2016; Tsiaras et al., 2018; Wakeford et al., 2019b). The scale height is typically computed using an atmospheric mean molecular weight corresponding to solar metallicity (2.3 g mol^{-1}) and a temperature equal to the planets' equilibrium temperature (T_{eq}). Higher metallicities are certainly possible, particularly for the lower mass planets, in which case assumptions of a solar metallicity scale height would underestimate the number of scale heights spanned by the observed water feature. The use of T_{eq} for defining the scale height is also approximate, since the temperature at the altitudes probed by transits could be higher or lower. These studies have found that aerosols diminish the water feature amplitude with respect to a clear atmosphere by 50%–70% on average. Some studies (Fu et al., 2017; Stevenson, 2016) have claimed that there may be a trend in water feature amplitude with T_{eq}, from ~600 to ~2,500 K, where hotter planets tend to have larger water feature amplitudes, suggesting deeper and/or more optically thin aerosol layers, while planet gravity appears to not significantly affect the feature. Crossfield and Kreidberg (2017), and Libby-Roberts et al. (2020) showed that a similar trend may exist for Neptune-mass and sub-Neptune planets with $T_{eq} < 1{,}000$ K, though higher atmospheric metallicity (i.e., higher mean molecular weight atmospheres) could also be responsible. However, this is in contrast with the recent discovery of a high amplitude water

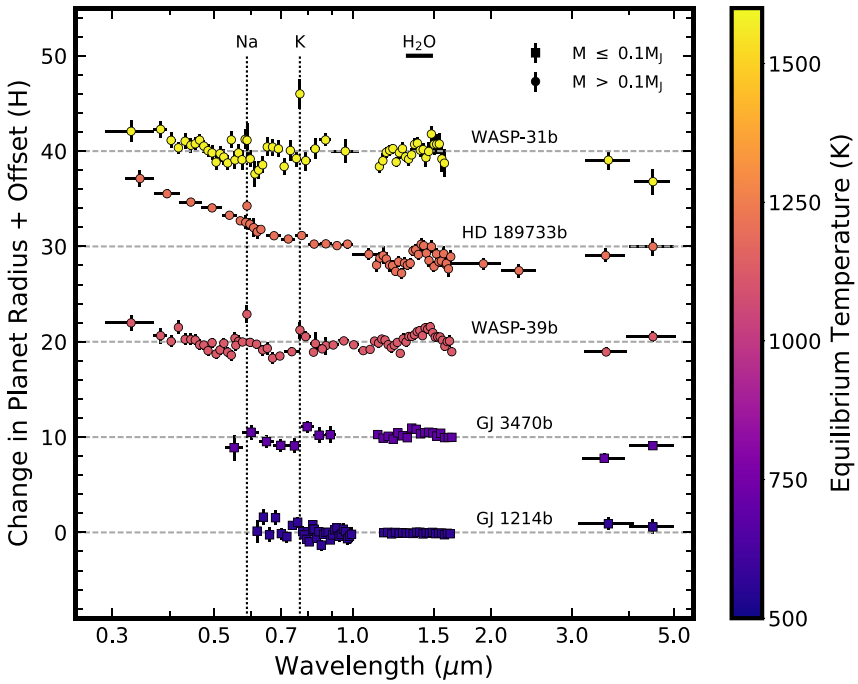

Figure 3. Transmission spectra of several exoplanets showing the various impacts of aerosols. Planets with masses >0.1 Jupiter masses are shown in circles, while lower mass planets are shown in squares. The colors of the datasets represent the equilibrium temperatures of the corresponding planet. Observations are taken from Bean et al. (2011), Désert et al. (2011), Kreidberg et al. (2014a), Sing et al. (2015, 2016), Benneke et al. (2019a), and Wakeford et al. (2018). The transmission spectra are offset for clarity, normalized to the mean transit depth, and shown in planetary scale heights calculated using parameters listed on exo.MAST (e.g., gravity and equilibrium temperature), assuming solar metallicity and atmospheres dominated by H/He, that is, an atmospheric mean molecular weight of 2.3 g mol^{-1}. We refer the reader to https://stellarplanet.org/science/exoplanet-transmission-spectra/ for an up to date database of published exoplanet transmission spectra.

feature for K2-18b, a sub-Neptune with Earth-like temperatures (Benneke et al., 2019b; Tsiaras et al., 2019). Moreover, Fisher and Heng (2018) found no significant trend between temperature and aerosol opacity in their combined analysis of giant and lower mass exoplanet near-infrared transmission spectra.

At optical wavelengths, Heng (2016) measured the amplitude of the atomic sodium and potassium absorption peaks and also claims a possible "cloudiness" trend with T_{eq}, with higher temperature planets being clearer. Sing et al. (2016) considered the relative increase in transit depths in the optical versus the mid-infrared as a measure of extinction by small particles, and found that aerosols are the primary factor that shape transmission spectra rather than variable water abundance. Also, several studies (Alderson et al., 2020; Chen et al., 2021; May et al., 2020; Pinhas et al., 2019; Welbanks et al., 2019) have measured optical spectral slopes steeper than that of Rayleigh scattering. This would require an opacity source that varies with altitude, such as highly scattering aerosols with variable particle size and/or vertical distribution (Lecavelier Des Etangs et al., 2008; Sing et al., 2011; Wakeford & Sing, 2015).

In addition to focusing on specific wavelength regions and spectral features, a number of studies have performed uniform, homogeneous retrieval analyses on a large number of planets' complete transmission spectra from optical to mid-infrared wavelengths. Retrievals are data-model parameter estimation procedures commonly used to infer the state properties (abundances, temperatures, cloud properties) of an atmosphere given a spectrum. Both Barstow et al. (2017) and Pinhas et al. (2019) performed a retrieval on the 10 planets presented in Sing et al. (2016). Although they both propose that non-monotonic trends with temperature exist in aerosol coverage at the limb of hot Jupiters, their results are incompatible. This highlights the sensitivity of retrieval studies to the details of the cloud parametrization (Barstow, 2020) and the many degeneracies present between aerosol physical parameters such as altitude range, latitudinal coverage, particle size distribution, etc. (see §4.1).

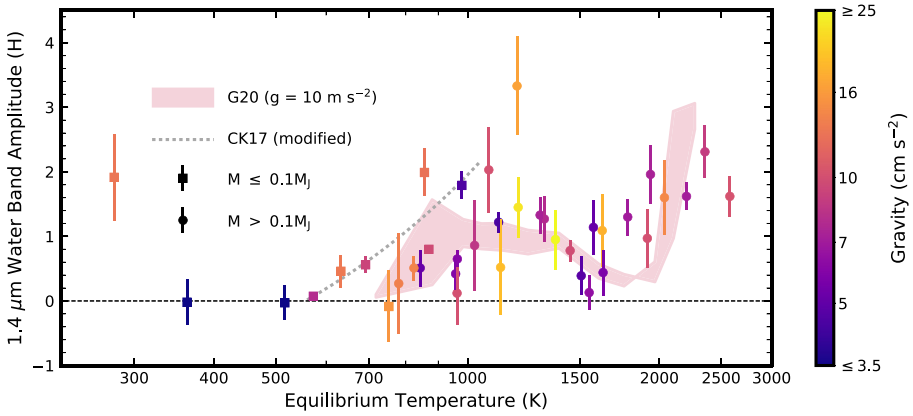

Figure 4. Amplitude of the 1.4 μm water feature in transmission spectra of exoplanets in units of atmospheric scale height H (defined as in Figure 3) as a function of gravity and equilibrium temperature. Planets with masses >0.1 Jupiter masses are shown as circles, with the water feature amplitude values taken from Fu et al. (2017), while lower mass planets are shown as squares. Water feature amplitudes for lower mass planets are taken from Crossfield and Kreidberg (2017), Libby-Roberts et al. (2020), and Kreidberg et al. (2020). The water feature amplitude for K2-18b in units of H, 1.915 ± 0.67, is calculated from the transmission spectrum presented in Benneke et al. (2019b) following the method of Stevenson (2016). The predicted water feature amplitude from Gao et al. (2020) for objects with gravity of 10 m s^{-2} and atmospheric metallicity between 1 and 10 × solar is shown in pink. The best fit linear trend to the Crossfield and Kreidberg (2017) data, modified from the original publication to take into account the slightly different definition of equilibrium temperature, is shown in the dotted line, and has the functional form of $A = 0.0044\mathrm{T} - 2.45$, where A is the water feature amplitude in units of H and T is the temperature in K.

3.2. Aerosols in Emission and Reflection

Thermal emission has been detected from two distinct populations of exoplanets: directly imaged young giant exoplanets in wide orbits about their host stars and transiting worlds on tight orbits ranging from hot Jupiters to rocky planets. Emission from a handful of non-transiting exoplanets have also been detected (Birkby et al., 2017; Brogi et al., 2012; Crossfield et al., 2010; Harrington et al., 2006; Lockwood et al., 2014; Piskorz et al, 2016, 2017; Webb et al., 2020), but these observations have not yet been used to infer aerosol properties. The nadir geometry of emission observations allows us to probe deeper into the atmosphere than transmission, with the emitted flux being a sensitive function of atmospheric thermal structure in addition to chemical composition and aerosol distribution. Thermal emission observations capture the average of the properties of a full hemisphere (often the dayside for transiting exoplanets), which makes them less sensitive to small variations in cloud properties and cloud coverage than transmission spectra. Thermal emission observed over a significant fraction of the rotation period of the object also gives information on longitudinal heterogeneity in the atmosphere; for transiting exoplanets, this is accomplished by observing the orbital phase curve over a significant fraction or all of the orbital period, as they are tidally locked to their stars, i.e. their rotation and orbital periods are the same.

3.2.1. The Brown Dwarfs Legacy

The large semi-major axes of directly imaged planets allow for analogies to be drawn between them and isolated field brown dwarfs, for which we have observations of higher quality and quantity (e.g., Helling & Casewell, 2014; Line et al., 2017; Liu et al., 2016). As Figure 5 shows, directly imaged companions and field brown dwarfs are similar in their near-infrared colors and luminosities, which in turn are controlled by the formation and evolution of clouds as brown dwarfs age (Bailey, 2014; Kirkpatrick, 2005; Lodders & Fegley, 2006): the M-L transition is characterized by the formation of titanium and vanadium clouds, removing TiO and VO gas absorption from the spectrum (Burrows & Sharp, 1999; Lodders, 1999, 2002). The reddening of the L dwarfs with decreasing luminosity is likely due to increasing cloud optical depth with the formation of silicate and iron clouds (Allard et al., 2001; Marley et al., 2002; Tsuji, 2002). The significant spread in J-K colors of L dwarfs have been attributed to variations in metallicity and gravity, though the existence of high altitude aerosol layers composed of submicron particles in addition to the mineral clouds have been suggested for the reddest field L dwarfs (Hiranaka et al., 2016). The departure of objects toward

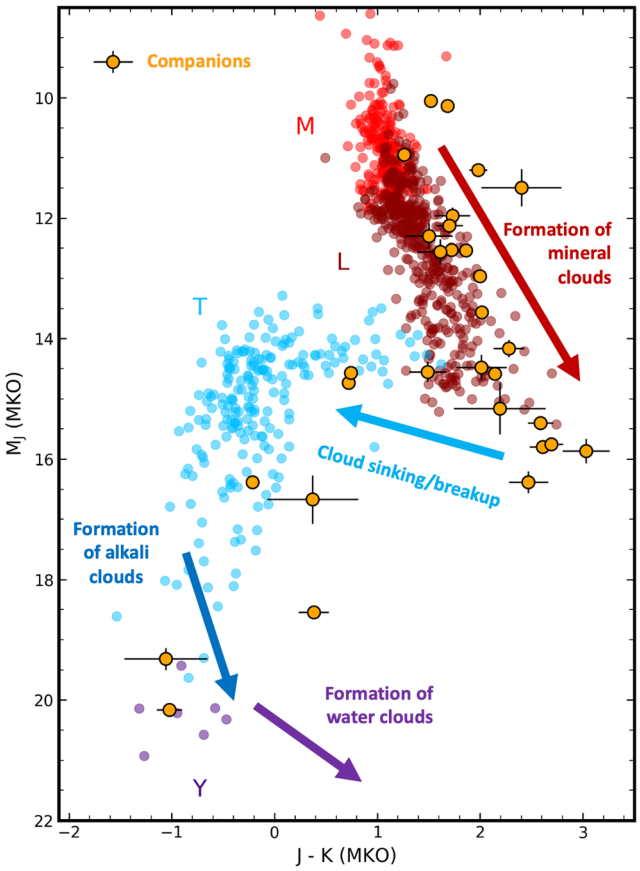

Figure 5. Color-magnitude diagram of field dwarfs (M dwarfs: red; L dwarfs: dark red; T dwarf: blue; Y dwarfs: indigo) and directly imaged companions (orange). Here we only include companions that may be exoplanets, which we take to be objects indicated by "Y," "Y?," and "N?" in the "exoplanet" column of Best et al. (2020a), along with objects with those designations that are part of binaries. We also include VHS J125601.92-125723.9 b and SDSSJ224953.46 + 004404.6A, which were stated to possess masses near the deuterium burning limit by Bowler (2016). Data are taken directly from Best et al. (2020a), which has been compiled by Dupuy and Liu (2012), Dupuy and Kraus (2013), Liu et al. (2016), and Best et al. (2018, 2020b). Only objects with near-infrared photometry available in MKO magnitudes are included. Annotations indicate our current understanding of cloud evolution on brown dwarfs.

bluer near-infrared colors at the L-T transition is partly due to increased methane absorption, but also the sinking of the clouds below the photosphere and/or breaking up of the clouds (Ackerman & Marley, 2001; Burgasser et al., 2002; Knapp et al., 2004; Marley et al., 2010; Stephens et al., 2009; Tsuji & Nakajima, 2003), though non-cloud explanations have also been proposed (Tremblin et al., 2016). The dimming and reddening of late T dwarfs is thought to be due to condensation of sulfides and chlorides (Line et al., 2017; Morley et al., 2012; Zalesky et al., 2019), while the transition to Y dwarfs occurs with the appearance of ammonia gas absorption, followed by water condensation for the coolest Y dwarfs discovered so far (Burrows et al., 2003; Cushing et al., 2011; Hubeny & Burrows, 2007; Leggett et al., 2015; Lodders & Fegley, 2002; Morley et al., 2014b, 2018). Similar condensation sequences and chemical transitions should occur in the atmospheres of directly imaged planets as they evolve.

In addition to luminosity and color variations over cosmic timescales, brown dwarfs also exhibit temporal variability in broadband emission and spectra as they rotate. This observed variability is indicative of heterogeneous aerosol distributions, including holes in aerosol layers, multiple layers, and variable layer thicknesses, with a possible higher concentration of variable objects at the L-T transition (Artigau, 2018; Artigau et al., 2009; B. Biller, 2017; B. A. Biller et al., 2013; Buenzli et al., 2014, 2015a; Burgasser et al., 2014; Crossfield et al., 2014; Cushing et al., 2016; Eriksson et al., 2019; Faherty et al., 2014; Heinze et al., 2013; Lew et al., 2020; Radigan, 2014; Radigan et al., 2012, 2014; Vos et al., 2020; Wilson et al., 2014). This points to cloud breakup as potentially contributing to the increasingly blue near-infrared colors of later spectral types. Furthermore, differences in variability amplitudes between atmospheric windows and absorption features can reveal the location of the aerosol layers. For example, the discovery that variability amplitudes in spectral windows are larger than those in wavelength-adjacent absorption features in several L-T transition objects shows that an aerosol layer with spatially variable thickness likely exists between the optical depth unity altitudes (where optical depth equals one) at these two wavelengths (Apai et al., 2013; Buenzli et al.,2015a, 2015b). Conversely, the variability amplitudes of some mid-L dwarfs are linear with wavelength across absorption bands, which is suggestive of an aerosol layer at high altitudes above the optical depth unity altitudes of the absorbers (Lew et al., 2016; Schlawin et al., 2017; H. Yang et al., 2015). This in turn implies that the sinking of aerosol layers also occurs as L dwarfs transition to T dwarfs. Complicating these analyses is the recognition that several brown dwarfs' light curves are aperiodic, indicating weather-like processes where aerosol distributions change within a timescale comparable to the rotation period, typically ranging from several hours to several days (Apai et al., 2017, 2021; Artigau et al., 2009; Gillon et al., 2013; Karalidi et al., 2016; Radigan et al., 2012; Tan & Showman, 2019; H. Yang et al., 2016).

3.2.2. Directly Imaged Planets

Near-infrared spectroscopy of directly imaged companions has shown that, like isolated brown dwarfs, aerosols are common in their atmospheres and that the distribution of aerosols appears to be heterogeneous, with some objects exhibiting temporal variability in photometry and spectra (B. A. Biller & Bonnefoy, 2018; Bonnefoy et al., 2013, 2016; Bowler et al., 2020; Currie et al., 2011; Delorme et al., 2017; Greenbaum et al., 2018; Ingraham et al., 2014; Lew et al., 2020; Macintosh et al., 2015; Manjavacas et al., 2019; Marley et al., 2012; Marois et al., 2008; Müller et al., 2018; Rajan et al., 2017; Samland et al., 2017; Skemer et al., 2012, 2014; J. J. Wang et al., 2020; Zhou et al., 2016, 2020). Trends in wavelength-dependent variability

with spectral type are also seen among companions, where L-type objects (those with spectra similar to L dwarfs) tend to have gray or linear dependence while L-T transition objects show lower variability amplitudes in absorption features (Manjavacas et al., 2018; Miles-Páez et al., 2019; Zhou et al., 2018). Importantly, these observations, along with those of young, low gravity, isolated objects (e.g., B. A. Biller et al., 2015, 2018; Faherty et al., 2016; Gizis et al., 2015; Liu et al., 2016; Metchev et al., 2015; Vos et al., 2019, 2020), show that lower gravity objects tend to be more variable and possess redder near-infrared colors (higher J-K) compared to higher gravity objects of the same effective temperature (Figure 5).

3.2.3. Transiting Exoplanets

While many transiting hot and warm Jupiters exhibit similar atmospheric temperatures as isolated brown dwarfs and wide orbit companions, the intense stellar irradiation that they experience while tidally locked to their host stars mean that they possess fundamentally different atmospheric thermal structures both vertically and horizontally. These differences have been revealed by observations of thermal emission from their permanent daysides (e.g., Arcangeli et al., 2018; Charbonneau et al., 2005, 2008; Deming et al., 2005, 2007; de Wit et al., 2012; Garhart et al., 2020; Knutson et al., 2008; Kreidberg et al., 2014b; Majeau et al., 2012; Mikal-Evans et al., 2019; Stevenson et al., 2010; Wallack et al., 2019) and phase curves (e.g., Cowan et al., 2012; Demory et al., 2016; Knutson et al., 2007, 2012; Kreidberg et al., 2018a, 2019; N. K. Lewis et al., 2013; Stevenson et al., 2014; I. Wong et al., 2015a, 2016; Zellem et al., 2014). Meanwhile, complementary observations of reflected light in the optical probe the longitudinal distribution of aerosols and the dayside albedo, as controlled by the reflectivity of aerosols and molecular absorption (e.g., Beatty et al., 2020; Borucki et al., 2009; Bourrier et al., 2020; Esteves et al., 2013; Jansen & Kipping, 2020; Kipping & Spiegel, 2011; Rowe et al., 2008; Shporer et al., 2014, 2019; Snellen et al., 2009; von Essen et al., 2020; I. Wong et al., 2020b). We refer the reader to Parmentier and Crossfield (2018) and Alonso (2018) for comprehensive reviews.

Combined optical and infrared observations have revealed significant longitudinal heterogeneity in the distribution of aerosols in transiting exoplanet atmospheres. For example, dayside near-infrared photometry and spectra can be explained without the need for optically thick aerosols down to the pressure levels probed, suggesting either a lack of aerosols altogether or that aerosols form at pressures higher than the planets' photosphere (Barstow et al., 2014; Kataria et al., 2015; J. M. Lee et al., 2012; Line et al., 2014). Similarly, the observed optical geometric albedos are low (≤0.1) for nearly all giant transiting planets (Figure 6; Angerhausen et al., 2015; Bell et al., 2017; Coughlin & López-Morales, 2012; Dai et al., 2017; Heng & Demory, 2013; Kane et al., 2020; Mallonn et al., 2019; Močnik et al., 2018; Niraula et al., 2018), consistent with significant gas absorption without substantial reflective aerosols (Marley et al., 1999; Seager et al., 2000; Sudarsky et al., 2000). One outlier, Kepler-7b, which possesses a geometric albedo ∼0.3 (Demory et al., 2011), also exhibits a maximum in its optical phase curve west of the substellar point; this has been interpreted as the presence of highly reflective aerosols covering a small fraction of the western limb (Demory et al., 2013; Garcia Munoz & Isaak, 2015; Webber et al., 2015). Westward-shifted maxima in optical phase curves have been observed for several objects (Figure 6), which all have T_{eq} < 2,000 K (Esteves et al., 2015; Shporer & Hu, 2015), suggesting that reflective aerosols may be common on the western limbs of hot and warm giant exoplanets, even though most of the dayside hemisphere may be clear. HD 189733b also exhibits a high albedo of 0.4 ± 0.12 at blue optical wavelengths, decreasing to <0.12 in the red optical (Evans et al., 2013), but this can be explained by Rayleigh scattering by atmospheric gas molecules alone (Barstow et al., 2014).

Several recent estimations of geometric albedos in the *TESS* bandpass have yielded high values (>0.2) for ultra-hot (T_{eq} > 2,000 K) giant exoplanets (Figure 6; von Essen et al., 2020; I. Wong et al., 2020b). However, because the measured flux in the TESS bandpass for ultra-hot Jupiters is dominated by thermal emission rather than reflected light, the estimated albedos are very sensitive to the assumptions made when estimating the thermal contamination. Assumptions about the stellar ellipsoidal effects (Shporer, 2017; I. Wong et al., 2020b), chemical profiles (Parmentier et al., 2018), thermal profiles (Lothringer et al., 2018), heat redistribution efficiency (Arcangeli et al., 2019), or the lack of 2D effects (Taylor, Parmentier, Irwin, et al., 2020) can all lead to an underestimation of the thermal emission contamination and thus an overestimation of the actual albedo. Cooler planets observed at shorter wavelengths (Shporer & Hu, 2015) are much more likely to yield precise albedo measurements. Finally, the geometric albedos of hot and warm (T_{eq} ≥ 600 K) Neptune-size, mini-Neptune, and rocky exoplanets in the *Kepler* bandpass have been constrained to low values (≤0.2) (Demory, 2014; Jansen & Kipping, 2018; Sheets & Deming, 2014, 2017). Though

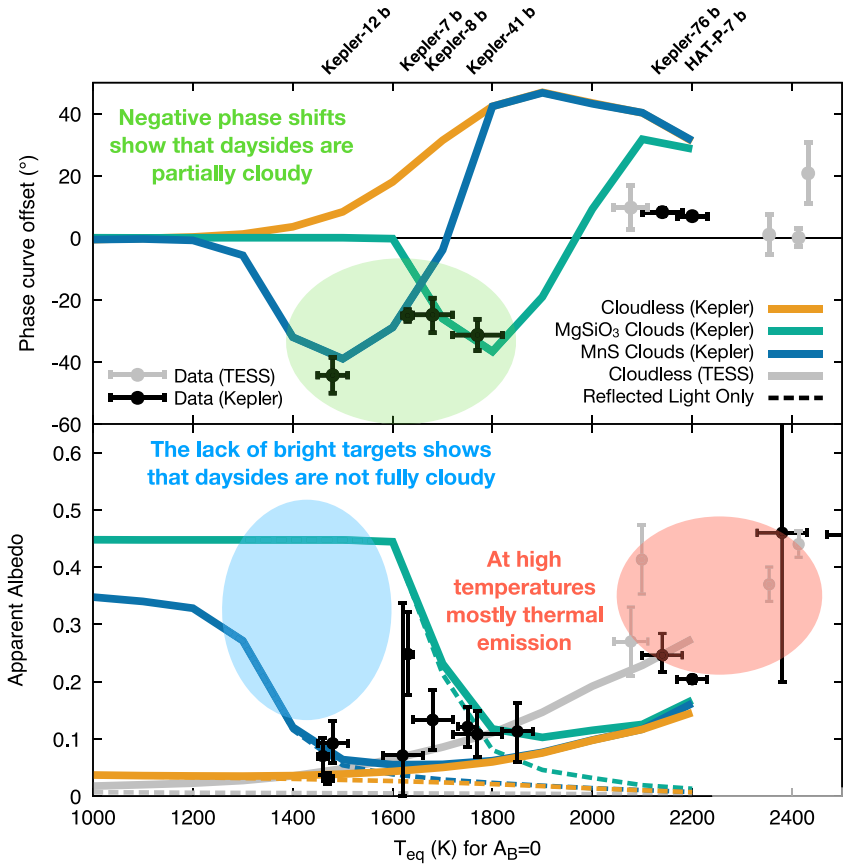

Figure 6. Optical phase curve offsets (top) and apparent albedos (bottom) of giant exoplanets in the Kepler (black points) and TESS (gray points) bandpasses compared to global circulation models assuming cloudless atmospheres (orange and gray curves for Kepler and TESS bandpasses, respectively) and atmospheres post-processed with $MgSiO_3$ (green curve) or MnS (blue curve) clouds. The apparent albedo includes both reflected and emitted light; the reflected light-only albedo is shown in the dashed curves, indicating that most of the photons received from the daysides of ultra-hot giant exoplanets are emitted rather than reflected. Two planets are not shown here, as they are situated beyond the plot limits: KELT-1b, which has an apparent albedo of 0.7 in the TESS bandpass (von Essen et al., 2020), and WASP-100b, which has a controversial hot spot measurement in the TESS bandpass (see Jansen and Kipping [2020] vs. I. Wong et al. [2020b]). The figure is updated from Parmentier et al. (2016). © AAS. Reproduced with permission.

the large measurement uncertainties have prevented solid conclusions to be drawn about aerosol properties in their atmospheres, reflective, spatially extensive aerosols are unlikely.

The nightsides of transiting giant exoplanets, as probed by thermal phase curves, show an intriguing pattern. Multiple studies (Beatty et al., 2019; Keating et al., 2019) have now shown that the nightside brightness temperature, as measured by *Spitzer*, is a nearly constant ~1,100 K, while the dayside brightness temperature increases linearly with T_{eq} (Figure 7). This pattern persists up to at least T_{eq} ~ 2,500 K. One possible explanation for this phenomenon is that observations of the nightside at near-infrared wavelengths probe the top of a cloud layer that persists on all transiting giant exoplanets with $T_{eq} \leq$ 2,500 K, such that the nightside brightness temperature is tied to the condensation temperature of that cloud (Beatty et al., 2019). Indeed, current efforts to interpret the amplitudes and phase shifts of hot Jupiter thermal phase curves using non-aerosol explanations, such as higher metallicity (Drummond et al., 2018a; Kataria et al., 2015) and disequilibrium chemistry (Drummond et al., 2018b; Mendonça et al., 2018; Steinrueck et al., 2019), have met limited success.

In summary, probes of exoplanet atmospheres by multiple observational methods have revealed an abundance of aerosols across all varieties of worlds. By taking advantage of the growing number of exoplanets amenable to characterization, we have found hints of trends in aerosol distribution with planet temperature

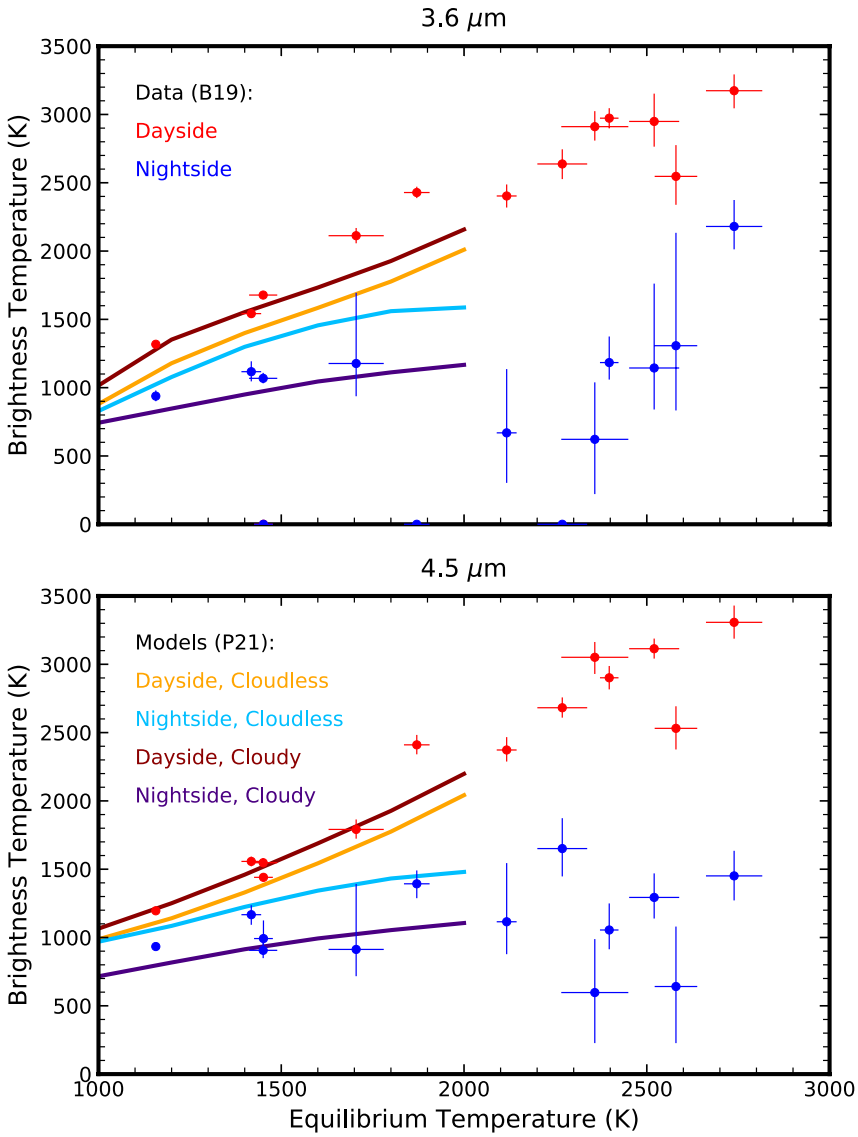

Figure 7. Observed brightness temperatures of the daysides (red) and nightsides (blue) of hot Jupiters at the 3.6 (top) and 4.5 μm (bottom) *Spitzer* bands from Beatty et al. (2019), which probe atmospheric temperature and opacity structures, including the effect of aerosols. Brightness temperatures computed by Parmentier et al. (2021) using a GCM for cloudless hot Jupiters (daysides: orange, nightsides: light blue) and hot Jupiters with cloudy nightsides (daysides: dark red, nightside: indigo) are shown for comparison.

and discovered the spatial heterogeneity of aerosols. Furthermore, we have shown through our discussions of both directly imaged exoplanets and transiting exoplanets that the level of stellar irradiation and orbital distance greatly affects aerosol distributions. In the next section, we overview the theoretical tools that have been brought to bear to explain our diverse observations.

4. Insights from Theory

The formation, evolution, and spatial and size distribution of aerosols depend on interactions between the atmospheric thermal structure, wind patterns, and microphysical processes (Pruppacher & Klett, 1978). For clouds, these processes include nucleation, the conversion of condensate vapor into solid or liquid either directly (homogeneous) or with the aid of a foreign surface (heterogeneous) often in the form of a "condensation nuclei"; condensation, the growth of cloud particles through the uptake of vapor; coagulation, the

growth of cloud particles through collision and sticking; evaporation, the decrease in particle mass due to loss of condensate molecules to the atmosphere; and transport by sedimentation, diffusion, and advection by winds. For hazes under our definition (§2), formation and growth through chemical reactions and coagulation, transport, and loss through thermal decomposition, nucleation (i.e. acting as condensation nuclei for clouds), and wet deposition are the primary processes. In this section, we review the extent to which current exoplanet models capture the aforementioned physical processes and what they can tell us about what we have observed.

4.1. Modeling Exoplanet Aerosols

4.1.1. Microphysical and Parametrized Models

Exoplanet aerosol models span a continuum in complexity, from single-variable parameterizations to computationally expensive simulations of aerosol microphysics in 3D, with each type of model serving a different purpose. Highly parameterized models are typically used for retrieval studies where rapid model execution is key. These models use a handful of variables (e.g., cloud top pressure) to capture only the first order impacts of aerosols on observations, such as changing/enhancing the spectral slope at optical wavelengths and reducing the amplitude of molecular features in the infrared, without treatment of specific physical processes (e.g., Barstow, 2020; Barstow et al., 2017, 2020; Benneke & Seager, 2012; Burningham et al., 2017; Goyal et al., 2018; Greene et al., 2016; Line et al., 2016; Mai & Line, 2019; Mollière et al., 2019; Pinhas et al., 2019; Tsiaras et al., 2018; M. Zhang et al., 2019). Some retrieval frameworks have included more complex aerosol models that consider various combinations of: Mie scattering by spherical particles (Benneke et al., 2019a; B. I. Lacy & Burrows, 2020b; J.-M. Lee et al., 2014; M. Zhang et al., 2019), aerosol layers that vary with altitude (Benneke et al., 2019a; Damiano & Hu, 2020; Lupu et al., 2016; M. Zhang et al., 2019), aerosol composition (Fisher & Heng, 2018; J.-M. Lee et al., 2014), and spatial heterogeneity (Feng et al., 2018; Line & Parmentier, 2016; MacDonald & Madhusudhan, 2017). These more complex models allow for more physical interpretations of how aerosols affect observations, but they come at a price of a greater number of parameters, some of which may not be well constrained by the data we currently possess (e.g., Fisher & Heng, 2018). In addition, Mai and Line (2019) and Barstow (2020) showed that the retrieved atmospheric temperature and composition from transmission spectra are largely insensitive to the chosen aerosol parameterization, as long as aerosols are not ignored in the retrieval. In contrast, the aerosol properties retrieved using the different parameterizations may be substantially different from each other, suggesting that consistent constraints on exoplanet aerosols may be difficult to obtain through retrievals that use simple aerosol parameterizations.

Aerosol models that include some of the physical processes that control aerosol distributions, but which are still parameterized to be computationally inexpensive are often found as a part of radiative-convective equilibrium models. While these models are more computationally expensive than retrievals, they are useful for generating model grids that elucidate the roles of specific parameters across populations of objects. In contrast, retrievals typically seek to extract physical parameters from observations by rapidly exploring the parameter space for a single object. These more complex aerosol models typically treat aerosol compositions computed from thermochemical equilibrium (see §2) and assume either a mean particle size or a functional form for the aerosol size distribution (Figure 8), allowing them to compute aerosol optical properties assuming Mie scattering. The differences between these models are due to how they parameterize aerosol microphysics. The cloud model of Ackerman and Marley (2001), for example, computes cloud distributions by balancing particle sedimentation with vertical mixing, while the vertical extent of the clouds is controlled by a sedimentation efficiency parameter. In contrast, the model of Cooper et al. (2003) computes the mean particle size by balancing the timescales of microphysical processes following Rossow (1978); free parameters include the supersaturation, which controls the nucleation and condensation timescales, and the sticking coefficient that controls the coagulation timescale. These two approaches both allow for relatively fast computations of profiles of particle sizes, cloud mass mixing ratios, and cloud optical properties. While these models' reliance on tunable parameters hinders their predictive powers, it also allows them to explore a large range of cloud properties and how they affect observations. Hu et al. (2012) describes an alternative aerosol model coupled to a photochemical model where the particle size is a free parameter, sedimentation is treated explicitly, and condensation and evaporation is computed through associated timescales. This

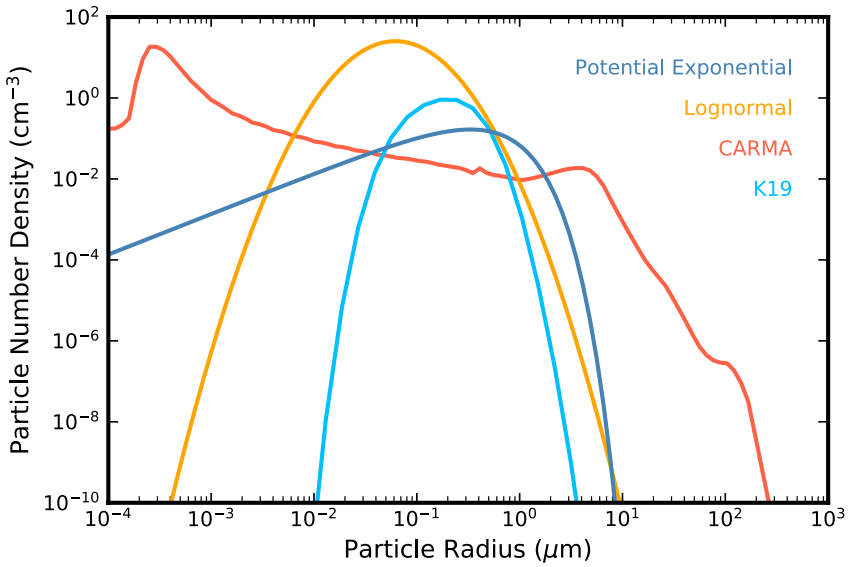

Figure 8. Example particle size distributions from aerosol models. Shown are the parameterized potential exponential (dark blue; e.g., Helling et al., 2008c) and lognormal (orange; e.g., Ackerman & Marley, 2001) functions, along with binned size distributions from the cloud simulations of Gao et al. (2020) using CARMA (red) and the haze simulations of Kawashima and Ikoma (2019) (K19; light blue).

model considers cloud compositions produced by photochemical reactions like sulfuric acid and sulfur (§2) and has been used mostly for terrestrial planet atmospheres thus far.

The most complex 1D aerosol models treat microphysical processes kinetically, producing particle distributions by balancing the rates of the individual processes. These models are used for exploring how different aerosol processes interact with each other and how aerosol distributions form and evolve. Table 1 shows how current kinetic models compare on several modeling techniques. Some of the models parameterize the particle size distribution using moments of that distribution, such that the actual shape of the distribution must be user-prescribed, while other models are able to resolve the size distribution using mass bins. Parameterizing the size distribution saves computation power, but may fail to capture multiple particle size modes (Figure 8), leading to significant differences in aerosol opacity and its wavelength dependence (Powell et al., 2019). The models also differ in whether they treat particles as being composed of a single composition or a mixture of multiple compositions. Given the large number of potential condensates at high temperatures (Figure 1), the existence of mixed composition particles is likely. DRIFT (not an acronym) and CARMA (Community Aerosol and Radiation Model for Atmospheres) treat mixed particles differently, however: DRIFT allows multiple species to condense onto the same cloud particle at the same time via numerous thermochemical reactions, forming well-mixed "dirty grains" (Helling & Woitke, 2006; Helling et al., 2008c), a procedure originating from models of mixed dust grains in stellar winds (Gail & Sedlmayr, 1988; Gail et al., 1984). In contrast, CARMA considers only layered particles, such that only the

Table 1
Properties of Microphysical Models of Exoplanet Aerosols

Model	Moment/bin	Mixed/pure	C/H	Nucleation	Haze formation	Transport	Reference
DRIFT	Moment	Mixed	C	Comp.	⋯	Relaxation	Helling et al. (2008b)
O17	Moment	Pure	C&H	Hybrid	Param.	Advection	Ohno and Okuzumi (2017)
L17	Bin	Pure	H	⋯	Hybrid	Diffusion	Lavvas and Koskinen (2017)
CARMA	Bin	Mixed	C&H	Comp.	Param.	Diffusion	Gao et al. (2018)
K18	Bin	Pure	H	⋯	Photo.	Diffusion	Kawashima and Ikoma (2018)
ARCiS	Moment	Pure	C	Param.	⋯	Diffusion	Ormel and Min (2019)

outer most layer can grow by condensation at any one time (Gao & Benneke, 2018). This strategy originates from CARMA's roots in Earth science (Toon et al., 1979; Turco et al., 1979) where condensing water vapor can completely envelope a condensation nucleus, but may not suffice for high temperature exoplanet clouds where multiple condensates may interact.

The considered kinetic models can be further divided between cloud models (C), haze models (H), and models capable of simulating both types of aerosols (C&H). Of the models capable of simulating clouds, an important attribute to consider is how they treat nucleation, as that ultimately controls the depletion of condensate vapor and the cloud particle number density and size. The ARCiS (ARtful modeling Code for exoplanet Science) framework (Ormel & Min, 2019) parameterizes (Param. in Table 1) their particle nucleation rate with a Gaussian profile and a user-defined column rate. The model of Ohno and Okuzumi (2017) uses a hybrid approach where the heterogeneous nucleation rate is computed based on user-input number densities and sizes of condensation nuclei. DRIFT (Helling et al., 2008b) and CARMA (Gao et al., 2018) both compute (Comp. in Table 1) homogeneous nucleation rates of condensation nuclei from classical nucleation theory (or modified versions of it); for subsequent condensation of other cloud compositions the former model considers grain chemistry while the latter model computes heterogeneous nucleation rates. While consideration of nucleation theory is more physical, it has been shown to differ from experimentally determined rates by orders of magnitude for some substances (see e.g., Anisimov et al., 2009; Oxtoby, 1992) and relies on material properties that may not have been measured at the appropriate temperatures, for example, surface energies (Gao et al., 2020).

Likewise, of the models capable of simulating hazes, a major source of uncertainty is how they compute the haze formation rate profile in the atmosphere, which ultimately determines the haze opacity. While no model has been able to fully simulate the chemical network from simple parent molecule to aerosol particles, some are more parameterized than others. CARMA and the Ohno and Okuzumi (2017) model (as described in Ohno & Kawashima, 2020) both fully parameterize (Param. in Table 1) haze formation rates through user-chosen production rate profiles and initial particle sizes. The model of Lavvas and Koskinen (2017) is similar except the column rate is computed from photochemical models (Hybrid in Table 1) under the assumption that some percentage of the pertinent photochemical reactions (a "haze formation efficiency"), typically involving the photolysis of hydrocarbons and nitriles, lead to haze formation. It is also the only model thus far to explicitly treat thermal decomposition of haze particles. The model of Kawashima and Ikoma (2018) takes this a step further by equating the production rate profile to some percentage of the rate profiles of the chosen photochemical reactions (Photo. in Table 1), though the initial particle size is still a free parameter. Similar strategies have also been adopted by other studies (Morley et al., 2013, 2015; Zahnle et al., 2016) that do not consider kinetic models of aerosol microphysics. In addition, several models have simulated exoplanet haze particles as fractal aggregates (Adams et al., 2019; G. N. Arney et al., 2017, 2018; Lavvas et al., 2019), much like haze particles on Titan (Lavvas et al., 2011b). Several cloud models have also considered aggregates composed of condensates (Ohno et al., 2020a; Samra et al., 2020).

4.1.2. Thermal Structure

The formation of clouds is intimately linked to the thermal structure of the atmosphere. For a given cloud species, too high of a temperature can prevent nucleation and condensation while too low of a temperature might shift cloud formation to deeper layers of the atmosphere that cannot be probed by current observations.

The thermal structure of exoplanets can be either calculated *a priori* using radiative-convective equilibrium models or retrieved directly from the planets' emission spectra. Radiative-convective models are often used in objects that experience no or little irradiation such as brown dwarfs and directly imaged planets where horizontal advection of heat is not significant. The radiative convective equilibrium profile can be further refined by using a combination of cloud and cloud-free atmospheric patches (e.g., Marley et al., 2010; Morley et al., 2014a). Parameterized thermal structures are often used for irradiated planets such as hot Jupiters (Guillot, 2010; Heng et al., 2012; Parmentier & Guillot, 2014), where the presence of trace species that are difficult to characterize, such as metal oxides or metal hydrides, can lead to large uncertainty in the expected thermal structures (Fortney et al., 2008; Gandhi & Madhusudhan, 2019). Furthermore, local radiative-convective equilibrium does not hold for specific parts of the planet, such as the dayside and the limb

that are probed by transmission and emission spectra, as their local thermal structure is determined by the global atmospheric circulation.

Aerosols have two main effects on the thermal structure of an atmosphere. First, they change the heat transport within the atmosphere: they warm up the atmosphere below the cloud by their increased opacity and cool down the atmosphere above the cloud top by efficiently radiating away heat. Second, aerosols change the albedo and thus the emissivity of the planet. The change in albedo leads to a change in the total energy received by the atmosphere and thus a change in the mean thermal structure of the planet. The change in emissivity leads to a change in the ability of the atmosphere to reemit light and thus a change in the relationship between thermal structure and observed spectra (Burningham et al., 2017; Lavie et al., 2017; J.-M. Lee et al., 2013; Mollière et al., 2020).

4.1.3. Atmospheric Transport

Atmospheric transport is needed both for aerosols to stay aloft in the atmosphere and for fresh gaseous species to replenish the depleted gas in the aerosol formation region. If no vertical mixing were present, all condensable species would rain out of the visible atmosphere. In 1D models, vertical mixing is usually assumed to be diffusive in nature and parameterized by an eddy diffusion coefficient K_{zz}, which is highly uncertain. As a diffusion coefficient, K_{zz} has units of length-squared per unit time. The "zz" subscript denotes motion in the z, i.e. vertical direction. In addition to being used in aerosol models to transport particles and condensate vapor, K_{zz} has also been frequently used in chemical kinetics/photochemistry models to approximate transport of gases (e.g., Moses et al., 2016). K_{zz} is an approximation of all large scale transport in a planetary atmosphere, including atmospheric circulation, gravity waves, and convection, most of which cannot be explicitly represented in 1D models. As some of these processes are not actually diffusive (X. Zhang & Showman, 2018a, 2018b), the use of K_{zz} to represent atmospheric transport and how its profile in the atmosphere is calculated require caution. For objects that are mainly convective, mixing length theory is often used to estimate the K_{zz} profile (e.g., Ackerman & Marley, 2001; Gierasch & Conrath, 1985). This is not valid for atmospheres that are predominantly radiative, such as those of transiting exoplanets.

On tidally locked planets, advection by the atmospheric circulation is likely the main source of vertical mixing, as opposed to turbulence or wave breaking. As first shown by Parmentier et al. (2013) using passive tracers in a 3D global circulation model (GCM), the mean vertical transport of particles in the atmospheres of hot Jupiters is surprisingly well represented by a 1D diffusion approach, resulting in a K_{zz} profile that increases with decreasing atmospheric pressure as a power law. The magnitude of K_{zz} is, however, a hundred times smaller than would be expected from extrapolating the mixing length parameterization or by multiplying the root mean square of the vertical velocities by the atmospheric scale height. X. Zhang and Showman (2018b) and X. Zhang and Showman (2018a) explored a wider range of atmospheric circulation patterns and showed that the K_{zz} used in 1D models should be different for different chemical and aerosol species. They further identified specific cases, such as when photochemical hazes form in the upper layers of a dayside updraft, which would require a negative K_{zz}, representing local concentration rather than dilution. Lastly, Komacek et al. (2019) proposed an analytical formula for K_{zz} that is based on the Earth stratosphere framework developed by Holton (1986); they showed that K_{zz} should depend on both the strength of the circulation and the timescale at which a given species is lost. Their formalism, however, was developed for gaseous chemical species only, which are not conserved. As such, it is not yet clear how to adapt it to aerosols that are usually conserved when settling vertically. In the deeper atmosphere, other processes likely start to dominate vertical mixing such as wave breaking (Fromang et al., 2016) or shear instability driven turbulence (Menou, 2019).

Not all 1D aerosol models treat transport as a diffusive process. The 1D version of DRIFT considers a Newtonian relaxation scheme for the chemical abundances instead of solving an actual diffusion equation (Woitke & Helling, 2004), and assumes that the particles are fully decoupled from the flow. In every atmospheric layer the gaseous composition relaxes toward the initial conditions. Though this approach is more straightforward numerically, it can lead to orders of magnitude differences in the cloud distribution compared to a model that uses a diffusion approach (Woitke et al., 2020). Ohno and Okuzumi (2017) also does not consider diffusion; instead, chemical species and particles are lifted upward by a constant advection along the 1D column. This approach is correct when modeling cloud formation in an updraft, but might be incorrect when modeling the spatially averaged atmosphere, where all updrafts are compensated by downdrafts.

4.1.4. 3D Aerosol Models

Aerosol models of various complexities have been incorporated into GCMs in an effort to understand the global aerosol distribution on exoplanets. On the more parameterized end, cloud particles have been treated as radiatively passive (Charnay, Meadows, & Leconte, 2015a; Komacek et al., 2019; Parmentier et al., 2013) and active (Charnay, Meadows, Misra, et al., 2015b) tracers that typically have a user-defined particle size distribution, are advected by the circulation, and may be removed through a parameterization of condensation and sedimentation. This technique has been useful in revealing how aerosols are transported in an atmosphere, particularly whether they can be lofted to high altitudes to explain muted gas spectral features. Alternatively, parameterized cloud distributions are prescribed onto the 3D grid of the GCM based on observations (M. Roman & Rauscher, 2017) or as 1D columns in which cloud formation is evaluated based on whether condensate vapor is locally supersaturated without advection of the clouds (Harada et al., 2019; Parmentier et al., 2016, 2018, 2021; M. Roman & Rauscher, 2019; M. T. Roman et al., 2020; Tan & Showman, 2017, 2020). More complex 1D cloud models, like DRIFT (Helling et al., 2016, 2019a, 2019b, 2020; G. Lee et al., 2015) and the Ackerman and Marley (2001) model (Lines et al., 2019) have also been incorporated into GCMs in this fashion. Both radiatively active and post-processed clouds (i.e. clouds added to the model atmosphere after a cloud-less GCM converged) have been considered. These studies have investigated how aerosols affect a planet's thermal emission and albedo, particle heating and cooling, and the impact of local aerosol formation on gas abundances. Several studies have more fully coupled DRIFT to GCMs (G. Lee et al., 2016, 2017; Lines et al., 2018a, 2018b), such that both particle advection, cloud microphysics, and cloud radiative feedback are considered simultaneously. While these models capture more of the interactions between the different physical processes, running them until all modeled processes can converge is currently computationally prohibitive.

4.2. Aerosol Model Predictions and Comparisons to Data

Exoplanet aerosol models have been used to interpret a variety of observations of exoplanet atmospheres and also predict future observations. In particular, many studies have focused on explaining observations of individual planets with aerosol models, either as part of retrieval frameworks (e.g., Benneke et al., 2019a; Kreidberg et al., 2014b; MacDonald & Madhusudhan, 2017; Mollière et al., 2020; Wakeford et al., 2018) and/or more complex forward models (e.g., Barman et al., 2011; Bonnefoy et al., 2013; Chachan et al., 2019; Fortney et al., 2005; G. Lee et al., 2015; Marley et al., 2012; Rajan et al., 2017). These studies have revealed a diversity of exoplanet atmospheres across planetary parameter space. However, due to limited data these comparisons often run into degeneracies and it is unknown how applicable their conclusions are to all exoplanets. Therefore, in this section we will mostly focus on studies that have attempted to explain or predict how aerosols impact whole populations of exoplanets, though we will also discuss several benchmark objects.

4.2.1. Transiting Exoplanets

As reviewed in §3, the proliferation of exoplanet transmission spectroscopy, emission photometry, and optical and infrared phase curves allow us to probe the vertical and horizontal extent of aerosols in exoplanet atmospheres across a wide range of planetary parameters. These efforts have yielded several important clues on how aerosol distributions vary with planet T_{eq} and longitude: (1) The daysides of giant transiting exoplanets are likely clear while the nightsides and western limbs likely host optically thick aerosols and (2) the vertical extent of aerosols at the limbs, as probed by transmission spectroscopy, may correlate with planet temperature. Several modeling studies have tried to explain these observations.

Parmentier et al. (2016) computed the total thermal emission and reflected light fluxes in the *Kepler* bandpass of a grid of hot giant exoplanets by adding post-processed, parameterized clouds to the output of a GCM and compared their results to observed optical phase shifts and apparent albedos (Figure 6). They found that a transition in cloud composition, as determined by local thermal stability of condensates predicted by thermochemistry models, could explain the data: at the highest temperatures, the dayside is devoid of aerosols with the flux dominated by thermal emission, which reaches a maximum toward the east limb; as temperatures decrease, silicate clouds form on the nightside and western limb, where the temperatures are the lowest, and begin extending eastward over the dayside, shifting the brightest longitude in the *Kepler*

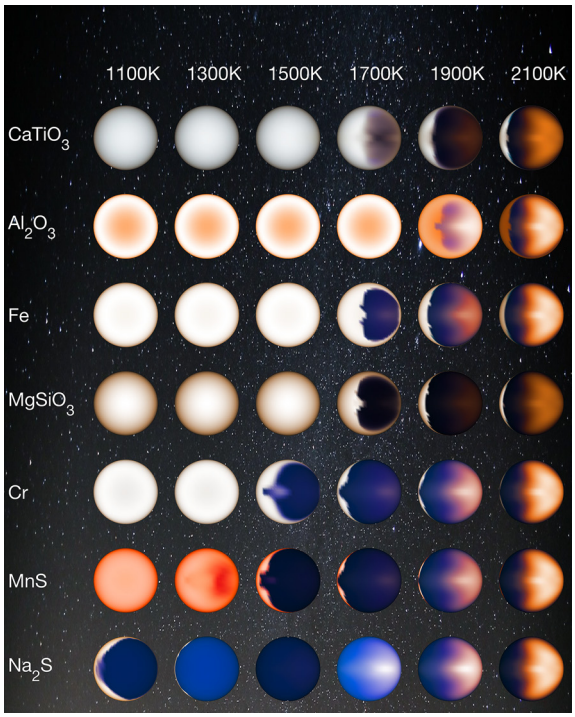

Figure 9. Visual appearance of the daysides of a set of exoplanet global circulation models with post-processed clouds (Parmentier et al., 2016), generated with the same approach as those of Harre and Heller (2021). Each column represents planets of a single equilibrium temperature while each row shows different cloud species. For low equilibrium temperatures, the dayside is often fully cloudy and the color of the cloud depends on its absorption bands in the optical. For intermediate temperatures, the cloud coverage is concentrated on the western part of the dayside, where the planet is cooler. The eastern part, dominated by the hot spot, is cloudless and has a dark blue appearance due to alkali absorption. At high equilibrium temperatures, the daysides are mostly cloudless, with their visual appearance dominated by the thermal emission of the hot spot. Image credit: NASA/JPL-Caltech/University of Arizona/V. Parmentier.

bandpass to the west and causing reflected light to dominate over thermal emission; at ∼1,600 K, the observed low albedo necessitates the disappearance of silicate clouds from the dayside, possibly due to sequestration in deeper atmospheric layers; at the same time, MnS clouds replace silicates as the dominant aerosol species on the western limb, perpetuating the westward optical phase curve shift (Figure 9). Parmentier et al. (2016) also found that cloud radiative feedback causes a net increase in the temperature of the planet due to the greenhouse effect of clouds on the nightside, producing a higher emission flux in the clear parts of the dayside and increasing the day-night temperature contrast, consistent with similar studies with prescribed clouds (M. Roman & Rauscher, 2019). Parmentier et al. (2021) and M. T. Roman et al. (2020) extended these works to show that the existence of nightside clouds is a likely explanation for the observed low uniform brightness nightside temperatures of hot Jupiters (Figure 7; Beatty et al., 2019; Keating et al., 2019) and thermal phase curve shifts, though the decrease in radiative timescale with increasing equilibrium temperature also strongly contributes.

The formation of spatially inhomogeneous clouds could also have a large impact on the spatial distribution of the gaseous species involved in cloud formation. For example, Helling et al. (2019a) found that the C/O ratio can vary from subsolar to supersolar (∼0.3 to ∼0.7) due to the evaporation and condensation of oxygen-bearing clouds (e.g., silicates) at different locations around the planet.

Studies that treat aerosols in GCMs as tracers showed that the atmospheric circulation of hot Jupiters tend to reduce the cloud cover at the equator compared to the midlatitudes (Komacek et al., 2019; Parmentier et al., 2013). Additionally, when aerosol microphysics is considered (G. Lee et al., 2016; Lines et al., 2018b), latitudinal variations in particle size and composition were predicted, with small particles made mainly of SiO_2 at the equator and larger particles dominated by Mg_2SiO_4 at midlatitudes. However, these works also found that the aerosol distribution was much more longitudinally homogeneous, in contrast with observations. This may be due to non-convergence of some of the processes considered in the models.

An important takeaway of the results of 3D models is that the aerosol distributions on the east and west limbs of hot Jupiters are unlikely to be the same, which could be observable via transmission spectroscopy (Kempton et al., 2017; Line & Parmentier, 2016; von Paris et al., 2016). Using the aerosol microphysics model CARMA combined with temperature profiles extracted from a GCM, Powell et al. (2018) showed that higher temperatures on the east limb promote cloud formation at higher altitudes, making it appear more cloudy than the cooler west limb, which hosts more massive but lower altitude clouds; this shifts abruptly above a critical temperature (∼1,700 K), determined by atmospheric circulation, however, when the clouds on the east limb become optically thin in transmission. As such, transmission spectra near this critical temperature may be especially diverse. Detection of patchy aerosols at exoplanet limbs have been difficult in broadband photometry due to a degeneracy between asymmetric limb atmospheres and uncertainties in the transit ephemeris, but this may be overcome by taking into account the chromatic variations in how aerosols impact transmission spectra (Powell et al., 2019).

Interpreting possible trends in transmission spectra is complementary to interpreting trends in emission and reflection. While the vertical extent of aerosols is vital in controlling the shape of transmission spectra, it does not strongly affect the emitted and reflected flux (Parmentier et al., 2016). As the vertical extent of aerosols is deeply connected to microphysical processes (Ackerman & Marley, 2001), a kinetic model is needed. Using CARMA, Gao et al. (2020) computed the amplitude of the 1.4 μm water feature of hot Jupiters in

transmission as a function of temperature, gravity, and atmospheric metallicity. Their results compare well to the data compiled by Fu et al. (2017), though there is more scatter in the data (Figure 4), which could be due to their usage of a 1D model that ignores east-west limb differences (e.g., Powell et al., 2018). The computed water feature amplitudes do not vary monotonically with temperature: CARMA predicts the formation of silicate, corundum, and titanium clouds at high temperatures, rapidly reducing the water feature amplitude compared to hotter, cloudless (1D) atmospheres; this is followed by the sinking of these clouds to lower altitudes at lower temperatures leading to an increase in the water feature amplitude; finally, at ~950 K, photochemical hazes form from methane photolysis, reducing the water feature amplitude once more. Importantly, Gao et al. (2020) predicts that optically thick iron and sulfide clouds, including MnS clouds, are difficult to form due to energy barriers associated with nucleation. These results are in contrast to those of Parmentier et al. (2016), who required silicate clouds to disappear for $T_{eq} < 1{,}600$ K and for MnS to become the primary aerosol species on the western limb. While a similar transition occurs in the work of Gao et al. (2020), it is set at a much lower temperature (~950 K) and is between silicates and methane-derived hazes rather than silicates and MnS clouds. A possible solution is if hazes could form at higher temperatures (e.g., Lavvas & Koskinen, 2017) such that it could replace MnS as the main source of aerosol opacity at the limb, while remaining optically thin in emission. An explanation for how silicate clouds disappear is also needed, as sequestration at depth may be difficult (Thorngren et al., 2019). In addition, Gao et al. (2020) does not explain the diversity of spectral slopes in the optical. Ohno and Kawashima (2020) offers a possible cause for such slopes by appealing to photochemical hazes. They found that variations in haze formation rates at high altitudes and the rates with which haze particles are mixed downwards naturally lead to a diversity of optical spectral slopes. In particular, they showed that "super-Rayleigh" slopes (Alderson et al., 2020; Chen et al., 2021; May et al., 2020; Pinhas et al., 2019; Welbanks et al., 2019) are possible when mixing is strong and the haze formation rate is moderate.

Modeling efforts for cooler, lower mass exoplanets have focused on understanding why certain benchmark objects, e.g., the mini-Neptune GJ 1214b and the "super-puffs" Kepler-51b and d have extremely flat transmission spectra (Kreidberg et al., 2014a; Libby-Roberts et al., 2020). A slew of studies have attempted to explain GJ 1214b's transmission spectra using 1D models, some relying on KCl and ZnS clouds (Gao & Benneke, 2018; Ohno & Okuzumi, 2018; Ohno et al., 2020a), some relying on photochemical hazes (Adams et al., 2019; Kawashima & Ikoma, 2018; Kawashima et al., 2019; Lavvas et al., 2019), and others relying on both (Morley et al., 2013, 2015). In general, a moderately high (>100 × solar) atmospheric metallicity is needed in addition to aerosol opacity to suppress the amplitude of molecular features to match the data. Studies focusing on clouds have required them to be extremely vertically extended, either due to extremely strong vertical mixing or low sedimentation velocities caused by high porosity. Charnay, Meadows, Misra, et al. (2015b) showed using a GCM that cloud particles can be lofted to low pressures by atmospheric circulation to explain the *Hubble da*ta (Kreidberg et al., 2014a), but the particle size required would be too small to explain the *Spitzer* data, which extends GJ 1214b's featureless transmission spectrum out to 5 μm. Studies that explored the impact of hazes frequently faced the same issue: the production of hazes at low pressures leads to small particles that are unable to explain the full spectrum. Adams et al. (2019) was able to explain the full spectrum with aggregate haze particles, though they relied on a parameterization of how the fractal dimension of aggregates scaled with the number of monomers within the aggregate that may not be realistic (Ohno et al., 2020a). Morley et al. (2015) was able to match the *Hubble* data for GJ 1214b with photochemical hazes and predicted that their existence may lead to atmospheric heating, resulting in a temperature inversion that would generate emission features in GJ 1214b's thermal infrared spectrum. In addition, Morley et al. (2015) showed that the haze production rate, parameterized from a photochemical model, peaks at a planet $T_{eq} \sim 800$ K with falling rates at higher temperatures due to lower methane abundances, and lower temperatures due to decreasing high energy UV photons. This could lead to increasing haze opacity with decreasing T_{eq} for $T_{eq} < 1{,}000$ K, which may explain the emerging trend in the amplitude of the 1.4 μm water feature seen in Crossfield and Kreidberg (2017).

The low gravities of super-puffs (e.g., Masuda, 2014) led to expectations of large (>1,000 ppm) amplitude spectral features in transmission, but observations showed a flat spectrum instead (Chachan et al., 2020; Libby-Roberts et al., 2020). Generating flat spectra for these objects using aerosols is difficult due to the extremely low pressures (<1 μbar) where they must persist. L. Wang and Dai (2019) and Gao and Zhang (2020) got around this issue by taking into account the outward wind that could exist on super-puffs due to ongoing

atmospheric loss, which could entrain aerosol particles and push them to higher altitudes. In particular, Gao and Zhang (2020) showed that such a phenomenon could occur on all young, low mass, temperate (T_{eq} < 1,000 K) planets, leading to an increase in the radius of a hazy-covered planet, as seen in transit, by as much as a factor of 2 compared to its clear-sky equivalent. On the other hand, nadir-geometry observations (emission and reflection) may be able to see past some of the aerosol opacity to reveal gas compositions and a smaller radius.

4.2.2. Directly Imaged Exoplanets

An important motivation of aerosol models of the current sample of directly imaged exoplanets is to explain why they are redder than brown dwarfs of the same effective temperature, given the general picture of cloud evolution on brown dwarfs outlined in §3. Marley et al. (2012) showed that the difference in gravity between field brown dwarfs and directly imaged exoplanets is the likely culprit: the atmospheric mass—and thus opacity—above a given pressure level is higher for a low gravity object than for a high gravity object, leading to the former object having higher temperatures at all pressures than the latter object for the same effective temperature. As such, the cloud base on the lower gravity object would be situated at lower pressures, allowing clouds to persist above the photosphere of the object to a lower effective temperature, leading to redder near-infrared colors due to aerosol opacity. Charnay et al. (2018) reaffirms this result but also shows that the location of the radiative-convective boundary is at lower pressures for lower gravity objects than for higher gravity objects of the same effective temperature, and thus lofting of cloud particles by convective turbulence may be more efficient for low gravity objects, further increasing cloud opacity. It is important to note, however, that these studies do not consider the kinetics of cloud formation, and thus how cloud opacity varies with gravity on directly imaged exoplanets is still uncertain. Furthermore, interpreting spectra of the reddest objects still requires the inclusion of high altitude submicron aerosols and/or highly vertically extended cloud layers (Allart et al., 2020; Burningham et al., 2017; Hiranaka et al., 2016; Kellogg et al., 2017; Lew et al., 2016; Manjavacas et al., 2018; Schlawin et al., 2017; Stone et al., 2020).

In addition to mineral clouds, the proximity of some directly imaged companions to their young, UV-bright host stars coupled with relatively cool stratospheres could permit the formation of photochemical hazes. Griffith et al. (1998) hypothesized that absorbing organic hazes could persist at several tens of bars in the atmosphere of the brown dwarf companion Gl 229 B, which would explain its low flux at red optical wavelengths. Photochemical modeling of directly imaged exoplanets (Moses et al., 2016; Zahnle et al., 2016) showed that optically thick hydrocarbon hazes are difficult to form, though there is great uncertainty in the chemical pathways involved. Interestingly, Zahnle et al. (2016) showed that H_2S photochemistry could produce elemental sulfur allotropes like S_8, which may condense to form optically thick sulfur clouds for planets with effective temperatures < 700 K. Such clouds would be highly reflective at red-optical and near-infrared wavelengths, but highly absorbing at wavelengths <0.4 μm (Gao et al., 2017).

Spatial inhomogeneity and temporal variability of cloud distributions on brown dwarfs and directly imaged exoplanets have been used to explain the variability in rotational light curves of these objects (§3), but what causes the inhomogeneity is uncertain. Showman and Kaspi (2013) showed using a cloudless GCM that there are likely large-scale upwelling and downwelling regions on these objects that would serve as areas of cloud formation and cloud depletion, respectively. Tan and Showman (2017) included a parameterization of silicate condensation and latent heating in their GCM study and found that isolated silicate storms can occur when the condensation level sinks below the radiative-convective boundary due to the onset of moist convection, which could explain the inferred patchiness of clouds and temporal variability of objects at the L-T transition. Variability is also likely impacted by the rotation rate and cloud radiative feedback (Tan & Showman, 2019, 2020, 2021), such that changes in the Coriolis force with latitude could lead to corresponding changes in cloud opacity and patchiness inline with observations of brown dwarfs at different inclinations, where objects viewed equator-on are redder and more variable than objects viewed pole-on (Vos et al., 2017).

In summary, exoplanet aerosol models have shown that aerosols are intimately linked with the atmospheric thermal structure and vertical mixing. Using models with a wide range of complexity, we have found that the composition of exoplanet aerosols likely transitions between several major compounds with temperature, including silicates, sulfides, and photochemical hazes. In addition, 3D models have shed light on the complexity of aerosol dynamics in both transiting and directly imaged exoplanets. However, all of these

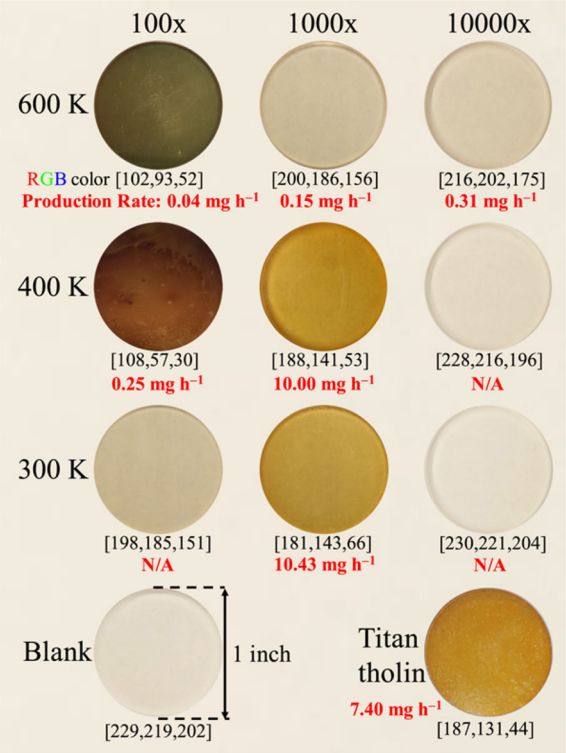

Figure 10. Laboratory hazes made from hydrogen-rich, water-rich, and carbon dioxide-rich atmospheres from 300 to 600 K have a range of colors at visible wavelengths, some unlike those seen in solar system hazes (He et al., 2018a). © AAS. Reproduced with permission.

models contain important assumptions on how aerosols form and evolve, many of which require laboratory experiments to validate. In the next section, we summarize the laboratory studies that have shed light on the potential complexity and diversity of exoplanet aerosols.

5. Insights From Laboratory Studies

The numerous parameterizations made by models in simulating exoplanet aerosols demonstrate the complexity in aerosol formation and evolution in exoplanet atmospheres, complexity that can often only be unveiled by experimental work. The few laboratory exoplanet studies that have been performed thus far have primarily focused on the formation and composition of hazes, as inspired by similar solar system studies such as investigations of Titan's hazes (see Cable et al., 2012, for a review), where haze formation in N_2/CH_4 gas mixtures at < 300 K are considered. These works all involve exposing various gas mixtures in a chamber under vacuum to an energy source, which dissociates and ionizes molecules that can then recombine and grow into larger haze particles. Experiments cover a range of possible atmospheric compositions and temperatures, from those of hot Jupiters to terrestrial planets. Each experimental study is distinct in its choice of temperatures, pressures, gas mixtures, gas flow mechanisms, and irradiation sources and thus drawing larger trends out of their results remains challenging at present. Since the actual atmospheric compositions of exoplanets are currently only loosely constrained, the choice of gas mixtures in many of these experiments is either based on equilibrium model predictions or earlier solar system studies.

Fleury et al. (2019) measured the photochemical output of a simple atmosphere of H_2 with 0.3% CO between temperatures of 600 and 1,500 K exposed to UV (Lyα, 121.6 nm) photons to simulate photochemistry in hot Jupiters. No solid aerosol material was observed for most of their temperature range except at 1,473 K and after very long UV exposure times, though contamination by the ambient atmosphere may have influenced their results. Hörst et al. (2018) and He et al. (2018b, 2020a, 2020b) conducted a series of experiments targeting hazes in mini-Neptunes and rocky planets with temperatures between 300 and 800 K incorporating gas mixtures dominated by H_2, H_2O, and CO_2, with varying amounts of CH_4, CO, NH_3, N_2, and H_2S, as determined by equilibrium chemistry calculations. Both plasma discharge and UV energy sources were used. These experiments showed that increasing H_2 tended to decrease aerosol particle production, while the water-dominated atmospheres actually produced more haze than Titan experiments, suggesting that some temperate terrestrial atmospheres may be extremely hazy (He et al., 2018b; Hörst et al., 2018). The visible appearance of these haze materials are highly diverse, as shown in Figure 10, hinting at a similar diversity in optical properties and compositions. In addition, the inclusion of sulfur species were found to dramatically increase haze production in terrestrial atmospheres and result in organosulfur haze compositions (He et al., 2020b; Vuitton et al., 2021), instead of the elemental sulfur allotropes (e.g., S_8) that have been predicted by some photochemical models (Hu & Seager, 2014; Zahnle et al., 2016). These conclusions are consistent with results from a recent, solar system-focused, experimental study of $N_2/CH_4/H_2S$ gas mixtures (Reed et al., 2020). Furthermore, the gas phase compositions resulting from these mini-Neptune and super-Earth experiments include a substantial abundance of organic species (He et al., 2019), which are then incorporated into the solids (Moran et al., 2020; Vuitton et al., 2021). Moran et al. (2020) demonstrated that oxygen is readily integrated into the haze particles along with nitrogen and carbon when oxygen-carrying gas species are present, which is consistent with previous studies investigating oxidized solar system hazes (Hasenkopf et al., 2010; Hörst & Tolbert, 2014; Trainer et al., 2006; Ugelow et al., 2018). Finally, preliminary characterization of the results of these exoplanet experiments suggests the production of a plethora of prebiotic species, such as amino acids, sugars, and nucleotide bases (Moran et al., 2020).

Critically, exoplanet aerosol experiments have demonstrated that methane, long used in the exoplanet literature as an essential component of haze formation (e.g., Gao et al., 2020; Kawashima & Ikoma, 2018; Morley et al., 2015), is not always needed to produce substantial amounts of haze (Fleury et al., 2019; He et al., 2018b, 2020a, 2020b; Hörst et al., 2018) and that exoplanet hazes likely contain more than just hydrocarbons or by-products of methane photolysis (Moran et al., 2020; Reed et al., 2020; Vuitton et al., 2021). While methane may be an intermediary gas product in some of the experiments that use CO and CO_2 as the primary carbon reservoir (e.g., Fleury et al., 2019), gas phase results show that it is not part of the chemical pathway in all cases, which instead seem more dependent on CO or CO_2 photolysis (He et al., 2019, 2020b). Additionally, photochemical models are typically limited to hydrocarbon species containing up to only five carbon atoms (e.g., G. Arney et al., 2016; Zahnle et al., 2016) or even fewer (Kawashima & Ikoma, 2018), but laboratory work focusing on Titan hazes shows that higher order reactions must be considered to realistically capture aerosol growth (Berry et al., 2019). Taken as a whole, laboratory results have clearly shown that the formation of haze in exoplanet atmospheres is not nearly as simple as that assumed in previous and current models (e.g., Gao et al., 2020), and that a greater appreciation for the chemistry and physics of haze formation at high temperatures is warranted.

Measuring the optical properties of exoplanet aerosol materials allow for a direct link to observations of exoplanet atmospheres and facilitates calculations of aerosol opacity in exoplanet atmospheric models. While refractive indices of a variety of cloud compositions exist (e.g., Wakeford & Sing, 2015), these measurements are not necessarily representative of exoplanet atmospheric conditions. Meanwhile, the most frequently used (e.g., Adams et al., 2019; Gao & Zhang, 2020; Howe & Burrows, 2012; Kawashima & Ikoma, 2018, 2019; Kitzmann & Heng, 2018; Morley et al., 2015; Ohno & Kawashima, 2020; Sing et al., 2013; Sudarsky et al., 2000, 2003; Wakeford & Sing, 2015) set of haze refractive indices in exoplanet investigations have come from the work of Khare et al. (1984), who measured the optical properties of Titan haze analogs ("tholins"). Other less frequently used optical properties include that of soots (Gao et al., 2020; Lavvas & Koskinen, 2017; Morley et al., 2013), also made predominately of hydrocarbons.

Gavilan et al. (2017) and Gavilan et al. (2018) conducted spectroscopy and ellipsometry of solid material produced from essentially Titan-like atmospheres at 300 K, with the addition of CO_2. They found that the aerosols they made were composed of complex organics, with prominent amide, hydroxyl, and carbonyl groups. In addition, the increased oxidation of the hazes were found to strongly increase their absorptivity in the UV and the mid-IR, particularly between 0.13 and 0.3 μm and 6 and 10 μm, as well as blueshift the absorption edge from the visible to the UV, consistent with an early Earth experiment of similar composition (Hasenkopf et al., 2010). In contrast, another similar composition early Earth-focused laboratory study, but which also contained molecular oxygen, found no UV absorption from oxidized hazes, though their experimental setup limited their results to discrete wavelength measurements at 405 and 450 nm (Ugelow et al., 2018). These works constitute the only measurements of spectra or refractive indices of exoplanet haze analogs thus far and likely represent only a tiny fraction of the potential diversity of haze optical properties. Solar system studies have shown that gas composition, pressure, temperature, and energy source all impact the spectral response of the resulting haze particles (Brassé et al., 2015; Imanaka et al., 2004).

The particle size distribution of aerosols offer a glimpse of the microphysical processes involved in aerosol formation and growth. Size distributions measured by He et al. (2018a) and He et al. (2018b, 2020b) for the temperate, high metallicity mini-Neptune and super-Earth atmospheres were unimodal and ranged between 20 and 200 nm for the temperatures, initial gas mixtures, and energy sources considered (Figure 11), which would be able to produce spectral slopes in optical and near-infrared exoplanet transmission spectra. Size distributions were wider for experiments conducted with UV as the energy source than for those conducted with plasma, but the plasma experiments generated more particles. This variance in particle sizes likely results from the difference in energy densities imparted by the UV versus the plasma discharge, but extrapolation to meaningful proxies for diverse stellar types is unclear. High temperatures produced narrower size distributions than cooler temperatures, but the cooler temperatures bore the largest particles. Higher metallicity atmospheres produce both more and larger particles, suggesting that the increased chemical complexity of the atmosphere is able to generate increasingly large, complex molecules. This is further displayed with the addition of sulfur in the form of H_2S to the initial gas mixture, which resulted not only in increased particle production (He et al., 2020b), but also in larger particle effective densities

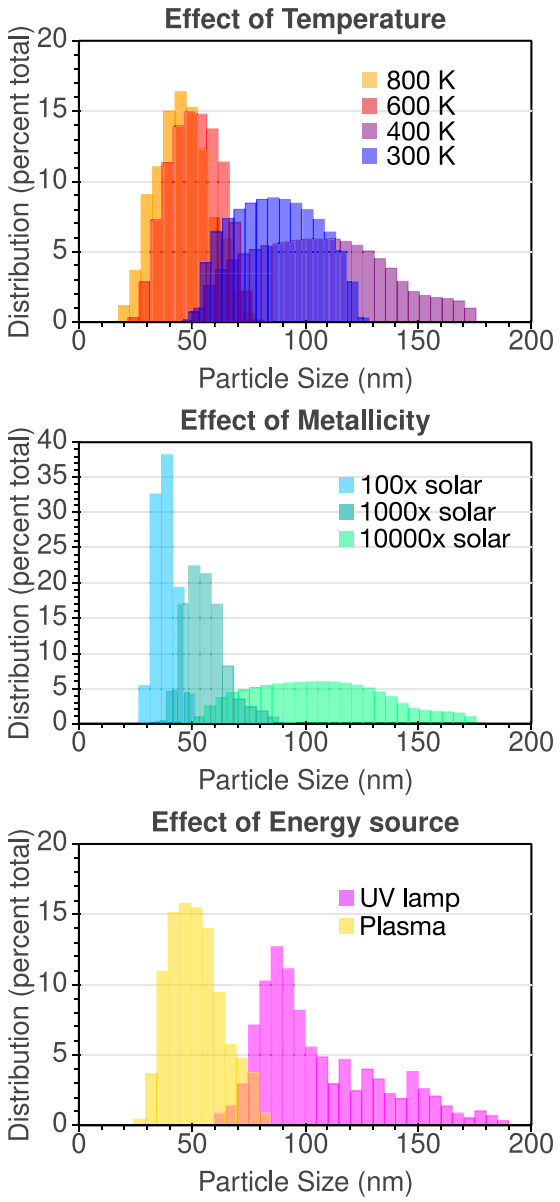

Figure 11. Summary of particle size distributions from the laboratory haze experiments of He et al. (2018a) and He et al. (2018b, 2020b) for 300–800 K (top), 100×–10000× solar metallicity (middle) atmospheres bombarded by UV photons and plasma discharges (bottom).

(Reed et al., 2020). Microscopy of the particles showed that not all of them are spherical, and that some particles clump into more aggregate structures, while some form linear chains. Though this is qualitatively consistent with modeling studies that consider aggregate particles (Adams et al., 2019; G. Arney et al., 2016; Ohno & Kawashima, 2020), the specific growth mechanisms of exoplanet hazes made in the laboratory remains highly uncertain past their initial formation, and the dynamics of haze particles in planetary atmospheres are unlikely to be fully captured by current experimental studies.

6. Summary and Future Prospects

6.1. An Emerging Picture

Aerosols are fundamental components of exoplanet atmospheres across a wide range of temperatures, gravities, compositions, and ages. The provenance and composition of aerosols vary with planetary parameters, leading to differences in the planets' emitted flux, geometric albedo, and transmission spectra. By combining state of the art observations with the latest theoretical models and laboratory data, we can summarize our current understanding of the nature of exoplanet aerosols.

On tidally locked, transiting exoplanets with hydrogen/helium-dominated atmospheres, the longitudinal variation in instellation coupled with atmospheric circulation result in daysides mostly devoid of aerosols for equilibrium temperatures ≥1,000 K, while the nightside and western limb possess optically thick aerosol layers up to ~2,500 K. This spatial inhomogeneity likely generates the observed low dayside albedos and nightside emission fluxes, as well as the westward shifted brightness maxima in optical phase curves. Clouds of silicates and other oxide minerals likely dominate the total aerosol opacity at high temperatures (≥1,500 K), while other types of aerosols, such as sulfide clouds and photochemical hazes, dominate at lower temperatures, causing the observed variations in the spectral slope and the amplitude of molecular features in transmission spectra. Exoplanet photochemical hazes are likely to possess diverse compositions, incorporating atomic species like carbon, oxygen, hydrogen, nitrogen, and sulfur. Clouds on the directly imaged exoplanets discovered to date should be similar in composition to their transiting cousins, though the evolution of these clouds with planetary parameters should be more akin to that on brown dwarfs. A major difference is that the lower gravity of directly imaged exoplanets, as compared to brown dwarfs, leads to the persistence of clouds above the photosphere to lower effective temperatures. The sinking and breaking up of clouds likely trigger the L-T transition in brown dwarfs and directly imaged exoplanets and cause the observed temporal variability in emission.

6.2. Outstanding Questions

While we are now able to construct a coherent picture of the formation and distribution of aerosols in exoplanet atmospheres, there are still many holes in our understanding. Below, we list a number of outstanding questions that will require detailed study in the next decade and beyond:

1. What are the compositions of exoplanet aerosols? Are they mixtures or mostly pure particles?
2. How porous are exoplanet aerosol particles? Are they dense or fluffy aggregates?
3. How do clouds initially form? What is the condensation sequence in exoplanet atmospheres?

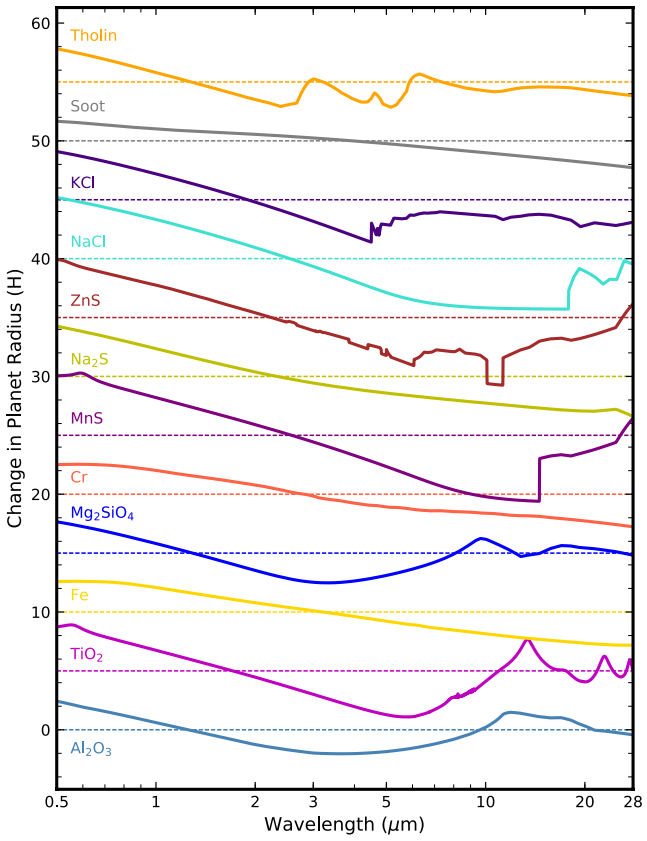

Figure 12. Aerosol transmission spectra for a variety of proposed cloud and haze species computed assuming monodisperse 0.1 μm particles distributed with a constant mass mixing ratio profile in the atmosphere. The spectra are offset for clarity, normalized to the mean transit depth, and shown in planetary scale heights. Optical constants for tholins are taken from Khare et al. (1984); those for soots are from Lavvas and Koskinen (2017); those for KCl, ZnS, Na_2S, MnS, and Cr are from Morley et al. (2012); those for NaCl are from Eldridge and Palik (1985) and Querry (1987); those for Mg_2SiO_4, Fe, and Al_2O_3 are from Wakeford and Sing (2015); and those for TiO_2 are from Posch et al. (2003) and Zeidler et al. (2011). The computed aerosol transmission spectra can be accessed from Gao et al. (2021).

4. What are the major parent molecules and chemical formation pathways of exoplanet photochemical hazes?
5. What physical processes lead to the cloud evolution hypothesized at the brown dwarf L-T transition and how do these change for directly imaged exoplanets?
6. What level of model complexity is necessary to capture the aerosol processes inferred from current and future observations to high fidelity? How should exoplanet aerosols be parameterized in retrievals?
7. How do aerosols respond to variations in planetary, atmospheric, and host star properties? Conversely, how do aerosols affect the composition, thermal structure, and dynamics of exoplanet atmospheres?

6.3. Future Observations

A major goal of future observational investigations of exoplanet aerosols should be to unveil their compositions, which are currently unknown due to the lack of any specific spectral features in current observations. Spectroscopy in the near-to-mid infrared (2–12 μm) with the *James Webb Space Telescope* (*JWST*) will be a critical next step to explore the composition of aerosols and their role in a 3D atmosphere. Many of the proposed aerosol species possess spectral features of their own, which are best measured in the mid-infrared and correspond to the vibrational mode between the dominant atoms in the material (Figure 12). Silicates such as enstatite ($MgSiO_3$) and forsterite (Mg_2SiO_4) have vibrational mode absorption dominated by the Si-O bond which produces prominent absorption at ~10 μm. These vibrational modes have been measured in an array of astrophysical contexts, including in the atmospheres of brown dwarfs (Cushing et al., 2006; Looper et al., 2008). Wakeford and Sing (2015) showed using Mie calculations and the optical properties of various cloud forming species that cloud vibrational-mode absorption features could reach observable amplitudes in exoplanet transmission spectra, though the amplitude is a strong function of the mean particle size and the width and shape of the size distribution, with larger particles and wider size distributions leading to smaller amplitudes. Follow up works investigated additional cloud species (Kitzmann & Heng, 2018; Wakeford et al., 2017b), the impact of different sized particle populations (Mai & Line, 2019), differences in cloud opacity at optical wavelengths (Pinhas & Madhusudhan, 2017), and the impact of taking into account cloud microphysics (Gao et al., 2020; Ormel & Min, 2019).

The observability of cloud spectral features will also depend on whether the cloud particles are pure, as predicted by equilibrium models, or mixtures, as predicted by kinetic cloud models. Helling et al. (2006) showed that consideration of kinetic cloud formation and mixed grains could result in the condensation of cloud species that are suppressed in equilibrium models, such as SiO_2, which exhibit mid-infrared absorption features different from those of enstatite and forsterite, the major silicate clouds predicted by equilibrium models. As such, the extent to which exoplanet cloud formation follows equilibrium or kinetic models may be testable using observations. However, it is not yet known how we can go a step further and, in the event that exoplanet clouds are better reproduced using kinetic models, use observations to differentiate between well-mixed cloud particles, like those modeled in DRIFT, and layered cloud particles, like those modeled in CARMA. In addition, the porosity of the cloud particles will also impact the spectral features, with more aggregate-like particles exhibiting stronger absorption (Samra et al., 2020).

Photochemical hazes may also exhibit spectral features in the near and mid-infrared (Figure 12; also see e.g., Gao & Zhang, 2020; Kawashima & Ikoma, 2018; Wakeford & Sing, 2015), which could shed light on their complex compositions by revealing the types of bonds that they contain. Many organic polymers that

contain mixtures of carbon, oxygen, nitrogen, and hydrogen possess absorption features at wavelengths ~3 and >6 μm (e.g., Laskina et al., 2014; Wang et al., 1998) corresponding to the vibrational modes of the various single and double bonds between C, O, N, and H in various functional groups. However, additional laboratory work is needed to measure the optical constants of exoplanet haze analogs before we can predict the amplitude, width, and exact locations of these features and interpret future exoplanet haze observations.

In addition to composition, *JWST*'s ability to continuously observe targets at high time cadence, as opposed to *Hubble*'s staccato way of observing brought on by its orbit around the Earth, will allow us to probe the east and west limbs separately. This will be critical for deciphering the 3D distribution of aerosols and how asymmetric limbs impact transmission spectra (Fortney et al., 2010; Kempton et al., 2017; Line & Parmentier, 2016; Powell et al., 2018, 2019; von Paris et al., 2016).

An alternative strategy for probing the composition of clouds is to look for the existence or absence of gas species that have been hypothesized to condense. In particular, as several groups of gasses are associated with clouds that condense at similar temperatures on hot Jupiters (e.g., TiO/VO, aluminum, and calcium at the highest temperatures, iron, magnesium, silicon, chromium, and manganese at moderate temperatures, and potassium and sodium at lower temperatures, see Figure 1), measuring the absolute abundances of these gases and their ratios as a function of planetary temperature and gravity could help constrain the condensation sequence in exoplanet atmospheres (Lothringer et al., 2020). However, while many species have been detected for ultra-hot Jupiters (e.g., Ben-Yami et al., 2020; Cabot et al., 2020; Fossati et al., 2010; Haswell et al., 2012; Hoeijmakers et al., 2018; Nugroho et al., 2020; Sing et al., 2019; von Essen et al., 2019; Yan et al., 2019), suggesting largely cloud-free atmospheres, efforts at lower temperatures have yielded mixed results due to controversial detections that are difficult to replicate (e.g., Chen et al., 2018; Cubillos et al., 2020; Espinoza et al., 2019; Gibson et al., 2019, 2017; McGruder et al., 2020; Sedaghati et al., 2017; Seidel et al., 2020; Sing et al., 2015; Vidal-Madjar et al., 2013) and aerosol opacity at optical wavelengths that reduce the amplitudes of atomic and molecular absorption features (Charbonneau et al., 2002; Heng, 2016; Pont et al., 2008; Sing et al., 2016).

Future high spectral resolution observations in the optical and near-ultraviolet by ground-based extremely large telescopes and space-based telescopes will be essential for accurate measurements of heavy element abundances in the upper atmospheres of exoplanets. The potential for constraining cloud and dynamical processes on hot Jupiters with high spectral resolution observations was shown by Ehrenreich et al. (2020), who recently detected the blue-shifted spectral signature of neutral iron on the eastern/dusk limb of the hot Jupiter WASP-76b but not on the western/dawn limb. This is suggestive of iron condensation on the nightside of the planet after it was transported there by eastward winds. In addition, high spectral resolution data can reveal the vertical distribution of aerosol layers, particularly for planets that exhibit low-resolution flat optical or near-infrared transmission spectra, by revealing the cores of spectral lines that extend above the aerosols (Gandhi et al., 2020; Hood et al., 2020; Pino et al., 2018); this was recently attempted for some hot Jupiters (Allart et al., 2020; Sánchez-López et al., 2020).

Future reflected light observations by ground-based extremely large telescopes and space-based telescopes will also allow for probes of exoplanet aerosols. Morley et al. (2015) and Charnay, Meadows, Misra, et al. (2015b) showed that mini-Neptunes like GJ 1214b that possess flat near-infrared transmission spectra may exhibit a variety of optical geometric albedo spectra that are diagnostic of aerosol compositions and particle sizes. Morley et al. (2014b), MacDonald et al. (2018), and Hu (2019) argued that water clouds on cooler giant exoplanets can boost their albedo such that the water and methane absorption bands in the red-optical become much more prominent, aiding retrievals of molecular abundances. However, degeneracies between retrieved cloud properties and molecular abundances could arise unless the planet could be observed at multiple orbital phases (Carrión-González et al., 2020; Damiano & Hu, 2020; Damiano et al., 2020). Sulfur clouds sourced from H_2S photochemistry can also boost planets' red-optical albedos, though their blue-optical and near-UV albedos would be much lower (~0.1; Gao et al., 2017). B. Lacy and Burrows (2020a) revealed that silicate clouds will greatly affect the optical spectrum of current directly imaged exoplanets by increasing their brightness and muting molecular and atomic absorption features. Mayorga et al. (2019) found that optical phases curve amplitudes in the *TESS* bandpass tend to be low (<10 ppm) for a variety of cloud species, but that amplitudes increase toward bluer wavelengths. In addition, measurements of the polarization of reflected light offer unique constraints on the composition, size, shape, and spatial distribution

of aerosol particles (Karalidi et al., 2013; Kopparla et al., 2016; Seager et al., 2000), though claims of detections so far have been controversial (e.g., Berdyugina et al., 2011; Bott et al., 2016; Wiktorowicz et al., 2015). Polarization of the thermal emission of brown dwarfs and directly imaged exoplanets can also constrain aerosol properties and distributions in their atmospheres (e.g., Marley & Sengupta, 2011; Millar-Blanchaer et al., 2020; Sanghavi & Shporer, 2018; Sengupta & Krishan, 2001; Stolker et al., 2017).

Further constraints on aerosol particle sizes and vertical distribution, important for shedding light on a myriad of microphysical and dynamical processes in the atmosphere, can be gleamed from current and future transmission and emission spectroscopy. Small particle sizes ($\leq$0.1 μm) have already been estimated from the spectral slopes in optical transmission spectra (e.g., Lecavelier Des Etangs et al., 2008; Wakeford & Sing, 2015; Wakeford et al., 2017b; I. Wong et al., 2020a), while extensions to the *Spitzer* bandpasses have yielded even tighter size constraints (Benneke et al., 2019a). Observations by *JWST* toward the mid-infrared will enhance these efforts by probing the decrease in opacity of larger particles, while the continuous wavelength coverage will allow for more precise measurements of the shape of the aerosol continuum, which contains information about the vertical distribution of aerosol particle sizes (Mai & Line, 2019). Meanwhile, tracking the wavelength-dependent light curve variability amplitude of L dwarfs has allowed for the measurement of aerosol particle sizes (Lew et al., 2016; Schlawin et al., 2017), since aerosol opacity impacts shorter wavelengths more than longer wavelengths. Future spectroscopic light curve surveys of L-type objects may be able to constrain cloud particle sizes as a function of effective temperature and gravity.

Finally, detections of weather/temporal variability in exoplanet atmospheres impose powerful constraints on dynamical processes therein, including how aerosol microphysics is coupled to the atmospheric circulation pattern. Future long time baseline, high precision observations will shed light on exoplanet weather in the same way rotational light curve measurements have informed our understanding of weather on L and T type objects. Brown dwarf surveys are already delving into cooler temperatures with measurements of variability on Y dwarfs (Cushing et al., 2016; Esplin et al., 2016; Leggett et al., 2016; Rajan et al., 2015) that could be probing patchy sulfide and chloride clouds and the onset of water clouds, thus bridging the gap between brown dwarfs and the giant planets in our own solar system. GCMs have predicted hot Jupiter atmospheric variability due to propagating waves and instabilities on spatial scales of thousands of kilometers to global scales (Dobbs-Dixon et al., 2010; Komacek & Showman, 2020; Lines et al., 2018b; Parmentier et al., 2013), which could lead to temporal variations in the spatial distribution of aerosols. Brightness variability has also been detected on hot Jupiters (Armstrong et al., 2016; Jackson et al., 2019), with interpretations ranging from clouds reacting to changing winds and temperatures to the coupling of atmospheric circulation with the planets' magnetic fields (Rogers, 2017; Rogers & Komacek, 2014).

6.4. Future Modeling Efforts and Laboratory Studies

The anticipated future exoplanet observations will necessitate the development of more sophisticated aerosol models and more detailed laboratory measurements. 3D models of exoplanet atmospheres coupled with kinetic models of aerosol microphysics that include cloud radiative and latent heat feedback will likely be required to fully understand these new observations due to the wavelength- and spatial-dependence of aerosol opacity. In particular, general, flexible models with the ability to simulate multiple particle size modes and multiple aerosol species (e.g., both clouds and hazes) for various background atmospheric compositions and thermal structures will need to be developed to interpret new data from hundreds, perhaps thousands of exoplanets. At the same time, non-hydrostatic atmospheric models capable of resolving and studying moist convection in H/He atmospheres (e.g., Freytag et al., 2010; Ge et al., 2020; Li & Chen, 2019) will allow for more rigorous investigations of cloud particle and condensate vapor transport, cloud formation, and cloud spatial inhomogeneity and temporal variability on giant exoplanets and brown dwarfs. Advances in computational efficiency will be essential for all of these innovations in modeling.

At the same time, intercomparisons between existing models are needed for understanding best modeling practices, evaluating model consistency, and placing interpretations of observations by different models on a more equal footing. As discussed in §4.1.1, comparisons of different treatments of aerosols in retrieval codes have been recently undertaken, showing a sensitivity of aerosol distribution parameters to the modeling assumptions (Barstow, 2020; Mai & Line, 2019). Helling et al. (2008a) compared several more complex aerosol models that were (at the time) used mostly for brown dwarf atmospheres, including DRIFT and the

Ackerman and Marley (2001) model, among others. They found that different models predicted different vertical and particle size distributions of clouds, leading to variations in the predicted brown dwarf near-infrared fluxes of several tens of %. Given the recent proliferation of complex aerosol microphysics models (Table 1), an update to Helling et al. (2008a) is warranted.

For 3D aerosol models, Lines et al. (2019) juxtaposed the advection of cloud distributions computed from DRIFT by a GCM with stationary cloudy atmospheric columns computed by the Ackerman and Marley (2001) model coupled to the same GCM. They found that the predominance of small, high altitude, scattering particles in DRIFT led to a decrease in global temperatures when compared to the larger, lower altitude particles predicted by the Ackerman and Marley (2001) model. Showman et al. (2020) compared several different aerosol treatments in GCMs, including passive tracers and microphysical models, and showed that all models found latitudinal variations in aerosol distributions, but whether the aerosol abundance increased or decreased with latitude is model dependent.

In addition to comparisons of models of similar complexity, lessons learned from complex aerosol models should be incorporated into simpler models used in retrievals and radiative-convective equilibrium models so that they can be made more physical and predictive, while allowing for connections between more subtler microphysical processes and exoplanet observations. Gao et al. (2018) attempted to place the sedimentation efficiency parameter of the Ackerman and Marley (2001) model into the context of microphysical processes by comparing it to CARMA for different planetary and aerosol parameters, but a more systematic and extensive effort is needed.

The measurement of a variety of material properties and aerosol processes through laboratory experiments is critical for interpreting future observations and building more physical models (Fortney et al., 2016). Many of the optical constants currently in use for exoplanet aerosols are decades old and not measured for the composition and temperature regimes of exoplanet atmospheres (Kitzmann & Heng, 2018; Morley et al., 2012; Wakeford & Sing, 2015), and thus updates are needed. This issue is exacerbated in the case of exoplanet hazes, which should have a diverse composition (*§*5). Saturation vapor pressures of certain exoplanet condensates must also be measured, as many are currently estimated from equilibrium chemistry models alone (e.g., Lodders, 2002; Visscher et al., 2010). The same is true for the surface energies of cloud species, which control their nucleation and condensation rates (Gao et al., 2018). In general, condensation in high temperature atmospheres has been rarely explored in the laboratory, and yet knowing which clouds predicted from equilibrium chemistry actually form, how they form, and how different condensates interact with each other (e.g., Helling & Woitke, 2006) are fundamental problems that can only be solved through laboratory experiments. These efforts would also shed light on whether exoplanet cloud particles are crystalline, amorphous, or mixtures of both, whether they are mostly spherical or irregularly shaped (Ohno et al., 2020a; Samra et al., 2020), and whether they are liquid or solid, all of which affect their optical properties and how they couple to the rest of the atmosphere. In addition, laboratory studies have yet to address the interplay of exoplanet clouds and hazes together as an interconnected set of processes, as seen in the solar system (e.g., Andreae & Rosenfeld, 2008; Lavvas et al., 2011a; M. L. Wong et al., 2017). Modeling studies have suggested that photochemical hazes may in some cases act as cloud condensation nuclei (Gao & Benneke, 2018). Preliminary measurements on the solubility of exoplanet haze analogs suggest that some may in fact enable cloud formation of polar condensates (Moran et al., 2020), but verification and generalization of such results are needed. Finally, laboratory efforts will be required to elucidate the photochemical pathways that lead from parent molecules to haze particles for different host star spectra and atmospheric composition. Such an effort will be essential for photochemical modeling of the entire haze formation process.

6.5. Toward Rocky Worlds

The atmospheres of rocky exoplanets are undoubtedly more diverse than the H/He-dominated atmospheres we have explored thus far, suggesting similarly diverse aerosol compositions. Importantly, aerosols in rocky exoplanets serve an additional role in their atmospheres as compared to gas giants: a major control on the surface climate and thus habitability. No molecular features have been robustly observed in rocky exoplanet atmospheres thus far (Burdanov et al., 2019; de Wit et al., 2016, 2018; Diamond-Lowe et al., 2018, 2020a, 2020b; Ducrot et al., 2018; Southworth et al., 2017; Wakeford et al., 2019a; Z. Zhang

et al., 2018), which could be caused by aerosols, a high mean molecular weight atmosphere, a combination thereof (Moran et al., 2018), or a lack of an atmosphere altogether (Kreidberg et al., 2019). We are therefore left with theoretical predictions about the aerosols that may be present in these atmospheres and their impacts.

The hottest rocky exoplanets, with $T_{eq} \geq 1{,}000$ K, are likely to have either no atmosphere or thin atmospheres in equilibrium with a molten surface. These atmospheres would be made of metal oxides like SiO, atomic and molecular oxygen, and atomic magnesium, sodium, iron, and other refractory elements, with abundance ratios dependent on the surface composition (Herbort et al., 2020; Ito et al., 2015; Kite et al., 2016; Miguel et al., 2011). Under these conditions, clouds of oxidized minerals (silicates, corundum, perovskite) and alkali salts, much like those proposed for hot Jupiter atmospheres, are likely to form (Mahapatra et al., 2017; Schaefer & Fegley, 2009; Schaefer et al., 2012).

Rocky exoplanets with temperatures more similar to those in the solar system may possess more familiar aerosols: clouds of water, sulfuric acid, and CO_2 in temperate, oxidizing atmospheres, clouds of hydrocarbons and nitriles, along with organic hazes in cool, reducing atmospheres, and dust elevated into the atmosphere by winds in a variety of atmospheres. Temperate, reducing atmospheres may also host organic hazes (e.g., G. Arney et al., 2016; He et al., 2020b, 2018b; Pavlov et al., 2001; Trainer et al., 2004; Vuitton et al., 2021; Wolf & Toon, 2010), as well as sulfur (S_8) clouds (Hu et al., 2013). Many of these aerosols are highly reflective at optical wavelengths, facilitating future reflected light observations. In particular, the detection of bright sulfuric acid clouds may point to active volcanism and the lack of significant oceans on the surface of temperate rocky exoplanets (Loftus et al., 2019; Misra et al., 2015).

Of particular interest are rocky exoplanets orbiting near the habitable zone of M dwarfs, as they are easier to characterize than those around Sun-like stars due to the more favorable planet-to-star radius ratio and short orbital periods. In regards to possible aerosols in their atmospheres, several differences between these planets and their solar cousins need to be considered: (1) they are most likely tidally locked to their host stars (Kasting et al., 1993), (2) they experience a prolonged period of high instellation during their host stars' pre-main sequence that could desiccate their upper mantles (Luger & Barnes, 2015), and (3) they are subjected to higher fluxes of high energy UV radiation and particle bombardment (France et al., 2013). A consequence of (1) is that a planet with a water ocean could exhibit vigorous convection at the subsolar point, leading to the formation of optically thick water clouds, with its high albedo acting as a stabilizing feedback against increasing instellation (Joshi, 2003; Way et al., 2018; J. Yang et al., 2013). Such cloud patterns are predicted to be sensitive to planet rotation rate (Komacek & Abbot, 2019; J. Yang et al., 2014) and lead to significant muting of molecular features in transmission (Komacek et al., 2020; Suissa et al., 2020). On the other hand, planets dried out from (2) could have clear or dusty atmospheres devoid of water clouds and sulfuric acid clouds (Lincowski et al., 2018; Lustig-Yaeger et al., 2019). Photochemical haze formation due to (3) depends on how different links in the reaction web that leads from simple parent molecules to haze particles react to the spectral energy distributions of M dwarfs. For example, G. Arney et al. (2018) showed that haze formation in temperate, anoxic atmospheres is more efficient for an M dwarf host star compared to a Sun-like host star, particularly in the presence of organic sulfur compounds.

6.6. Exoplanet-Solar System Synergies

Lessons learned from studying aerosols in the atmospheres of solar system worlds have been and will continue to be vital for our understanding of exoplanet aerosols. As shown in this review, the theoretical frameworks used to understand exoplanet aerosols are heavily influenced by what we know of aerosols in the solar system, and in fact several exoplanet aerosol models are derived directly from models of Earth and solar system aerosols (e.g., CARMA and the Ackerman and Marley [2001] model). Laboratory investigations of exoplanet aerosols are even more intimately linked to efforts to experimentally characterize aerosols closer to home, with many deriving from investigations of Titan's haze.

As the quality of exoplanet observations improve in the coming decades, it would be beneficial for analyses of these data to draw inspiration from efforts to analyze solar system data. For example, Irwin et al. (2015) retrieved the imaginary refractive index of the aerosols in Uranus's atmosphere from reflected light spectra in the near-infrared instead of assuming any particular aerosol composition; this strategy may become

necessary for future reflected light and thermal emission observations of exoplanets and brown dwarfs (e.g., Taylor, Parmentier, Line, et al., 2020). In addition, several studies have focused on treating observations of solar system worlds as analogs of future exoplanet data. Mayorga et al. (2016); Dyudina et al. (2016) investigated how the brightness and color of Jupiter and Saturn varied with phase and found significant deviations from a Lambertian model, indicating complex vertical distributions of aerosol particles, with implications for directly imaging exoplanets in reflected light. Simon et al. (2016) and Ge et al. (2019) analyzed rotational light curves of Neptune and Jupiter, respectively, as analogies of brown dwarf light curves, and discovered that light curve variability is controlled largely by discrete features like the Great Red Spot, and that the shape of the light curve depends strongly on the heterogeneous cloud cover and gas opacity. These efforts not only provide cautionary tales of how complicated planetary atmospheres can be, but they also provide benchmarks to which exoplanet aerosol models can be compared. Karalidi et al. (2015), for example, applied their mapping code to both Jupiter and brown dwarfs and were able to retrieve several major atmospheric features on the former object. Similarly, Lupu et al. (2016) applied a multi-aerosol-layer retrieval code to reflected light observations of Jupiter and Saturn in preparation for future observations of wide-orbit giant exoplanets, and were able to retrieve methane mixing ratios and cloud single scattering albedos consistent with the observed values for those two planets. As we increasingly focus on cooler targets like Y dwarfs and temperate exoplanets with temperatures and atmospheric compositions approaching that of our own giant planets (e.g., Benneke et al., 2019b; Dalba & Tamburo, 2019; Morley et al., 2018; Vanderburg et al., 2020), forging connections with solar system science will become ever more important.

As with giant planets, much of our predictions of rocky exoplanet aerosols are based on the examples in our solar system (see §6.5), including sulfuric acid and water clouds on potential Venus-like and Earth-like worlds, respectively (Lincowski et al., 2018; J. Yang et al., 2014). Organic hazes inspired by aerosols that may have existed on the Archean Earth have also been invoked for exoplanets (G. N. Arney et al., 2017). Understanding how these aerosols impact surface temperatures and ionizing radiation fluxes are vital for predictions of habitability (Parisi & Downs, 2004; J. Yang et al., 2013). Recent discoveries of nearby worlds with inferred temperatures much cooler than that of Earth (Damasso et al., 2020; Ribas et al., 2018) have also placed a spotlight on exoplanets that may be similar to the icy satellites and Kuiper Belt objects in the solar system that are enshrouded by organic hazes, such as Titan, Triton, and Pluto. Several studies have investigated the surface temperature (Gilliam & McKay, 2011) and transmission spectra and geometric albedo (Checlair et al., 2016; Robinson et al., 2014) of Titan-like exoplanets, all of which are strongly dependent on the haze properties. In addition, Lora et al. (2018) used a photochemical model to show that haze production on Titan-like exoplanets for host stars of various stellar types may be similar, though the photochemical pathways require further laboratory studies.

As we have shown in this review, the study of aerosols in exoplanet atmospheres touches upon nearly every aspect of exoplanet science and every method that we use to learn about exoplanets. In the years to come, the study of exoplanet aerosols must continue to advance on two major fronts: (1) understanding the composition and spatial and size distributions of exoplanet aerosols to better constrain their influence on exoplanet atmospheres and (2) leveraging the impact of aerosols on observations so that we can constrain the gaseous composition and thermal structure of the atmosphere. These two goals are intertwined since the aerosol composition and distribution depend strongly on the overall atmospheric composition and thermal structure, while constraining these two attributes through observations requires a more detailed picture of the nature of aerosols. Accomplishing these goals will demand greater synergy between observations, modeling, and laboratory work, as well as between the exoplanet, solar system, and Earth sciences. Ultimately, deciphering the aerosol puzzle will get us one step closer to understanding the atmospheres and origins of exoplanets and their potential for life.

Data Availability Statement

Data sets for this research are available in these in-text data citation references: Fu et al. (2017), Crossfield and Kreidberg (2017), Libby-Roberts et al. (2020), Kreidberg et al. (2020), Best et al. (2020a), Parmentier et al. (2016), Beatty et al. (2019), and Gao et al. (2021). The authors are grateful for NASA's Astrophysics Data System, without which this review would not have been possible. The authors thank X. Zhang and J.

J. Fortney for valuable discussions about the structure of this review. The authors also thank I. J. M. Crossfield, L. Kreidberg, Y. Kawashima, and C. He for contributing to the production of several figures.

Acknowledgments
P. Gao acknowledges support from H. Zhang, W. Z. Gao, H. Y. Dai, H. P. Zhang, the 51 Pegasi b Fellowship sponsored by the Heising-Simons Foundation, and NASA through the NASA Hubble Fellowship grant HST-HF2-51456.001-A awarded by the Space Telescope Science Institute, which is operated by the Association of Universities for Research in Astronomy, Inc., for NASA, under contract NAS5-26555. S. E. Moran acknowledges support from NASA Earth and Space Science Fellowship Grant 80NSSC18K1109.

References

Ackerman, A. S., & Marley, M. S. (2001). Precipitating condensation clouds in substellar atmospheres. *The Astrophysical Journal*, *556*(2), 872–884. https://doi.org/10.1086/321540

Adams, D., Gao, P., de Pater, I., & Morley, C. V. (2019). Aggregate hazes in exoplanet atmospheres. *The Astrophysical Journal*, *874*(1), 61. https://doi.org/10.3847/1538-4357/ab074c

Alderson, L., Kirk, J., López-Morales, M., Wheatley, P. J., Skillen, I., Henry, G. W., et al. (2020). LRG-BEASTS: Ground-based detection of sodium and a steep optical slope in the atmosphere of the highly inflated hot-saturn WASP-21b. *Monthly Notices of the Royal Astronomical Society*, *497*(4), 5182–5202. https://doi.org/10.1093/mnras/staa2315

Allard, F., Hauschildt, P. H., Alexander, D. R., & Starrfield, S. (1997). Model atmospheres of very low mass stars and brown dwarfs. *Annual Review of Astronomy and Astrophysics*, *35*(1), 137–177. https://doi.org/10.1146/annurev.astro.35.1.137

Allard, F., Hauschildt, P. H., Alexander, D. R., Tamanai, A., & Schweitzer, A. (2001). The limiting effects of dust in brown dwarf model atmospheres. *The Astrophysical Journal*, *556*(1), 357–372. https://doi.org/10.1086/321547

Allart, R., Pino, L., Lovis, C., Sousa, S. G., Casasayas-Barris, N., Zapatero Osorio, M. R., et al. (2020). *WASP-127b: A misaligned planet with a partly cloudy atmosphere and tenuous sodium signature seen by ESPRESSO*. arXiv e-prints, arXiv:2010.15143.

Alonso, R. (2018). Characterization of exoplanets: Secondary eclipses. In H. J. Deeg& J. A. Belmonte (Eds.), *Handbook of exoplanets* (pp. 1441–1467). Cham: Springer International Publishing. Retrieved from https://doi.org/10.1007/978-3-319-55333-7_40

Andreae, M., & Rosenfeld, D. (2008). Aerosol–cloud–precipitation interactions. Part 1. The nature and sources of cloud-active aerosols. *Earth-Science Reviews*, *89*(1–2), 13–41. https://doi.org/10.1016/j.earscirev.2008.03.001

Angerhausen, D., DeLarme, E., & Morse, J. A. (2015). A comprehensive study of Kepler phase curves and secondary eclipses: Temperatures and albedos of confirmed Kepler giant planets. *Publications of the Astronomical Society of the Pacific*, *127*(957), 1113. https://doi.org/10.1086/683797

Anisimov, M. P., Fominykh, E. G., Akimov, S. V., & Hopke, P. K. (2009). Vapor–gas/liquid nucleation experiments: A review of the challenges. *Journal of Aerosol Science*, *40*(9), 733–746. https://doi.org/10.1016/j.jaerosci.2009.06.002

Apai, D., Karalidi, T., Marley, M. S., Yang, H., Flateau, D., Metchev, S., et al. (2017). Zones, spots, and planetary-scale waves beating in brown dwarf atmospheres. *Science*, *357*(6352), 683–687. https://doi.org/10.1126/science.aam9848

Apai, D., Nardiello, D., & Bedin, L. R. (2021). TESS observations of the Luhman 16 AB brown dwarf system: Rotational periods, lightcurve evolution, and zonal circulation. *The Astrophysical Journal*, *906*(1), 64. https://doi.org/10.3847/1538-4357/abcb97

Apai, D., Radigan, J., Buenzli, E., Burrows, A., Reid, I. N., & Jayawardhana, R. (2013). HST spectral mapping of L/T transition brown dwarfs reveals cloud thickness variations. *The Astrophysical Journal*, *768*(2), 121. https://doi.org/10.1088/0004-637X/768/2/121

Arcangeli, J., Désert, J.-M., Line, M. R., Bean, J. L., Parmentier, V., Stevenson, K. B., et al. (2018). H^- opacity and water dissociation in the dayside atmosphere of the very hot gas giant WASP-18b. *The Astrophysical Journal Letters*, *855*(2), L30. https://doi.org/10.3847/2041-8213/aab272

Arcangeli, J., Désert, J.-M., Parmentier, V., Stevenson, K. B., Bean, J. L., Line, M. R., et al. (2019). Climate of an ultra hot Jupiter. Spectroscopic phase curve of WASP-18b with HST/WFC3. *Astronomy & Astrophysics*, *625*, A136. https://doi.org/10.1051/0004-6361/201834891

Armstrong, D. J., de Mooij, E., Barstow, J., Osborn, H. P., Blake, J., & Saniee, N. F. (2016). Variability in the atmosphere of the hot giant planet HAT-P-7 b. *Nature Astronomy*, *1*, 0004. https://doi.org/10.1038/s41550-016-0004

Arney, G., Domagal-Goldman, S. D., & Meadows, V. S. (2018). Organic haze as a biosignature in anoxic Earth-like atmospheres. *Astrobiology*, *18*(3), 311–329. https://doi.org/10.1089/ast.2017.1666

Arney, G., Domagal-Goldman, S. D., Meadows, V. S., Wolf, E. T., Schwieterman, E., Charnay, B., et al. (2016). The pale orange dot: The spectrum and habitability of hazy Archean Earth. *Astrobiology*, *16*(11), 873–899. https://doi.org/10.1089/ast.2015.1422

Arney, G. N., Meadows, V. S., Domagal-Goldman, S. D., Deming, D., Robinson, T. D., Tovar, G., et al. (2017). Pale orange dots: The impact of organic haze on the habitability and detectability of Earthlike exoplanets. *The Astrophysical Journal*, *836*(1), 49. https://doi.org/10.3847/1538-4357/836/1/49

Artigau, É. (2018). Variability of brown dwarfs. In H. J. Deeg& J. A. Belmonte (Eds.), *Handbook of exoplanets* (pp. 555–573). Cham: Springer International Publishing. Retrieved from https://doi.org/10.1007/978-3-319-55333-7_94

Artigau, É., Bouchard, S., Doyon, R., & Lafrenière, D. (2009). Photometric variability of the T2.5 brown dwarf SIMP J013656.5+093347: Evidence for evolving weather patterns. *The Astrophysical Journal*, *701*(2), 1534–1539. https://doi.org/10.1088/0004-637X/701/2/1534

Bailey, J. (2014). The Dawes review 3: The atmospheres of extrasolar planets and brown dwarfs. *Publications of the Astronomical Society of Australia*, *31*, e043. https://doi.org/10.1017/pasa.2014.38

Baines, K. H., Delitsky, M. L., Momary, T. W., Brown, R. H., Buratti, B. J., Clark, R. N., & Nicholson, P. D. (2009). Storm clouds on Saturn: Lightning-induced chemistry and associated materials consistent with Cassini/VIMS spectra. *Planetary and Space Science*, *57*(14), 1650–1658. https://doi.org/10.1016/j.pss.2009.06.025

Baraffe, I., Chabrier, G., Barman, T. S., Allard, F., & Hauschildt, P. H. (2003). Evolutionary models for cool brown dwarfs and extrasolar giant planets. The case of HD 209458. *Astronomy & Astrophysics*, *402*, 701–712. https://doi.org/10.1051/0004-6361:20030252

Barman, T. S., Hauschildt, P. H., & Allard, F. (2001). Irradiated planets. *The Astrophysical Journal*, *556*(2), 885–895. https://doi.org/10.1086/321610

Barman, T. S., Macintosh, B., Konopacky, Q. M., & Marois, C. (2011). Clouds and chemistry in the atmosphere of extrasolar planet HR8799b. *The Astrophysical Journal*, *733*(1), 65. https://doi.org/10.1088/0004-637X/733/1/65

Barstow, J. K. (2020). *Unveiling cloudy exoplanets: The influence of cloud model choices on retrieval solutions*. arXiv e-prints, arXiv:2002.02945.

Barstow, J. K., Aigrain, S., Irwin, P. G. J., Hackler, T., Fletcher, L. N., Lee, J. M., & Gibson, N. P. (2014). Clouds on the hot Jupiter HD189733b: Constraints from the reflection spectrum. *The Astrophysical Journal*, *786*(2), 154. https://doi.org/10.1088/0004-637X/786/2/154

Barstow, J. K., Aigrain, S., Irwin, P. G. J., & Sing, D. K. (2017). A consistent retrieval analysis of 10 hot Jupiters observed in transmission. *The Astrophysical Journal*, *834*(1), 50. https://doi.org/10.3847/1538-4357/834/1/50

Barstow, J. K., Changeat, Q., Garland, R., Line, M. R., Rocchetto, M., & Waldmann, I. P. (2020). A comparison of exoplanet spectroscopic retrieval tools. *Monthly Notices of the Royal Astronomical Society*, *493*(4), 4884–4909. https://doi.org/10.1093/mnras/staa548

Bean, J. L., Désert, J.-M., Kabath, P., Stalder, B., Seager, S., Miller-Ricci Kempton, E., et al. (2011). The optical and near-infrared transmission spectrum of the super-Earth GJ 1214b: Further evidence for a metal-rich atmosphere. *The Astrophysical Journal*, *743*(1), 92. https://doi.org/10.1088/0004-637X/743/1/92

Bean, J. L., Miller-Ricci Kempton, E., & Homeier, D. (2010). A ground-based transmission spectrum of the super-Earth exoplanet GJ 1214b. *Nature*, *468*(7324), 669–672. https://doi.org/10.1038/nature09596

Beatty, T. G., Marley, M. S., Gaudi, B. S., Colón, K. D., Fortney, J. J., & Showman, A. P. (2019). Spitzer phase curves of KELT-1b and the signatures of nightside clouds in thermal phase observations. *The Astronomical Journal*, *158*(4), 166. https://doi.org/10.3847/1538-3881/ab33fc

Beatty, T. G., Wong, I., Fetherolf, T., Line, M. R., Shporer, A., Stassun, K. G., et al. (2020). *The TESS phase curve of KELT-1b suggests a high dayside albedo*. arXiv e-prints, arXiv:2006.10292.

Bell, T. J., Nikolov, N., Cowan, N. B., Barstow, J. K., Barman, T. S., Crossfield, I. J. M., et al. (2017). The very low albedo of WASP-12b from spectral eclipse observations with hubble. *The Astrophysical Journal Letters*, *847*(1), L2. https://doi.org/10.3847/2041-8213/aa876c

Benneke, B., Knutson, H. A., Lothringer, J., Crossfield, I. J. M., Moses, J. I., Morley, C., et al. (2019a). A sub-Neptune exoplanet with a low-metallicity methane-depleted atmosphere and Mie-scattering clouds. *Nature Astronomy*, *3*(9), 813–821. https://doi.org/10.1038/s41550-019-0800-5

Benneke, B., & Seager, S. (2012). Atmospheric retrieval for super-Earths: Uniquely constraining the atmospheric composition with transmission spectroscopy. *The Astrophysical Journal*, *753*(2), 100. https://doi.org/10.1088/0004-637X/753/2/100

Benneke, B., Wong, I., Piaulet, C., Knutson, H. A., Lothringer, J., Morley, C. V., et al. (2019b). Water vapor and clouds on the habitable-zone sub-Neptune exoplanet K2-18b. *The Astrophysical Journal Letters*, *887*(1), L14. https://doi.org/10.3847/2041-8213/ab59dc

Ben-Yami, M., Madhusudhan, N., Cabot, S. H. C., Constantinou, S., Piette, A., Gandhi, S., & Welbanks, L. (2020). *Neutral Cr and V in the atmosphere of ultra hot Jupiter WASP-121 b*. arXiv e-prints, arXiv:2006.05995.

Berdyugina, S. V., Berdyugin, A. V., Fluri, D. M., & Piirola, V. (2011). Polarized reflected light from the exoplanet HD189733b: First multicolor observations and confirmation of detection. *The Astrophysical Journal Letters*, *728*(1), L6. https://doi.org/10.1088/2041-8205/728/1/L6

Berry, J. L., Ugelow, M. S., Tolbert, M. A., & Browne, E. C. (2019). The influence of gas-phase chemistry on organic haze formation. *The Astrophysical Journal Letters*, *885*(1), L6. https://doi.org/10.3847/2041-8213/ab4b5b

Best, W. M. J., Dupuy, T. J., Liu, M. C., Siverd, R. J., & Zhang, Z. (2020a). *The UltracoolSheet: Photometry, astrometry, spectroscopy, and multiplicity for 3000+ ultracool dwarfs and imaged exoplanets*. Zenodo. Retrieved from https://doi.org/10.5281/zenodo.4169085

Best, W. M. J., Liu, M. C., Magnier, E. A., & Dupuy, T. J. (2020b). The Hawaii Infrared Parallax Program. IV. A Comprehensive Parallax Survey of L0-T8 Dwarfs with UKIRT. *The Astronomical Journal*, *159*(6), 257. https://doi.org/10.3847/1538-3881/ab84f4

Best, W. M. J., Magnier, E. A., Liu, M. C., Aller, K. M., Zhang, Z., Burgett, W. S., et al. (2018). Photometry and Proper Motions of M, L, and T Dwarfs from the Pan-STARRS1 3π Survey. *The Astrophysical Journal Supplement Series*, *234*(1), 1. https://doi.org/10.3847/1538-4365/aa9982

Biller, B. (2017). The time domain for brown dwarfs and directly imaged giant exoplanets: The power of variability monitoring. *The Astronomical Review*, *13*(1), 1–27. https://doi.org/10.1080/21672857.2017.1303105

Biller, B. A., & Bonnefoy, M. (2017). Exoplanet atmosphere measurements from direct imaging. In H. J. Deeg & J. A. Belmonte (Eds.), *Handbook of exoplanets* (pp. 1–28). Cham: Springer International Publishing. https://doi.org/10.1007/978-3-319-30648-3_101-1

Biller, B. A., Crossfield, I. J. M., Mancini, L., Ciceri, S., Southworth, J., Kopytova, T. G., et al. (2013). Weather on the nearest brown dwarfs: Resolved simultaneous multi-wavelength variability monitoring of WISE J104915.57-531906.1AB. *The Astrophysical Journal Letters*, *778*(1), L10. https://doi.org/10.1088/2041-8205/778/1/L10

Biller, B. A., Vos, J., Bonavita, M., Buenzli, E., Baxter, C., Crossfield, I. J. M., et al. (2015). Variability in a young, L/T transition planetary-mass object. *The Astrophysical Journal Letters*, *813*(2), L23. https://doi.org/10.1088/2041-8205/813/2/L23

Biller, B. A., Vos, J., Buenzli, E., Allers, K., Bonnefoy, M., Charnay, B., et al. (2018). Simultaneous multiwavelength variability characterization of the free-floating planetary-mass object PSO J318.5-22. *The Astronomical Journal*, *155*(2), 95. https://doi.org/10.3847/1538-3881/aaa5a6

Birkby, J. L., de Kok, R. J., Brogi, M., Schwarz, H., & Snellen, I. A. G. (2017). Discovery of water at high spectral resolution in the atmosphere of 51 Peg b. *The Astronomical Journal*, *153*(3), 138. https://doi.org/10.3847/1538-3881/aa5c87

Bjoraker, G. L., Wong, M. H., de Pater, I., Hewagama, T., Ádámkovics, M., & Orton, G. S. (2018). The gas composition and deep cloud structure of Jupiter's great red spot. *The Astronomical Journal*, *156*(3), 101. https://doi.org/10.3847/1538-3881/aad186

Bolton, S. J., Adriani, A., Adumitroaie, V., Allison, M., Anderson, J., Atreya, S., et al. (2017). Jupiter's interior and deep atmosphere: The initial pole-to-pole passes with the Juno spacecraft. *Science*, *356*(6340), 821–825. https://doi.org/10.1126/science.aal2108

Bonnefoy, M., Boccaletti, A., Lagrange, A. M., Allard, F., Mordasini, C., Beust, H., et al. (2013). The near-infrared spectral energy distribution of β Pictoris b. *Astronomy & Astrophysics*, *555*, A107. https://doi.org/10.1051/0004-6361/201220838

Bonnefoy, M., Zurlo, A., Baudino, J. L., Lucas, P., Mesa, D., Maire, A. L., et al. (2016). First light of the VLT planet finder SPHERE. IV. Physical and chemical properties of the planets around HR8799. *Astronomy & Astrophysics*, *587*, A58. https://doi.org/10.1051/0004-6361/201526906

Borucki, W. J., Koch, D., Jenkins, J., Sasselov, D., Gilliland, R., Batalha, N., et al. (2009). Kepler's optical phase curve of the exoplanet HAT-P-7b. *Science*, *325*(5941), 709. https://doi.org/10.1126/science.1178312

Bott, K., Bailey, J., Kedziora-Chudczer, L., Cotton, D. V., Lucas, P. W., Marshall, J. P., & Hough, J. H. (2016). The polarization of HD 189733. *Monthly Notices of the Royal Astronomical Society*, *459*(1), L109–L113. https://doi.org/10.1093/mnrasl/slw046

Bourrier, V., Kitzmann, D., Kuntzer, T., Nascimbeni, V., Lendl, M., Lavie, B., et al. (2020). Optical phase curve of the ultra-hot Jupiter WASP-121b. *Astronomy & Astrophysics*, *637*, A36. https://doi.org/10.1051/0004-6361/201936647

Bowler, B. P. (2016). Imaging extrasolar giant planets. *Publications of the Astronomical Society of the Pacific*, *128*(968), 102001. https://doi.org/10.1088/1538-3873/128/968/102001

Bowler, B. P., Zhou, Y., Morley, C. V., Kataria, T., Bryan, M. L., Benneke, B., & Batygin, K. (2020). Strong Near-infrared Spectral Variability of the Young Cloudy L Dwarf Companion VHS J1256-1257 b. *The Astrophysical Journal Letters*, *893*(2), L30. https://doi.org/10.3847/2041-8213/ab8197

Brassé, C., Muñoz, O., Coll, P., & Raulin, F. (2015). Optical constants of Titan aerosols and their tholins analogs: Experimental results and modeling/observational data. *Planetary and Space Science*, *109*, 159–174. https://doi.org/10.1016/j.pss.2015.02.012

Brogi, M., Snellen, I. A. G., de Kok, R. J., Albrecht, S., Birkby, J., & de Mooij, E. J. W. (2012). The signature of orbital motion from the dayside of the planet τ Boötis b. *Nature*, *486*(7404), 502–504. https://doi.org/10.1038/nature11161

Brooke, T., Knacke, R., Encrenaz, T., Drossart, P., Crisp, D., & Feuchtgruber, H. (1998). Models of the ISO 3-μm reflection spectrum of Jupiter. *Icarus*, *136*(1), 1–13. https://doi.org/10.1006/icar.1998.6013

Brown, M. E., Bouchez, A. H., & Griffith, C. A. (2002). Direct detection of variable tropospheric clouds near Titan's south pole. *Nature*, *420*(6917), 795–797. https://doi.org/10.1038/nature01302

Bruno, G., Lewis, N. K., Stevenson, K. B., Filippazzo, J., Hill, M., Fraine, J. D., et al. (2018). A comparative study of WASP-67 b and HAT-P-38 b from WFC3 data. *The Astronomical Journal*, *155*(2), 55. https://doi.org/10.3847/1538-3881/aaa0c7

Buenzli, E., Apai, D., Radigan, J., Reid, I. N., & Flateau, D. (2014). Brown dwarf photospheres are patchy: A Hubble Space Telescope near-infrared spectroscopic survey finds frequent low-level variability. *The Astrophysical Journal*, *782*(2), 77. https://doi.org/10.1088/0004-637X/782/2/77

Buenzli, E., Marley, M. S., Apai, D., Saumon, D., Biller, B. A., Crossfield, I. J. M., & Radigan, J. (2015a). Cloud structure of the nearest brown dwarfs. II. High-amplitude variability for Luhman 16 A and B in and out of the 0.99 μm FeH feature. *The Astrophysical Journal*, *812*(2), 163. https://doi.org/10.1088/0004-637X/812/2/163

Buenzli, E., Saumon, D., Marley, M. S., Apai, D., Radigan, J., Bedin, L. R., et al. (2015b). Cloud structure of the nearest brown dwarfs: Spectroscopic variability of Luhman 16AB from the Hubble Space Telescope. *The Astrophysical Journal*, *798*(2), 127. https://doi.org/10.1088/0004-637X/798/2/127

Burdanov, A. Y., Lederer, S. M., Gillon, M., Delrez, L., Ducrot, E., de Wit, J., et al. (2019). Ground-based follow-up observations of TRAPPIST-1 transits in the near-infrared. *Monthly Notices of the Royal Astronomical Society*, *487*(2), 1634–1652. https://doi.org/10.1093/mnras/stz1375

Burgasser, A. J., Gillon, M., Faherty, J. K., Radigan, J., Triaud, A. H. M. J., Plavchan, P., et al. (2014). A monitoring campaign for Luhman 16AB. I. Detection of resolved near-infrared spectroscopic variability. *The Astrophysical Journal*, *785*(1), 48. https://doi.org/10.1088/0004-637X/785/1/48

Burgasser, A. J., Marley, M. S., Ackerman, A. S., Saumon, D., Lodders, K., Dahn, C. C., et al. (2002). Evidence of cloud disruption in the L/T dwarf transition. *The Astrophysical Journal Letters*, *571*(2), L151–L154. https://doi.org/10.1086/341343

Burningham, B., Marley, M. S., Line, M. R., Lupu, R., Visscher, C., Morley, C. V., et al. (2017). Retrieval of atmospheric properties of cloudy L dwarfs. *Monthly Notices of the Royal Astronomical Society*, *470*(1), 1177–1197. https://doi.org/10.1093/mnras/stx1246

Burrows, A., Burgasser, A. J., Kirkpatrick, J. D., Liebert, J., Milsom, J. A., Sudarsky, D., & Hubeny, I. (2002). Theoretical spectral models of T dwarfs at short wavelengths and their comparison with data. *The Astrophysical Journal*, *573*(1), 394–417. https://doi.org/10.1086/340584

Burrows, A., Marley, M., Hubbard, W. B., Lunine, J. I., Guillot, T., Saumon, D., et al. (1997). A nongray theory of extrasolar giant planets and brown dwarfs. *The Astrophysical Journal*, *491*(2), 856–875. https://doi.org/10.1086/305002

Burrows, A., Marley, M. S., & Sharp, C. M. (2000). The near-infrared and optical spectra of methane dwarfs and brown dwarfs. *The Astrophysical Journal*, *531*(1), 438–446. https://doi.org/10.1086/308462

Burrows, A., & Sharp, C. M. (1999). Chemical equilibrium abundances in brown dwarf and extrasolar giant planet atmospheres. *The Astrophysical Journal*, *512*(2), 843–863. https://doi.org/10.1086/306811

Burrows, A., Sudarsky, D., & Lunine, J. I. (2003). Beyond the T dwarfs: Theoretical spectra, colors, and detectability of the coolest brown dwarfs. *The Astrophysical Journal*, *596*(1), 587–596. https://doi.org/10.1086/377709

Cable, M. L., Hörst, S. M., Hodyss, R., Beauchamp, P., Smith, M. A., & Willis, P. (2012). Titan tholins: Simulating Titan organic chemistry in the Cassini-Huygens era. *Chemical Reviews*, *112*(3), 1882–1909. https://doi.org/10.1021/cr200221x

Cabot, S. H. C., Madhusudhan, N., Welbanks, L., Piette, A., & Gandhi, S. (2020). Detection of neutral atomic species in the ultra-hot Jupiter WASP-121b. *Monthly Notices of the Royal Astronomical Society*, *494*(1), 363–377. https://doi.org/10.1093/mnras/staa748

Carlson, B. E., Rossow, W. B., & Orton, G. S. (1988). Cloud microphysics of the giant planets. *Journal of the Atmospheric Sciences*, *45*(14), 2066–2081.

Carrión-González, Ó., García Muñoz, A., Cabrera, J., Csizmadia, S., Santos, N. C., & Rauer, H. (2020). Directly imaged exoplanets in reflected starlight: The importance of knowing the planet radius. *Astronomy & Astrophysics*, *640*, A136. https://doi.org/10.1051/0004-6361/202038101

Chabrier, G., Baraffe, I., Allard, F., & Hauschildt, P. (2000). Evolutionary models for very low-mass stars and brown dwarfs with dusty atmospheres. *The Astrophysical Journal*, *542*(1), 464–472. https://doi.org/10.1086/309513

Chachan, Y., Jontof-Hutter, D., Knutson, H. A., Adams, D., Gao, P., Benneke, B., et al. (2020). A featureless infrared transmission spectrum for the super-puff planet Kepler-79d. *The Astronomical Journal*, *160*(5), 201. https://doi.org/10.3847/1538-3881/abb23a

Chachan, Y., Knutson, H. A., Gao, P., Kataria, T., Wong, I., Henry, G. W., et al. (2019). A Hubble PanCET Study of HAT-P-11b: A cloudy Neptune with a low atmospheric metallicity. *The Astronomical Journal*, *158*(6), 244. https://doi.org/10.3847/1538-3881/ab4e9a

Charbonneau, D., Allen, L. E., Megeath, S. T., Torres, G., Alonso, R., Brown, T. M., et al. (2005). Detection of thermal emission from an extrasolar planet. *The Astrophysical Journal*, *626*(1), 523–529. https://doi.org/10.1086/429991

Charbonneau, D., Brown, T. M., Noyes, R. W., & Gilliland, R. L. (2002). Detection of an extrasolar planet atmosphere. *The Astrophysical Journal*, *568*(1), 377–384. https://doi.org/10.1086/338770

Charbonneau, D., Knutson, H. A., Barman, T., Allen, L. E., Mayor, M., Megeath, S. T., et al. (2008). The broadband infrared emission spectrum of the exoplanet HD 189733b. *The Astrophysical Journal*, *686*(2), 1341–1348. https://doi.org/10.1086/591635

Charnay, B., Bézard, B., Baudino, J. L., Bonnefoy, M., Boccaletti, A., & Galicher, R. (2018). A self-consistent cloud model for brown dwarfs and young giant exoplanets: Comparison with photometric and spectroscopic observations. *The Astrophysical Journal*, *854*(2), 172. https://doi.org/10.3847/1538-4357/aaac7d

Charnay, B., Meadows, V., & Leconte, J. (2015a). 3D modeling of GJ1214b's atmosphere: Vertical mixing driven by an anti-Hadley circulation. *The Astrophysical Journal*, *813*, 15. https://doi.org/10.1088/0004-637X/813/1/15

Charnay, B., Meadows, V., Misra, A., Leconte, J., & Arney, G. (2015b). 3D modeling of GJ1214b's atmosphere: Formation of inhomogeneous high clouds and observational implications. *The Astrophysical Journal Letters*, *813*, L1. https://doi.org/10.1088/2041-8205/813/1/L1

Checlair, J., McKay, C. P., & Imanaka, H. (2016). Titan-like exoplanets: Variations in geometric albedo and effective transit height with haze production rate. *Planetary and Space Science*, *129*, 1–12. https://doi.org/10.1016/j.pss.2016.03.012

Chen, G., Pallé, E., Parviainen, H., Wang, H., van Boekel, R., Murgas, F., et al. (2021). An enhanced slope in the transmission spectrum of the hot Jupiter WASP-104b. *Monthly Notices of the Royal Astronomical Society*, *500*(4), 5420–5435. https://doi.org/10.1093/mnras/staa3555

Chen, G., Pallé, E., Welbanks, L., Prieto-Arranz, J., Madhusudhan, N., Gandhi, S., et al. (2018). The GTC exoplanet transit spectroscopy survey. IX. Detection of haze, Na, K, and Li in the super-Neptune WASP-127b. *Astronomy & Astrophysics*, *616*, A145. https://doi.org/10.1051/0004-6361/201833033

Cooper, C. S., Sudarsky, D., Milsom, J. A., Lunine, J. I., & Burrows, A. (2003). Modeling the formation of clouds in brown dwarf atmospheres. *The Astrophysical Journal*, *586*(2), 1320–1337. https://doi.org/10.1086/367763

Coughlin, J. L., & López-Morales, M. (2012). A uniform search for secondary eclipses of hot Jupiters in Kepler Q2 light curves. *The Astronomical Journal*, *143*(2), 39. https://doi.org/10.1088/0004-6256/143/2/39

Cowan, N. B., Machalek, P., Croll, B., Shekhtman, L. M., Burrows, A., Deming, D., et al. (2012). Thermal phase variations of WASP-12b: Defying predictions. *The Astrophysical Journal*, *747*(1), 82. https://doi.org/10.1088/0004-637X/747/1/82

Crossfield, I. J. M., Barman, T., Hansen, B. M. S., & Howard, A. W. (2013). Warm ice giant GJ 3470b. I. A flat transmission spectrum indicates a hazy, low-methane, and/or metal-rich atmosphere. *Astronomy & Astrophysics*, *559*, A33. https://doi.org/10.1051/0004-6361/201322278

Crossfield, I. J. M., Biller, B., Schlieder, J. E., Deacon, N. R., Bonnefoy, M., Homeier, D., et al. (2014). A global cloud map of the nearest known brown dwarf. *Nature*, *505*(7485), 654–656. https://doi.org/10.1038/nature12955

Crossfield, I. J. M., Hansen, B. M. S., Harrington, J., Cho, J. Y. K., Deming, D., Menou, K., & Seager, S. (2010). A new 24 μm phase curve for υ Andromedae b. *The Astrophysical Journal*, *723*(2), 1436–1446. https://doi.org/10.1088/0004-637X/723/2/1436

Crossfield, I. J. M., & Kreidberg, L. (2017). Trends in atmospheric properties of Neptune-size exoplanets. *The Astronomical Journal*, *154*, 261. https://doi.org/10.3847/1538-3881/aa9279

Cubillos, P. E., Fossati, L., Koskinen, T., Young, M. E., Salz, M., France, K., et al. (2020). Near-ultraviolet Transmission Spectroscopy of HD 209458b: Evidence of Ionized Iron Beyond the Planetary Roche Lobe. *The Astronomical Journal*, *159*(3), 111. https://doi.org/10.3847/1538-3881/ab6a0b

Currie, T., Burrows, A., Itoh, Y., Matsumura, S., Fukagawa, M., Apai, D., et al. (2011). A combined Subaru/VLT/MMT 1-5 μm study of planets orbiting HR 8799: Implications for atmospheric properties, masses, and formation. *The Astrophysical Journal*, *729*(2), 128. https://doi.org/10.1088/0004-637X/729/2/128

Cushing, M. C., Hardegree-Ullman, K. K., Trucks, J. L., Morley, C. V., Gizis, J. E., Marley, M. S., et al. (2016). The first detection of photometric variability in a Y dwarf: WISE J140518.39+553421.3. *The Astrophysical Journal*, *823*(2), 152. https://doi.org/10.3847/0004-637X/823/2/152

Cushing, M. C., Kirkpatrick, J. D., Gelino, C. R., Griffith, R. L., Skrutskie, M. F., Mainzer, A., et al. (2011). The discovery of Y dwarfs using data from the wide-field infrared survey explorer (WISE). *The Astrophysical Journal*, *743*(1), 50. https://doi.org/10.1088/0004-637X/743/1/50

Cushing, M. C., Roellig, T. L., Marley, M. S., Saumon, D., Leggett, S. K., Kirkpatrick, J. D., et al. (2006). A Spitzer Infrared Spectrograph spectral sequence of M, L, and T Dwarfs. *The Astrophysical Journal*, *648*(1), 614–628. https://doi.org/10.1086/505637

Dai, F., Winn, J. N., Yu, L., & Albrecht, S. (2017). The stellar obliquity, planet mass, and very low albedo of Qatar-2 from K2 photometry. *The Astronomical Journal*, *153*(1), 40. https://doi.org/10.3847/1538-3881/153/1/40

Dalba, P. A., & Tamburo, P. (2019). Spitzer detection of the transiting Jupiter-analog exoplanet Kepler-167e. *The Astrophysical Journal Letters*, *873*(2), L17. https://doi.org/10.3847/2041-8213/ab0bb4

Damasso, M., Del Sordo, F., Anglada-Escudé, G., Giacobbe, P., Sozzetti, A., Morbidelli, A., et al. (2020). A low-mass planet candidate orbiting Proxima Centauri at a distance of 1.5 AU. *Science Advances*, *6*(3), eaax7467. https://doi.org/10.1126/sciadv.aax7467

Damiano, M., & Hu, R. (2020). EXOREL$^{\mathfrak{R}}$: A Bayesian inverse retrieval framework for exoplanetary reflected light spectra. *The Astronomical Journal*, *159*(4), 175. https://doi.org/10.3847/1538-3881/ab79a5

Damiano, M., Hu, R., & Hildebrandt, S. R. (2020). Multi-orbital-phase and multiband characterization of exoplanetary atmospheres with reflected light spectra. *The Astronomical Journal*, *160*(5), 206. https://doi.org/10.3847/1538-3881/abb76a

Delorme, P., Schmidt, T., Bonnefoy, M., Desidera, S., Ginski, C., Charnay, B., et al. (2017). In-depth study of moderately young but extremely red, very dusty substellar companion HD 206893B. *Astronomy & Astrophysics*, *608*, A79. https://doi.org/10.1051/0004-6361/201731145

Deming, D., Harrington, J., Laughlin, G., Seager, S., Navarro, S. B., Bowman, W. C., & Horning, K. (2007). Spitzer transit and secondary eclipse photometry of GJ 436b. *The Astrophysical Journal Letters*, *667*(2), L199–L202. https://doi.org/10.1086/522496

Deming, D., Seager, S., Richardson, L. J., & Harrington, J. (2005). Infrared radiation from an extrasolar planet. *Nature*, *434*(7034), 740–743. https://doi.org/10.1038/nature03507

Deming, D., Wilkins, A., McCullough, P., Burrows, A., Fortney, J. J., Agol, E., et al. (2013). Infrared transmission spectroscopy of the exoplanets HD 209458b and XO-1b using the Wide Field Camera-3 on the Hubble Space Telescope. *The Astrophysical Journal*, *774*(2), 95. https://doi.org/10.1088/0004-637X/774/2/95

Demory, B.-O. (2014). The albedos of Kepler's close-in super-Earths. *The Astrophysical Journal Letters*, *789*(1), L20. https://doi.org/10.1088/2041-8205/789/1/L20

Demory, B.-O., de Wit, J., Lewis, N., Fortney, J., Zsom, A., Seager, S., et al. (2013). Inference of inhomogeneous clouds in an exoplanet atmosphere. *The Astrophysical Journal Letters*, *776*, L25. https://doi.org/10.1088/2041-8205/776/2/L25

Demory, B.-O., Gillon, M., de Wit, J., Madhusudhan, N., Bolmont, E., Heng, K., et al. (2016). A map of the large day-night temperature gradient of a super-Earth exoplanet. *Nature*, *532*(7598), 207–209. https://doi.org/10.1038/nature17169

Demory, B.-O., Seager, S., Madhusudhan, N., Kjeldsen, H., Christensen-Dalsgaard, J., Gillon, M., et al. (2011). The high albedo of the hot Jupiter Kepler-7 b. *The Astrophysical Journal Letters*, *735*(1), L12. https://doi.org/10.1088/2041-8205/735/1/L12

de Pater, I., Fletcher, L. N., Luszcz-Cook, S., DeBoer, D., Butler, B., Hammel, H. B., et al. (2014). Neptune's global circulation deduced from multi-wavelength observations. *Icarus*, *237*, 211–238. https://doi.org/10.1016/j.icarus.2014.02.030

Désert, J.-M., Bean, J., Miller-Ricci Kempton, E., Berta, Z. K., Charbonneau, D., Irwin, J., et al. (2011). Observational evidence for a metal-rich atmosphere on the super-Earth GJ1214b. *The Astrophysical Journal Letters*, *731*(2), L40. https://doi.org/10.1088/2041-8205/731/2/L40

de Wit, J., Gillon, M., Demory, B. O., & Seager, S. (2012). Towards consistent mapping of distant worlds: Secondary-eclipse scanning of the exoplanet HD 189733b. *Astronomy & Astrophysics*, *548*, A128. https://doi.org/10.1051/0004-6361/201219060

de Wit, J., Wakeford, H. R., Gillon, M., Lewis, N. K., Valenti, J. A., Demory, B.-O., et al. (2016). A combined transmission spectrum of the Earth-sized exoplanets TRAPPIST-1 b and c. *Nature*, *537*(7618), 69–72. https://doi.org/10.1038/nature18641

de Wit, J., Wakeford, H. R., Lewis, N. K., Delrez, L., Gillon, M., Selsis, F., et al. (2018). Atmospheric reconnaissance of the habitable-zone Earth-sized planets orbiting TRAPPIST-1. *Nature Astronomy*, *2*(3), 214–219. https://doi.org/10.1038/s41550-017-0374-z

Diamond-Lowe, H., Berta-Thompson, Z., Charbonneau, D., Dittmann, J., & Kempton, E. M. R. (2020a). Simultaneous Optical Transmission Spectroscopy of a Terrestrial, Habitable-zone Exoplanet with Two Ground-based Multiobject Spectrographs. *The Astronomical Journal*, *160*(1), 27. https://doi.org/10.3847/1538-3881/ab935f

Diamond-Lowe, H., Berta-Thompson, Z., Charbonneau, D., & Kempton, E. M. R. (2018). Ground-based optical transmission spectroscopy of the small, rocky exoplanet GJ 1132b. *The Astronomical Journal*, *156*(2), 42. https://doi.org/10.3847/1538-3881/aac6dd

Diamond-Lowe, H., Charbonneau, D., Malik, M., Kempton, E. M. R., & Beletsky, Y. (2020b). Optical Transmission Spectroscopy of the Terrestrial Exoplanet LHS 3844b from 13 Ground-based Transit Observations. *The Astronomical Journal*, *160*(4), 188. https://doi.org/10.3847/1538-3881/abaf4f

Dobbs-Dixon, I., Cumming, A., & Lin, D. N. C. (2010). Radiative hydrodynamic simulations of HD209458b: Temporal variability. *The Astrophysical Journal*, *710*(2), 1395–1407. https://doi.org/10.1088/0004-637X/710/2/1395

Drummond, B., Mayne, N. J., Baraffe, I., Tremblin, P., Manners, J., Amundsen, D. S., et al. (2018a). The effect of metallicity on the atmospheres of exoplanets with fully coupled 3D hydrodynamics, equilibrium chemistry, and radiative transfer. *Astronomy & Astrophysics*, *612*, A105. https://doi.org/10.1051/0004-6361/201732010

Drummond, B., Mayne, N. J., Manners, J., Baraffe, I., Goyal, J., Tremblin, P., et al. (2018b). The 3D thermal, dynamical, and chemical structure of the atmosphere of HD 189733b: Implications of wind-driven chemistry for the emission phase curve. *The Astrophysical Journal*, *869*(1), 28. https://doi.org/10.3847/1538-4357/aaeb28

Ducrot, E., Sestovic, M., Morris, B. M., Gillon, M., Triaud, A. H. M. J., De Wit, J., et al. (2018). The 0.8-4.5 μm broadband transmission spectra of TRAPPIST-1 planets. *The Astronomical Journal*, *156*(5), 218. https://doi.org/10.3847/1538-3881/aade94

Dupuy, T. J., & Kraus, A. L. (2013). Distances, luminosities, and temperatures of the coldest known substellar objects. *Science*, *341*(6153), 1492–1495. https://doi.org/10.1126/science.1241917

Dupuy, T. J., & Liu, M. C. (2012). The Hawaii infrared parallax program. I. Ultracool binaries and the L/T transition. *The Astrophysical Journal Supplement*, *201*(2), 19. https://doi.org/10.1088/0067-0049/201/2/19

Dyudina, U., Zhang, X., Li, L., Kopparla, P., Ingersoll, A. P., Dones, L., et al. (2016). Reflected light curves, spherical and bond albedos of Jupiter- and Saturn-like exoplanets. *The Astrophysical Journal*, *822*(2), 76. https://doi.org/10.3847/0004-637X/822/2/76

Ebel, D. S. (2006). Condensation of rocky material in astrophysical environments. In D. S. Lauretta & H. Y. McSween (Eds.), *Meteorites and the early solar system II* (p. 253), University of Arizona Press, Tucson.

Ehrenreich, D., Lovis, C., Allart, R., Zapatero Osorio, M. R., Pepe, F., Cristiani, S., et al. (2020). Nightside condensation of iron in an ultra-hot giant exoplanet. *Nature*, *580*(7805), 597–601. https://doi.org/10.1038/s41586-020-2107-1

Eldridge, J., & Palik, E. D. (1985). Sodium chloride (NaCl). In E. D. Palik (Ed.), *Handbook of optical constants of solids* (p. 775–793). Boston, MA: Academic Press. Retrieved from http://www.sciencedirect.com/science/article/pii/B9780080547213500435

Eriksson, S. C., Janson, M., & Calissendorff, P. (2019). Detection of new strongly variable brown dwarfs in the L/T transition. *Astronomy & Astrophysics*, *629*, A145. https://doi.org/10.1051/0004-6361/201935671

Espinoza, N., Rackham, B. V., Jordán, A., Apai, D., López-Morales, M., Osip, D. J., et al. (2019). ACCESS: A featureless optical transmission spectrum for WASP-19b from Magellan/IMACS. *Monthly Notices of the Royal Astronomical Society*, *482*(2), 2065–2087. https://doi.org/10.1093/mnras/sty2691

Esplin, T. L., Luhman, K. L., Cushing, M. C., Hardegree-Ullman, K. K., Trucks, J. L., Burgasser, A. J., & Schneider, A. C. (2016). Photometric monitoring of the coldest known brown dwarf with the Spitzer Space Telescope. *The Astrophysical Journal*, *832*(1), 58. https://doi.org/10.3847/0004-637X/832/1/58

Esteves, L. J., De Mooij, E. J. W., & Jayawardhana, R. (2013). Optical phase curves of Kepler exoplanets. *The Astrophysical Journal*, *772*(1), 51. https://doi.org/10.1088/0004-637X/772/1/51

Esteves, L. J., De Mooij, E. J. W., & Jayawardhana, R. (2015). Changing phases of alien worlds: Probing atmospheres of Kepler planets with high-precision photometry. *The Astrophysical Journal*, *804*(2), 150. https://doi.org/10.1088/0004-637X/804/2/150

Evans, T. M., Pont, F., Sing, D. K., Aigrain, S., Barstow, J. K., Désert, J.-M., et al. (2013). The deep blue color of HD 189733b: Albedo measurements with Hubble Space Telescope/space telescope imaging spectrograph at visible wavelengths. *The Astrophysical Journal Letters*, *772*(2), L16. https://doi.org/10.1088/2041-8205/772/2/L16

Faherty, J. K., Beletsky, Y., Burgasser, A. J., Tinney, C., Osip, D. J., Filippazzo, J. C., & Simcoe, R. A. (2014). Signatures of cloud, temperature, and gravity from spectra of the closest brown dwarfs. *The Astrophysical Journal*, *790*(2), 90. https://doi.org/10.1088/0004-637X/790/2/90

Faherty, J. K., Riedel, A. R., Cruz, K. L., Gagne, J., Filippazzo, J. C., Lambrides, E., et al. (2016). Population properties of brown dwarf analogs to exoplanets. *The Astrophysical Journal Supplement Series*, *225*(1), 10. https://doi.org/10.3847/0067-0049/225/1/10

Feng, Y. K., Robinson, T. D., Fortney, J. J., Lupu, R. E., Marley, M. S., Lewis, N. K., et al. (2018). Characterizing Earth analogs in reflected light: Atmospheric retrieval studies for future space telescopes. *The Astronomical Journal*, *155*(5), 200. https://doi.org/10.3847/1538-3881/aab95c

Fisher, C., & Heng, K. (2018). Retrieval analysis of 38 WFC3 transmission spectra and resolution of the normalization degeneracy. *Monthly Notices of the Royal Astronomical Society*, *481*(4), 4698–4727. https://doi.org/10.1093/mnras/sty2550

Fleury, B., Gudipati, M. S., Henderson, B. L., & Swain, M. (2019). Photochemistry in hot H_2-dominated exoplanet atmospheres. *The Astrophysical Journal*, *871*(2), 158. https://doi.org/10.3847/1538-4357/aaf79f

Fortney, J. J. (2005). The effect of condensates on the characterization of transiting planet atmospheres with transmission spectroscopy. *Monthly Notices of the Royal Astronomical Society*, *364*(2), 649–653. https://doi.org/10.1111/j.1365-2966.2005.09587.x

Fortney, J. J., Marley, M. S., Lodders, K., Saumon, D., & Freedman, R. (2005). Comparative planetary atmospheres: Models of TrES-1 and HD 209458b. *The Astrophysical Journal*, *627*(1), L69–L72. https://doi.org/10.1086/431952

Fortney, J. J., Marley, M. S., Saumon, D., & Lodders, K. (2008). Synthetic spectra and colors of young giant planet atmospheres: Effects of initial conditions and atmospheric metallicity. *The Astrophysical Journal*, *683*(2), 1104–1116. https://doi.org/10.1086/589942

Fortney, J. J., Robinson, T. D., Domagal-Goldman, S., Skålid Amundsen, D., Brogi, M., Claire, M., et al. (2016). *The need for laboratory work to aid in the understanding of exoplanetary atmospheres.* arXiv e-prints, arXiv:1602.06305.

Fortney, J. J., Shabram, M., Showman, A. P., Lian, Y., Freedman, R. S., Marley, M. S., & Lewis, N. K. (2010). Transmission spectra of three-dimensional hot Jupiter model atmospheres. *The Astrophysical Journal*, *709*, 1396–1406. https://doi.org/10.1088/0004-637X/709/2/1396

Fortney, J. J., Sudarsky, D., Hubeny, I., Cooper, C. S., Hubbard, W. B., Burrows, A., & Lunine, J. I. (2003). On the indirect detection of sodium in the atmosphere of the planetary companion to HD 209458. *The Astrophysical Journal*, *589*(1), 615–622. https://doi.org/10.1086/374387

Fossati, L., Haswell, C. A., Froning, C. S., Hebb, L., Holmes, S., Kolb, U., et al. (2010). Metals in the exosphere of the highly irradiated planet WASP-12b. *The Astrophysical Journal Letters*, *714*(2), L222–L227. https://doi.org/10.1088/2041-8205/714/2/L222

France, K., Froning, C. S., Linsky, J. L., Roberge, A., Stocke, J. T., Tian, F., et al. (2013). The ultraviolet radiation environment around M dwarf exoplanet host stars. *The Astrophysical Journal*, *763*(2), 149. https://doi.org/10.1088/0004-637X/763/2/149

Freytag, B., Allard, F., Ludwig, H. G., Homeier, D., & Steffen, M. (2010). The role of convection, overshoot, and gravity waves for the transport of dust in M dwarf and brown dwarf atmospheres. *Astronomy & Astrophysics*, *513*, A19. https://doi.org/10.1051/0004-6361/200913354

Fromang, S., Leconte, J., & Heng, K. (2016). Shear-driven instabilities and shocks in the atmospheres of hot Jupiters. *Astronomy & Astrophysics*, *591*, A144. https://doi.org/10.1051/0004-6361/201527600

Fu, G., Deming, D., Knutson, H., Madhusudhan, N., Mandell, A., & Fraine, J. (2017). Statistical analysis of hubble/WFC3 transit spectroscopy of extrasolar planets. *The Astrophysical Journal Letters*, *847*, L22. https://doi.org/10.3847/2041-8213/aa8e40

Gail, H. P., Keller, R., & Sedlmayr, E. (1984). Dust formation in stellar winds. I - A rapid computational method and application to graphite condensation. *Astronomy & Astrophysics*, *133*(2), 320–332.

Gail, H. P., & Sedlmayr, E. (1988). Dust formation in stellar winds. IV. Heteromolecular carbon grain formation and growth. *Astronomy & Astrophysics*, *206*, 153–168.
Gandhi, S., Brogi, M., & Webb, R. K. (2020). Seeing above the clouds with high-resolution spectroscopy. *Monthly Notices of the Royal Astronomical Society*, *498*(1), 194–204. https://doi.org/10.1093/mnras/staa2424
Gandhi, S., & Madhusudhan, N. (2019). New avenues for thermal inversions in atmospheres of hot Jupiters. *Monthly Notices of the Royal Astronomical Society*, *485*(4), 5817–5830. https://doi.org/10.1093/mnras/stz751
Gao, P., & Benneke, B. (2018). Microphysics of KCl and ZnS Clouds on GJ 1214 b. *The Astrophysical Journal*, *863*(2), 165. https://doi.org/10.3847/1538-4357/aad461
Gao, P., Marley, M. S., & Ackerman, A. S. (2018). Sedimentation efficiency of condensation clouds in substellar atmospheres. *The Astrophysical Journal*, *855*(2), 86. https://doi.org/10.3847/1538-4357/aab0a1
Gao, P., Marley, M. S., Zahnle, K., Robinson, T. D., & Lewis, N. K. (2017). Sulfur hazes in giant exoplanet atmospheres: Impacts on reflected light spectra. *The Astrophysical Journal*, *153*(3), 139. https://doi.org/10.3847/1538-3881/aa5fab
Gao, P., Thorngren, D. P., Lee, G. K. H., Fortney, J. J., Morley, C. V., Wakeford, H. R., et al. (2020). Aerosol composition of hot giant exoplanets dominated by silicates and hydrocarbon hazes. *Nature Astronomy*, *4*, 951–956. https://doi.org/10.1038/s41550-020-1114-3
Gao, P., Wakeford, H. R., Moran, S. E., & Parmentier, V. (2021). *Exoplanet aerosol transmission spectra*. Zenodo. Retrieved from https://doi.org/10.5281/zenodo.4444278
Gao, P., & Zhang, X. (2020). Deflating Super-puffs: Impact of Photochemical Hazes on the Observed Mass-Radius Relationship of Low-mass Planets. *The Astrophysical Journal*, *890*(2), 93. https://doi.org/10.3847/1538-4357/ab6a9b
Garcia Munoz, A., & Isaak, K. G. (2015). Probing exoplanet clouds with optical phase curves. *Proceedings of the National Academy of Sciences*, *112*(44), 13461–13466. https://doi.org/10.1073/pnas.1509135112
Garhart, E., Deming, D., Mandell, A., Knutson, H. A., Wallack, N., Burrows, A., et al. (2020). Statistical characterization of hot Jupiter atmospheres using Spitzer's secondary eclipses. *The Astronomical Journal*, *159*(4), 137. https://doi.org/10.3847/1538-3881/ab6cff
Gavilan, L., Broch, L., Carrasco, N., Fleury, B., & Vettier, L. (2017). Organic aerosols in the presence of CO_2 in the early Earth and exoplanets: UV-Vis refractive indices of oxidized tholins. *The Astrophysical Journal Letters*, *848*(1), L5. https://doi.org/10.3847/2041-8213/aa8cc4
Gavilan, L., Carrasco, N., Hoffmann, S. V., Jones, N. C., & Mason, N. J. (2018). Organic aerosols in anoxic and oxic atmospheres of Earth-like exoplanets: VUV-MIR spectroscopy of CHON tholins. *The Astrophysical Journal*, *861*(2), 110. https://doi.org/10.3847/1538-4357/aac8df
Ge, H., Li, C., Zhang, X., & Lee, D. (2020). A global nonhydrostatic atmospheric model with a mass- and energy-conserving vertically implicit correction (VIC) scheme. *The Astrophysical Journal*, *898*(2), 130. https://doi.org/10.3847/1538-4357/ab9ec7
Ge, H., Zhang, X., Fletcher, L. N., Orton, G. S., Sinclair, J., Fernandes, J., et al. (2019). Rotational light curves of Jupiter from ultraviolet to mid-infrared and implications for brown dwarfs and exoplanets. *The Astronomical Journal*, *157*(2), 89. https://doi.org/10.3847/1538-3881/aafba7
Gibson, N. P., Aigrain, S., Pont, F., Sing, D. K., Désert, J. M., Evans, T. M., et al. (2012). Probing the haze in the atmosphere of HD 189733b with Hubble Space Telescope/WFC3 transmission spectroscopy. *Monthly Notices of the Royal Astronomical Society*, *422*(1), 753–760. https://doi.org/10.1111/j.1365-2966.2012.20655.x
Gibson, N. P., de Mooij, E. J. W., Evans, T. M., Merritt, S., Nikolov, N., Sing, D. K., & Watson, C. (2019). Revisiting the potassium feature of WASP-31b at high resolution. *Monthly Notices of the Royal Astronomical Society*, *482*(1), 606–615. https://doi.org/10.1093/mnras/sty2722
Gibson, N. P., Nikolov, N., Sing, D. K., Barstow, J. K., Evans, T. M., Kataria, T., & Wilson, P. A. (2017). VLT/FORS2 comparative transmission spectroscopy II: Confirmation of a cloud deck and Rayleigh scattering in WASP-31b, but no potassium? *Monthly Notices of the Royal Astronomical Society*, *467*(4), 4591–4605. https://doi.org/10.1093/mnras/stx353
Gierasch, P. J., & Conrath, B. J. (1985). Energy conversion processes in the outer planets. In G. E. Hunt (Ed.), *Recent advances in planetary meteorology* (p. 121–146), Cambridge, UK. Cambridge University Press.
Gilliam, A. E., & McKay, C. P. (2011). Titan under a red dwarf star and as a rogue planet: Requirements for liquid methane. *Planetary and Space Science*, *59*(9), 835–839. https://doi.org/10.1016/j.pss.2011.03.012
Gillon, M., Triaud, A. H. M. J., Jehin, E., Delrez, L., Opitom, C., Magain, P., et al. (2013). Fast-evolving weather for the coolest of our two new substellar neighbours. *Astronomy & Astrophysics*, *555*, L5. https://doi.org/10.1051/0004-6361/201321620
Gizis, J. E., Allers, K. N., Liu, M. C., Harris, H. C., Faherty, J. K., Burgasser, A. J., & Kirkpatrick, J. D. (2015). WISEP J004701.06+680352.1: An intermediate surface gravity, dusty brown dwarf in the AB Dor Moving Group. *The Astrophysical Journal*, *799*(2), 203. https://doi.org/10.1088/0004-637X/799/2/203
Gladstone, G. R., Stern, S. A., Ennico, K., Olkin, C. B., Weaver, H. A., Young, L. A., et al. (2016). The atmosphere of Pluto as observed by New Horizons. *Science*, *351*(6279), 1280. https://doi.org/10.1126/science.aad8866
Goyal, J. M., Mayne, N., Sing, D. K., Drummond, B., Tremblin, P., Amundsen, D. S., et al. (2018). A library of ATMO forward model transmission spectra for hot Jupiter exoplanets. *Monthly Notices of the Royal Astronomical Society*, *474*(4), 5158–5185. https://doi.org/10.1093/mnras/stx3015
Greenbaum, A. Z., Pueyo, L., Ruffio, J.-B., Wang, J. J., De Rosa, R. J., Aguilar, J., et al. (2018). GPI Spectra of HR 8799 c, d, and e from 1.5 to 2.4 μm with KLIP Forward Modeling. *The Astronomical Journal*, *155*(6), 226. https://doi.org/10.3847/1538-3881/aabcb8
Greene, T. P., Line, M. R., Montero, C., Fortney, J. J., Lustig-Yaeger, J., & Luther, K. (2016). Characterizing transiting exoplanet atmospheres with JWST. *The Astrophysical Journal*, *817*(1), 17. https://doi.org/10.3847/0004-637X/817/1/17
Griffith, C. A., Yelle, R. V., & Marley, M. S. (1998). The dusty atmosphere of the brown dwarf Gliese 229B. *Science*, *282*, 2063. https://doi.org/10.1126/science.282.5396.2063
Guillot, T. (2010). On the radiative equilibrium of irradiated planetary atmospheres. *Astronomy & Astrophysics*, *520*, A27. https://doi.org/10.1051/0004-6361/200913396
Guillot, T., Burrows, A., Hubbard, W. B., Lunine, J. I., & Saumon, D. (1996). Giant planets at small orbital distances. *The Astrophysical Journal Letters*, *459*(1), L35. https://doi.org/10.1086/309935
Hansen, J. E., & Hovenier, J. W. (1974). Interpretation of the polarization of Venus. *Journal of the Atmospheric Sciences*, *31*(4), 1137–1160.
Harada, C. K., Kempton, E. M. R., Rauscher, E., Roman, M., & Brinjikji, M. (2019). *Signatures of clouds in hot Jupiter atmospheres: Modeled high resolution emission spectra from 3D general circulation models*. arXiv e-prints, arXiv:1912.02268.
Harre, J.-V., & Heller, R. (2021). *Digital color codes of stars*. arXiv e-prints, arXiv:2101.06254.
Harrington, J., Hansen, B. M., Luszcz, S. H., Seager, S., Deming, D., Menou, K., et al. (2006). The phase-dependent infrared brightness of the extrasolar planet υ Andromedae b. *Science*, *314*(5799), 623–626. https://doi.org/10.1126/science.1133904

Hasenkopf, C. A., Beaver, M. R., Trainer, M. G., Langley Dewitt, H., Freedman, M. A., Toon, O. B., et al. (2010). Optical properties of Titan and early Earth haze laboratory analogs in the mid-visible. *Icarus*, *207*(2), 903–913. https://doi.org/10.1016/j.icarus.2009.12.015

Haswell, C. A., Fossati, L., Ayres, T., France, K., Froning, C. S., Holmes, S., et al. (2012). Near-ultraviolet absorption, chromospheric activity, and star-planet interactions in the WASP-12 system. *The Astrophysical Journal*, *760*(1), 79. https://doi.org/10.1088/0004-637X/760/1/79

He, C., Hörst, S. M., Lewis, N. K., Moses, J. I., Kempton, E. M. R., Marley, M. S., et al. (2019). Gas phase chemistry of cool exoplanet atmospheres: Insight from laboratory simulations. *ACS Earth and Space Chemistry*, *3*(1), 39–50. https://doi.org/10.1021/acsearthspacechem.8b00133

He, C., Hörst, S. M., Lewis, N. K., Yu, X., Moses, J. I., Kempton, E. M.-R., et al. (2018a). Laboratory simulations of haze formation in the atmospheres of super-Earths and mini-Neptunes: Particle color and size distribution. *The Astrophysical Journal Letters*, *856*(1), L3. https://doi.org/10.3847/2041-8213/aab42b

He, C., Hörst, S. M., Lewis, N. K., Yu, X., Moses, J. I., Kempton, E. M. R., et al. (2018b). Photochemical haze formation in the atmospheres of super-Earths and mini-Neptunes. *The Astronomical Journal*, *156*(1), 38. https://doi.org/10.3847/1538-3881/aac883

He, C., Hörst, S. M., Lewis, N. K., Yu, X., Moses, J. I., McGuiggan, P., et al. (2020a). Haze formation in warm H_2-rich exoplanet atmospheres. *The Planetary Science Journal*, *1*(2), 51. https://doi.org/10.3847/PSJ/abb1a4

He, C., Hörst, S. M., Lewis, N. K., Yu, X., Moses, J. I., McGuiggan, P., et al. (2020b). Sulfur-driven haze formation in warm CO_2-rich exoplanet atmospheres. *Nature Astronomy*, *4*(10), 986–993. https://doi.org/10.1038/s41550-020-1072-9

Heinze, A. N., Metchev, S., Apai, D., Flateau, D., Kurtev, R., Marley, M., et al. (2013). Weather on other worlds. I. Detection of periodic variability in the L3 dwarf DENIS-P J1058.7-1548 with precise multi-wavelength photometry. *The Astrophysical Journal*, *767*(2), 173. https://doi.org/10.1088/0004-637X/767/2/173

Helling, C., Ackerman, A., Allard, F., Dehn, M., Hauschildt, P., Homeier, D., et al. (2008a). A comparison of chemistry and dust cloud formation in ultracool dwarf model atmospheres. *Monthly Notices of the Royal Astronomical Society*, *391*(4), 1854–1873. https://doi.org/10.1111/j.1365-2966.2008.13991.x

Helling, C., & Casewell, S. (2014). Atmospheres of brown dwarfs. *The Astronomy and Astrophysics Review*, *22*, 80. https://doi.org/10.1007/s00159-014-0080-0

Helling, C., Dehn, M., Woitke, P., & Hauschildt, P. H. (2008b). Consistent simulations of substellar atmospheres and nonequilibrium dust cloud formation. *The Astrophysical Journal Letters*, *675*(2), L105. https://doi.org/10.1086/533462

Helling, C., Gourbin, P., Woitke, P., & Parmentier, V. (2019a). Sparkling nights and very hot days on WASP-18b: The formation of clouds and the emergence of an ionosphere. *Astronomy & Astrophysics*, *626*, A133. https://doi.org/10.1051/0004-6361/201834085

Helling, C., Iro, N., Corrales, L., Samra, D., Ohno, K., Alam, M. K., et al. (2019b). Understanding the atmospheric properties and chemical composition of the ultra-hot Jupiter HAT-P-7b. I. Cloud and chemistry mapping. *Astronomy & Astrophysics*, *631*, A79. https://doi.org/10.1051/0004-6361/201935771

Helling, C., Kawashima, Y., Graham, V., Samra, D., Chubb, K. L., Min, M., et al. (2020). *Mineral cloud and hydrocarbon haze particles in the atmosphere of the hot Jupiter JWST target WASP-43b*. arXiv e-prints, arXiv:2005.14595.

Helling, C., Lee, G., Dobbs-Dixon, I., Mayne, N., Amundsen, D. S., Khaimova, J., et al. (2016). The mineral clouds on HD 209458b and HD 189733b. *Monthly Notices of the Royal Astronomical Society*, *460*(1), 855–883. https://doi.org/10.1093/mnras/stw662

Helling, C., Oevermann, M., Lüttke, M. J. H., Klein, R., & Sedlmayr, E. (2001). Dust in brown dwarfs. I. Dust formation under turbulent conditions on microscopic scales. *Astronomy & Astrophysics*, *376*(1), 194–212.

Helling, C., Thi, W. F., Woitke, P., & Fridlund, M. (2006). Detectability of dirty dust grains in brown dwarf atmospheres. *Astronomy & Astrophysics*, *451*(2), L9–L12. https://doi.org/10.1051/0004-6361:20054598

Helling, C., Tootill, D., Woitke, P., & Lee, G. (2017). Dust in brown dwarfs and extrasolar planets. V. Cloud formation in carbon- and oxygen-rich environments. *Astronomy & Astrophysics*, *603*, A123. https://doi.org/10.1051/0004-6361/201629696

Helling, C., & Woitke, P. (2006). Dust in brown dwarfs. V. Growth and evaporation of dirty dust grains. *Astronomy & Astrophysics*, *455*(1), 325–338. http://doi.org/10.1051/0004-6361:20054598

Helling, C., Woitke, P., & Thi, W.-F. (2008c). Dust in brown dwarfs and extra-solar planets. I. Chemical composition and spectral appearance of quasi-static cloud layers. *Astronomy & Astrophysics*, *485*(2), 547–560. https://doi.org/10.1051/0004-6361:20078220

Heng, K. (2016). A cloudiness index for transiting exoplanets based on the sodium and potassium lines: Tentative evidence for hotter atmospheres being less cloudy at visible wavelengths. *The Astrophysical Journal Letters*, *826*(1), L16. https://doi.org/10.3847/2041-8205/826/1/L16

Heng, K., & Demory, B.-O. (2013). Understanding trends associated with clouds in irradiated exoplanets. *The Astrophysical Journal*, *777*(2), 100. https://doi.org/10.1088/0004-637X/777/2/100

Heng, K., Hayek, W., Pont, F., & Sing, D. K. (2012). On the effects of clouds and hazes in the atmospheres of hot Jupiters: Semi-analytical temperature-pressure profiles. *Monthly Notices of the Royal Astronomical Society*, *420*(1), 20–36. https://doi.org/10.1111/j.1365-2966.2011.19943.x

Herbort, O., Woitke, P., Helling, C., & Zerkle, A. (2020). The atmospheres of rocky exoplanets. I. Outgassing of common rock and the stability of liquid water. *Astronomy & Astrophysics*, *636*, A71. https://doi.org/10.1051/0004-6361/201936614

Hiranaka, K., Cruz, K. L., Douglas, S. T., Marley, M. S., & Baldassare, V. F. (2016). Exploring the role of sub-micron-sized dust grains in the atmospheres of red L0–L6 dwarfs. *The Astrophysical Journal*, *830*(2), 96. https://doi.org/10.3847/0004-637X/830/2/96

Hoeijmakers, H. J., Ehrenreich, D., Heng, K., Kitzmann, D., Grimm, S. L., Allart, R., et al. (2018). Atomic iron and titanium in the atmosphere of the exoplanet KELT-9b. *Nature*, *560*(7719), 453–455. https://doi.org/10.1038/s41586-018-0401-y

Holton, J. R. (1986). A dynamically based transport parameterization for one-dimensional photochemical models of the stratosphere. *Journal of Geophysical Research*, *91*(D2), 2681–2686.

Hood, C. E., Fortney, J. J., Line, M. R., Martin, E. C., Morley, C. V., Birkby, J. L., et al. (2020). Prospects for characterizing the haziest sub-Neptune exoplanets with high-resolution spectroscopy. *The Astronomical Journal*, *160*(5), 198. https://doi.org/10.3847/1538-3881/abb46b

Hörst, S. (2016). *Clouds and haze and dust, oh my!* The Planetary Society. Retrieved from https://www.planetary.org/blogs/guest-blogs/2016/0324-clouds-and-haze-and-dust-oh-my.html

Hörst, S. M., He, C., Lewis, N. K., Kempton, E. M.-R., Marley, M. S., Morley, C. V., et al. (2018). Haze production rates in super-Earth and mini-Neptune atmosphere experiments. *Nature Astronomy*, *2*(4), 303–306. https://doi.org/10.1038/s41550-018-0397-0

Hörst, S. M., & Tolbert, M. A. (2014). The effect of carbon monoxide on planetary haze formation. *The Astrophysical Journal*, *781*(1), 53. https://doi.org/10.1088/0004-637X/781/1/53

Howe, A. R., & Burrows, A. S. (2012). Theoretical transit spectra for GJ 1214b and other "super-Earths". *The Astrophysical Journal*, *756*(2), 176. https://doi.org/10.1088/0004-637X/756/2/176

Hu, R. (2019). Information in the reflected-light spectra of widely separated giant exoplanets. *The Astrophysical Journal*, *887*(2), 166. https://doi.org/10.3847/1538-4357/ab58c7

Hu, R., & Seager, S. (2014). Photochemistry in terrestrial exoplanet atmospheres. III. Photochemistry and thermochemistry in thick atmospheres on super Earths and mini Neptunes. *The Astrophysical Journal*, *784*(1), 63. http://stacks.iop.org/0004-637X/784/i=1/a=63

Hu, R., Seager, S., & Bains, W. (2012). Photochemistry in terrestrial exoplanet atmospheres. I. Photochemistry model and benchmark cases. *The Astrophysical Journal*, *761*(2), 166. https://doi.org/10.1088/0004-637X/761/2/166

Hu, R., Seager, S., & Bains, W. (2013). Photochemistry in terrestrial exoplanet atmospheres. II. H_2S and SO_2 photochemistry in anoxic atmospheres. *The Astrophysical Journal*, *769*(1), 6. https://doi.org/10.1088/0004-637X/769/1/6

Hubbard, W. B., Fortney, J. J., Lunine, J. I., Burrows, A., Sudarsky, D., & Pinto, P. (2001). Theory of extrasolar giant planet transits. *The Astrophysical Journal*, *560*(1), 413–419. https://doi.org/10.1086/322490

Hubeny, I., & Burrows, A. (2007). A systematic study of departures from chemical equilibrium in the atmospheres of substellar mass objects. *The Astrophysical Journal*, *669*(2), 1248–1261. https://doi.org/10.1086/522107

Hueso, R., & Sánchez-Lavega, A. (2006). Moist convective storms in the atmospheres of Jupiter and Saturn atmospheric storms in Jupiter and Saturn. In J.Del Toro Iniesta, E. Alfaro, J. Gorgas, E. Salvador-Solé, H.Butcher (Eds.), *The many scales in the universe: Jenam 2004 astrophysics reviews* (pp. 211–220). Dordrecht: Springer Netherlands. Retrieved from https://doi.org/10.1007/1-4020-4526-3_18

Imanaka, H., Khare, B. N., Elsila, J. E., Bakes, E. L. O., McKay, C. P., Cruikshank, D. P., et al. (2004). Laboratory experiments of Titan tholin formed in cold plasma at various pressures: implications for nitrogen-containing polycyclic aromatic compounds in Titan haze. *Icarus*, *168*(2), 344–366. https://doi.org/10.1016/j.icarus.2003.12.014

Ingraham, P., Marley, M. S., Saumon, D., Marois, C., Macintosh, B., Barman, T., et al. (2014). Gemini Planet Imager Spectroscopy of the HR 8799 Planets c and d. *The Astrophysical Journal Letters*, *794*(1), L15. https://doi.org/10.1088/2041-8205/794/1/L15

Irwin, P. G. J., Tice, D. S., Fletcher, L. N., Barstow, J. K., Teanby, N. A., Orton, G. S., & Davis, G. R. (2015). Reanalysis of Uranus' cloud scattering properties from IRTF/SpeX observations using a self-consistent scattering cloud retrieval scheme. *Icarus*, *250*, 462–476. https://doi.org/10.1016/j.icarus.2014.12.020

Ito, Y., Ikoma, M., Kawahara, H., Nagahara, H., Kawashima, Y., & Nakamoto, T. (2015). Theoretical emission spectra of atmospheres of hot rocky super-Earths. *The Astrophysical Journal*, *801*(2), 144. https://doi.org/10.1088/0004-637X/801/2/144

Iyer, A. R., Swain, M. R., Zellem, R. T., Line, M. R., Roudier, G., Rocha, G., & Livingston, J. H. (2016). A characteristic transmission spectrum dominated by H_2O applies to the majority of HST/WFC3 exoplanet observations. *The Astrophysical Journal*, *823*, 109. https://doi.org/10.3847/0004-637X/823/2/109

Jackson, B., Adams, E., Sandidge, W., Kreyche, S., & Briggs, J. (2019). Variability in the atmosphere of the hot Jupiter Kepler-76b. *The Astronomical Journal*, *157*(6), 239. https://doi.org/10.3847/1538-3881/ab1b30

Jansen, T., & Kipping, D. (2018). Kepler's dark worlds: A low albedo for an ensemble of Neptunian and Terran exoplanets. *Monthly Notices of the Royal Astronomical Society*, *478*(3), 3025–3041. https://doi.org/10.1093/mnras/sty1149

Jansen, T., & Kipping, D. (2020). Detection of the phase curve and occultation of WASP-100b with TESS. *Monthly Notices of the Royal Astronomical Society*, *494*(3), 4077–4089. https://doi.org/10.1093/mnras/staa814

Joshi, M. (2003). Climate model studies of synchronously rotating planets. *Astrobiology*, *3*(2), 415–427. https://doi.org/10.1089/153110703769016488

Kane, S. R., Fetherolf, T., & Hill, M. L. (2020). The dark planets of the WASP-47 planetary system. *The Astronomical Journal*, *159*(4), 176. https://doi.org/10.3847/1538-3881/ab7818

Karalidi, T., Apai, D., Marley, M. S., & Buenzli, E. (2016). Maps of evolving cloud structures in Luhman 16AB from HST time-resolved spectroscopy. *The Astrophysical Journal*, *825*(2), 90. https://doi.org/10.3847/0004-637X/825/2/90

Karalidi, T., Apai, D., Schneider, G., Hanson, J. R., & Pasachoff, J. M. (2015). Aeolus: A Markov chain Monte Carlo code for mapping ultracool atmospheres. An Application on Jupiter and brown dwarf HST light curves. *The Astrophysical Journal*, *814*(1), 65. https://doi.org/10.1088/0004-637X/814/1/65

Karalidi, T., Stam, D. M., & Guirado, D. (2013). Flux and polarization signals of spatially inhomogeneous gaseous exoplanets. *Astronomy & Astrophysics*, *555*, A127. https://doi.org/10.1051/0004-6361/201321492

Kasting, J. F., Whitmire, D. P., & Reynolds, R. T. (1993). Habitable zones around main sequence stars. *Icarus*, *101*(1), 108–128. https://doi.org/10.1006/icar.1993.1010

Kataria, T., Showman, A. P., Fortney, J. J., Stevenson, K. B., Line, M. R., Kreidberg, L., et al. (2015). The atmospheric circulation of the hot Jupiter WASP-43b: Comparing three-dimensional models to spectrophotometric data. *The Astrophysical Journal*, *801*(2), 86. https://doi.org/10.1088/0004-637X/801/2/86

Kawashima, Y., Hu, R., & Ikoma, M. (2019). Detectable molecular features above hydrocarbon haze via transmission spectroscopy with JWST: Case studies of GJ 1214b-, GJ 436b-, HD 97658b-, and Kepler-51b-like planets. *The Astrophysical Journal Letters*, *876*(1), L5. https://doi.org/10.3847/2041-8213/ab16f6

Kawashima, Y., & Ikoma, M. (2018). Theoretical transmission spectra of exoplanet atmospheres with hydrocarbon haze: Effect of creation, growth, and settling of haze particles. I. Model description and first results. *The Astrophysical Journal*, *853*(1), 7. https://doi.org/10.3847/1538-4357/aaa0c5

Kawashima, Y., & Ikoma, M. (2019). Theoretical transmission spectra of exoplanet atmospheres with hydrocarbon haze: Effect of creation, growth, and settling of haze particles. II. Dependence on UV irradiation intensity, metallicity, C/O ratio, eddy diffusion coefficient, and temperature. *The Astrophysical Journal*, *877*(2), 109. https://doi.org/10.3847/1538-4357/ab1b1d

Keating, D., Cowan, N. B., & Dang, L. (2019). Uniformly hot nightside temperatures on short-period gas giants. *Nature Astronomy*, *3*(12), 1092–1098. https://doi.org/10.1038/s41550-019-0859-z

Kellogg, K., Metchev, S., Miles-Páez, P. A., & Tannock, M. E. (2017). A statistical survey of peculiar L and T dwarfs in SDSS, 2MASS, and WISE. *The Astronomical Journal*, *154*(3), 112. https://doi.org/10.3847/1538-3881/aa83b0

Kempton, E. M. R., Bean, J. L., & Parmentier, V. (2017). An observational diagnostic for distinguishing between clouds and haze in hot exoplanet atmospheres. *The Astrophysical Journal Letters*, *845*(2), L20. https://doi.org/10.3847/2041-8213/aa84ac

Khare, B. N., Sagan, C., Arakawa, K. T., Suits, F., Callcott, T. A., & Williams, M. W. (1984). Optical constants of organic tholins produced in a simulated Titanian atmosphere: From soft X-ray to microwave frequencies. *Icarus*, *60*(1), 127–137.

Kilpatrick, B. M., Cubillos, P. E., Stevenson, K. B., Lewis, N. K., Wakeford, H. R., MacDonald, R. J., et al. (2018). Community targets of JWST's early release science program: Evaluation of WASP-63b. *The Astronomical Journal*, *156*(3), 103. https://doi.org/10.3847/1538-3881/aacea7

Kipping, D. M., & Spiegel, D. S. (2011). Detection of visible light from the darkest world. *Monthly Notices of the Royal Astronomical Society*, *417*(1), L88–L92. https://doi.org/10.1111/j.1745-3933.2011.01127.x

Kirkpatrick, J. D. (2005). New spectral types L and T. *Annual Review of Astronomy & Astrophysics*, *43*(1), 195–245. https://doi.org/10.1146/annurev.astro.42.053102.134017

Kite, E. S., Fegley, B., Jr., Schaefer, L., & Gaidos, E. (2016). Atmosphere-interior exchange on hot, rocky exoplanets. *The Astrophysical Journal*, *828*(2), 80. https://doi.org/10.3847/0004-637X/828/2/80

Kitzmann, D., & Heng, K. (2018). Optical properties of potential condensates in exoplanetary atmospheres. *Monthly Notices of the Royal Astronomical Society*, *475*(1), 94–107. https://doi.org/10.1093/mnras/stx3141

Knapp, G. R., Leggett, S. K., Fan, X., Marley, M. S., Geballe, T. R., Golimowski, D. A., et al. (2004). Near-infrared photometry and spectroscopy of L and T dwarfs: The effects of temperature, clouds, and gravity. *The Astronomical Journal*, *127*(6), 3553–3578. https://doi.org/10.1086/420707

Knutson, H. A., Benneke, B., Deming, D., & Homeier, D. (2014). A featureless transmission spectrum for the Neptune-mass exoplanet GJ436b. *Nature*, *505*(7481), 66. https://doi.org/10.1038/nature12887

Knutson, H. A., Charbonneau, D., Allen, L. E., Burrows, A., & Megeath, S. T. (2008). The 3.6-8.0 μm broadband emission spectrum of HD 209458b: Evidence for an atmospheric temperature inversion. *The Astrophysical Journal*, *673*(1), 526–531. https://doi.org/10.1086/523894

Knutson, H. A., Charbonneau, D., Allen, L. E., Fortney, J. J., Agol, E., Cowan, N. B., et al. (2007). A map of the day-night contrast of the extrasolar planet HD 189733b. *Nature*, *447*(7141), 183–186. https://doi.org/10.1038/nature05782

Knutson, H. A., Lewis, N., Fortney, J. J., Burrows, A., Showman, A. P., Cowan, N. B., et al. (2012). 3.6 and 4.5 μm phase curves and evidence for non-equilibrium chemistry in the atmosphere of extrasolar planet HD 189733b. *The Astrophysical Journal*, *754*(1), 22. https://doi.org/10.1088/0004-637X/754/1/22

Komacek, T. D., & Abbot, D. S. (2019). The atmospheric circulation and climate of terrestrial planets orbiting Sun-like and M dwarf stars over a broad range of planetary parameters. *The Astrophysical Journal*, *871*(2), 245. https://doi.org/10.3847/1538-4357/aafb33

Komacek, T. D., Fauchez, T. J., Wolf, E. T., & Abbot, D. S. (2020). Clouds will likely prevent the detection of water vapor in JWST transmission spectra of terrestrial exoplanets. *The Astrophysical Journal Letters*, *888*(2), L20. https://doi.org/10.3847/2041-8213/ab6200

Komacek, T. D., & Showman, A. P. (2020). Temporal variability in hot Jupiter atmospheres. *The Astrophysical Journal*, *888*(1), 2. https://doi.org/10.3847/1538-4357/ab5b0b

Komacek, T. D., Showman, A. P., & Parmentier, V. (2019). Vertical tracer mixing in hot Jupiter atmospheres. *The Astrophysical Journal*, *881*(2), 152. https://doi.org/10.3847/1538-4357/ab338b

Kopparla, P., Natraj, V., Zhang, X., Swain, M. R., Wiktorowicz, S. J., & Yung, Y. L. (2016). A multiple scattering polarized radiative transfer model: Application to HD 189733b. *The Astrophysical Journal*, *817*(1), 32. https://doi.org/10.3847/0004-637X/817/1/32

Kreidberg, L. (2018). Exoplanet atmosphere measurements from transmission spectroscopy and other planet star combined light observations. In H. J. Deeg& J. A.Belmonte (Eds.), *Handbook of exoplanets* (pp. 2083–2105). Cham: Springer International Publishing. Retrieved fromhttps://doi.org/10.1007/978-3-319-55333-7_100

Kreidberg, L., Bean, J. L., Désert, J.-M., Benneke, B., Deming, D., Stevenson, K. B., et al. (2014a). Clouds in the atmosphere of the super-Earth exoplanet GJ1214b. *Nature*, *505*(7481), 69–72. https://doi.org/10.1038/nature12888

Kreidberg, L., Bean, J. L., Désert, J.-M., Line, M. R., Fortney, J. J., Madhusudhan, N., et al. (2014b). A precise water abundance measurement for the hot Jupiter WASP-43b. *The Astrophysical Journal Letters*, *793*(2), L27. https://doi.org/10.1088/2041-8205/793/2/L27

Kreidberg, L., Koll, D. D. B., Morley, C., Hu, R., Schaefer, L., Deming, D., et al. (2019). Absence of a thick atmosphere on the terrestrial exoplanet LHS 3844b. *Nature*, *573*(7772), 87–90. https://doi.org/10.1038/s41586-019-1497-4

Kreidberg, L., Line, M. R., Parmentier, V., Stevenson, K. B., Louden, T., Bonnefoy, M., et al. (2018a). Global climate and atmospheric composition of the ultra-hot Jupiter WASP-103b from HST and Spitzer phase curve observations. *The Astronomical Journal*, *156*(1), 17. https://doi.org/10.3847/1538-3881/aac3df

Kreidberg, L., Line, M. R., Thorngren, D., Morley, C. V., & Stevenson, K. B. (2018b). Water, high-altitude condensates, and possible methane depletion in the atmosphere of the warm super-Neptune WASP-107b. *The Astrophysical Letter Letters*, *858*(1), L6. https://doi.org/10.3847/2041-8213/aabfce

Kreidberg, L., Mollière, P., Crossfield, I. J. M., Thorngren, D. P., Kawashima, Y., Morley, C. V., et al. (2020). *Tentative evidence for water vapor in the atmosphere of the Neptune-size exoplanet HD 106315 c*. arXiv e-prints, arXiv:2006.07444.

Lacy, B., & Burrows, A. (2020a). Prospects for directly imaging young giant planets at optical wavelengths. *The Astrophysical Journal*, *892*(2), 151. https://doi.org/10.3847/1538-4357/ab7017

Lacy, B. I., & Burrows, A. (2020b). JWST transit spectra. II. Constraining aerosol species, particle-size distributions, temperature, and metallicity for cloudy exoplanets. *The Astrophysical Journal*, *904*(1), 25. https://doi.org/10.3847/1538-4357/abbc6c

Laskina, O., Young, M. A., Kleiber, P. D., & Grassian, V. H. (2014). Infrared optical constants of organic aerosols: Organic acids and model humic-like substances (HULIS). *Aerosol Science and Technology*, *48*(6), 630–637. https://doi.org/10.1080/02786826.2014.904499

Lavie, B., Mendonça, J. M., Mordasini, C., Malik, M., Bonnefoy, M., Demory, B.-O., et al. (2017). HELIOS-RETRIEVAL: An open-source, nested sampling atmospheric retrieval code; application to the HR 8799 exoplanets and inferred constraints for planet formation. *The Astronomical Journal*, *154*(3), 91. https://doi.org/10.3847/1538-3881/aa7ed8

Lavvas, P., Griffith, C. A., & Yelle, R. V. (2011a). Condensation in Titan's atmosphere at the Huygens landing site. *Icarus*, *215*(2), 732–750. https://doi.org/10.1016/j.icarus.2011.06.040

Lavvas, P., & Koskinen, T. (2017). Aerosol properties of the atmospheres of extrasolar giant planets. *The Astrophysical Journal*, *847*(1), 32. https://doi.org/10.3847/1538-4357/aa88ce

Lavvas, P., Koskinen, T., Steinrueck, M. E., García Muñoz, A., & Showman, A. P. (2019). Photochemical hazes in sub-Neptunian atmospheres with a focus on GJ 1214b. *The Astrophysical Journal*, *878*(2), 118. https://doi.org/10.3847/1538-4357/ab204e

Lavvas, P., Lellouch, E., Strobel, D. F., Gurwell, M. A., Cheng, A. F., Young, L. A., & Gladstone, G. R. (2020). A major ice component in Pluto's haze. *Nature Astronomy*. https://doi.org/10.1038/s41550-020-01270-3

Lavvas, P., Sander, M., Kraft, M., & Imanaka, H. (2011b). Surface chemistry and particle shape: Processes for the evolution of aerosols in Titan's atmosphere. *The Astrophysical Journal*, *728*(2), 80. https://doi.org/10.1088/0004-637X/728/2/80

Lavvas, P., Yelle, R. V., Koskinen, T., Bazin, A., Vuitton, V., Vigren, E., et al. (2013). Aerosol growth in Titan's ionosphere. *Proceedings of the National Academy of Sciences*, *110*(8), 2729–2734.

Lecavelier Des Etangs, A., Pont, F., Vidal-Madjar, A., & Sing, D. (2008). Rayleigh scattering in the transit spectrum of HD 189733b. *Astronomy & Astrophysics*, *481*(2), L83–L86. https://doi.org/10.1051/0004-6361:200809388

Lee, G., Dobbs-Dixon, I., Helling, C., Bognar, K., & Woitke, P. (2016). Dynamic mineral clouds on HD 189733b. I. 3D RHD with kinetic, non-equilibrium cloud formation. *Astronomy & Astrophysics*, *594*, A48. https://doi.org/10.1051/0004-6361/201628606

Lee, G., Helling, C., Dobbs-Dixon, I., & Juncher, D. (2015). Modelling the local and global cloud formation on HD 189733b. *Astronomy & Astrophysics*, *580*, A12. https://doi.org/10.1051/0004-6361/201525982

Lee, G. K. H., Wood, K., Dobbs-Dixon, I., Rice, A., & Helling, C. (2017). Dynamic mineral clouds on HD 189733b. II. Monte Carlo radiative transfer for 3D cloudy exoplanet atmospheres: Combining scattering and emission spectra. *Astronomy & Astrophysics*, *601*, A22. https://doi.org/10.1051/0004-6361/201629804

Lee, J. M., Fletcher, L. N., & Irwin, P. G. J. (2012). Optimal estimation retrievals of the atmospheric structure and composition of HD 189733b from secondary eclipse spectroscopy. *Monthly Notices of the Royal Astronomical Society*, *420*(1), 170–182. https://doi.org/10.1111/j.1365-2966.2011.20013.x

Lee, J.-M., Heng, K., & Irwin, P. G. J. (2013). Atmospheric retrieval analysis of the directly imaged exoplanet HR 8799b. *The Astrophysical Journal*, *778*(2), 97. https://doi.org/10.1088/0004-637X/778/2/97

Lee, J.-M., Irwin, P. G. J., Fletcher, L. N., Heng, K., & Barstow, J. K. (2014). Constraining the atmospheric composition of the day-night terminators of HD 189733b: Atmospheric retrieval with aerosols. *The Astrophysical Journal*, *789*(1), 14. https://doi.org/10.1088/0004-637X/789/1/14

Leggett, S. K., Cushing, M. C., Hardegree-Ullman, K. K., Trucks, J. L., Marley, M. S., Morley, C. V., et al. (2016). Observed variability at 1 and 4 μm in the Y0 brown dwarf WISEP J173835.52+273258.9. *The Astrophysical Journal*, *830*(2), 141. https://doi.org/10.3847/0004-637X/830/2/141

Leggett, S. K., Morley, C. V., Marley, M. S., & Saumon, D. (2015). Near-infrared photometry of Y dwarfs: Low ammonia abundance and the onset of water clouds. *The Astrophysical Journal*, *799*(1), 37. https://doi.org/10.1088/0004-637X/799/1/37

Lew, B. W. P., Apai, D., Zhou, Y., Radigan, J., Marley, M., Schneider, G., et al. (2020). Cloud atlas: weak color modulations due to rotation in the planetary-mass companion GU Psc b and 11 other brown dwarfs. *The Astronomical Journal*, *159*(3), 125. https://doi.org/10.3847/1538-3881/ab5f59

Lew, B. W. P., Apai, D., Zhou, Y., Schneider, G., Burgasser, A. J., Karalidi, T., et al. (2016). Cloud atlas: discovery of patchy clouds and high-amplitude rotational modulations in a young, extremely red L-type brown dwarf. *The Astrophysical Journal Letters*, *829*(2), L32. https://doi.org/10.3847/2041-8205/829/2/L32

Lewis, J. S. (1969). The clouds of Jupiter and the NH_3—H_2O and NH_3—H_2S systems. *Icarus*, *10*(3), 365–378. https://doi.org/10.1016/0019-1035(69)90091-8

Lewis, N. K., Knutson, H. A., Showman, A. P., Cowan, N. B., Laughlin, G., Burrows, A., et al. (2013). Orbital phase variations of the eccentric giant planet HAT-P-2b. *The Astrophysical Journal*, *766*(2), 95. https://doi.org/10.1088/0004-637X/766/2/95

Li, C., & Chen, X. (2019). Simulating Nonhydrostatic Atmospheres on Planets (SNAP): Formulation, validation, and application to the Jovian atmosphere. *The Astrophysical Journal Supplement Series*, *240*(2), 37. https://doi.org/10.3847/1538-4365/aafdaa

Li, C., & Ingersoll, A. P. (2015). Moist convection in hydrogen atmospheres and the frequency of Saturn's giant storms. *Nature Geoscience*, *8*(5), 398–403. https://doi.org/10.1038/ngeo2405

Libby-Roberts, J. E., Berta-Thompson, Z. K., Désert, J.-M., Masuda, K., Morley, C. V., Lopez, E. D., et al. (2020). The featureless transmission spectra of two super-puff planets. *The Astronomical Journal*, *159*(2), 57. https://doi.org/10.3847/1538-3881/ab5d36

Lincowski, A. P., Meadows, V. S., Crisp, D., Robinson, T. D., Luger, R., Lustig-Yaeger, J., & Arney, G. N. (2018). Evolved climates and observational discriminants for the TRAPPIST-1 planetary system. *The Astrophysical Journal*, *867*(1), 76. https://doi.org/10.3847/1538-4357/aae36a

Line, M. R., Knutson, H., Wolf, A. S., & Yung, Y. L. (2014). A systematic retrieval analysis of secondary eclipse spectra. II. A uniform analysis of nine planets and their C to O ratios. *The Astrophysical Journal*, *783*(2), 70. https://doi.org/10.1088/0004-637X/783/2/70

Line, M. R., Marley, M. S., Liu, M. C., Burningham, B., Morley, C. V., Hinkel, N. R., et al. (2017). Uniform atmospheric retrieval analysis of ultracool dwarfs. II. Properties of 11 T dwarfs. *The Astrophysical Journal*, *848*(2), 83. https://doi.org/10.3847/1538-4357/aa7ff0

Line, M. R., & Parmentier, V. (2016). The influence of nonuniform cloud cover on transit transmission spectra. *The Astrophysical Journal*, *820*(1), 78. https://doi.org/10.3847/0004-637X/820/1/78

Line, M. R., Stevenson, K. B., Bean, J., Desert, J.-M., Fortney, J. J., Kreidberg, L., et al. (2016). No thermal inversion and a solar water abundance for the hot Jupiter HD 209458b from HST/WFC3 spectroscopy. *The Astronomical Journal*, *152*(6), 203. https://doi.org/10.3847/0004-6256/152/6/203

Lines, S., Manners, J., Mayne, N. J., Goyal, J., Carter, A. L., Boutle, I. A., et al. (2018a). Exonephology: Transmission spectra from a 3D simulated cloudy atmosphere of HD 209458b. *Monthly Notices of the Royal Astronomical Society*, *481*(1), 194–205. https://doi.org/10.1093/mnras/sty2275

Lines, S., Mayne, N. J., Boutle, I. A., Manners, J., Lee, G. K. H., Helling, C., et al. (2018b). *Simulating the cloudy atmospheres of HD 209458 b and HD 189733 b with the 3D Met Office Unified Model*. ArXiv e-prints.

Lines, S., Mayne, N. J., Manners, J., Boutle, I. A., Drummond, B., Mikal-Evans, T., et al. (2019). Overcast on Osiris: 3D radiative-hydrodynamical simulations of a cloudy hot Jupiter using the parametrized, phase-equilibrium cloud formation code EDDYSED. *Monthly Notices of the Royal Astronomical Society*, *488*(1), 1332–1355. https://doi.org/10.1093/mnras/stz1788

Liu, M. C., Dupuy, T. J., & Allers, K. N. (2016). The Hawaii infrared parallax program. II. Young ultracool field dwarfs. *The Astrophysical Journal*, *833*(1), 96. https://doi.org/10.3847/1538-4357/833/1/96

Lockwood, A. C., Johnson, J. A., Bender, C. F., Carr, J. S., Barman, T., Richert, A. J. W., & Blake, G. A. (2014). Near-IR direct detection of water vapor in Tau Boötis b. *The Astrophysical Journal Letters*, *783*(2), L29. https://doi.org/10.1088/2041-8205/783/2/L29

Lodders, K. (1999). Alkali element chemistry in cool dwarf atmospheres. *The Astrophysical Journal*, *519*(2), 793.

Lodders, K. (2002). Titanium and vanadium chemistry in low-mass dwarf stars. *The Astrophysical Journal*, *577*(2), 974–985. https://doi.org/10.1086/342241

Lodders, K. (2010). Solar system abundances of the elements. *Astrophysics and Space Science Proceedings*, *16*, 379. https://doi.org/10.1007/978-3-642-10352-0_8

Lodders, K., & Fegley, B. (1998). *The planetary scientist's companion/Katharina Lodders, Bruce Fegley*. New York, NY: Oxford University Press.

Lodders, K., & Fegley, B. (2002). Atmospheric chemistry in giant planets, brown dwarfs, and low-mass dwarf stars. I. Carbon, nitrogen, and oxygen. *Icarus*, *155*(2), 393–424. https://doi.org/10.1006/icar.2001.6740

Lodders, K., & Fegley, B., Jr. (2006). Chemistry of low mass substellar objects. In J. W. Mason (Ed.), Astrophysics update (Vol. 2, p. 1), Springer Praxis Books. Springer, Berlin, Heidelberg. https://doi.org/10.1007/3-540-30313-8_1

Loftus, K., Wordsworth, R. D., & Morley, C. V. (2019). Sulfate aerosol hazes and SO_2 gas as constraints on rocky exoplanets' surface liquid water. *The Astrophysical Journal*, *887*(2), 231. https://doi.org/10.3847/1538-4357/ab58cc

Looper, D. L., Kirkpatrick, J. D., Cutri, R. M., Barman, T., Burgasser, A. J., Cushing, M. C., et al. (2008). Discovery of two nearby peculiar L dwarfs from the 2MASS proper-motion survey: Young or metal-rich? *The Astrophysical Journal*, *686*(1), 528–541. https://doi.org/10.1086/591025

Lora, J. M., Kataria, T., & Gao, P. (2018). Atmospheric circulation, chemistry, and infrared spectra of Titan-like exoplanets around different stellar types. *The Astrophysical Journal*, *853*(1), 58. https://doi.org/10.3847/1538-4357/aaa132
Lothringer, J. D., Barman, T., & Koskinen, T. (2018). Extremely irradiated hot Jupiters: Non-oxide inversions, H^- opacity, and thermal dissociation of molecules. *The Astrophysical Journal*, *866*(1), 27. https://doi.org/10.3847/1538-4357/aadd9e
Lothringer, J. D., Fu, G., Sing, D. K., & Barman, T. S. (2020). UV exoplanet transmission spectral features as probes of metals and rainout. *The Astrophysical Journal Letters*, *898*(1), L14. https://doi.org/10.3847/2041-8213/aba265
Luger, R., & Barnes, R. (2015). Extreme water loss and abiotic O_2 buildup on planets throughout the habitable zones of M dwarfs. *Astrobiology*, *15*(2), 119–143. https://doi.org/10.1089/ast.2014.1231
Lunine, J. I. (1993). The atmospheres of Uranus and Neptune. *Annual Review of Astronomy and Astrophysics*, *31*, 217–263. https://doi.org/10.1146/annurev.aa.31.090193.001245
Lunine, J. I., Hubbard, W. B., Burrows, A., Wang, Y. P., & Garlow, K. (1989). The effect of gas and grain opacity on the cooling of brown dwarfs. *The Astrophysical Journal*, *338*, 314. https://doi.org/10.1086/167201
Lupu, R. E., Marley, M. S., Lewis, N., Line, M., Traub, W. A., & Zahnle, K. (2016). Developing atmospheric retrieval methods for direct imaging spectroscopy of gas giants in reflected light. I. Methane abundances and basic cloud properties. *The Astronomical Journal*, *152*(6), 217. https://doi.org/10.3847/0004-6256/152/6/217
Lustig-Yaeger, J., Meadows, V. S., & Lincowski, A. P. (2019). The detectability and characterization of the TRAPPIST-1 exoplanet atmospheres with JWST. *The Astronomical Journal*, *158*(1), 27. https://doi.org/10.3847/1538-3881/ab21e0
MacDonald, R. J., & Madhusudhan, N. (2017). HD 209458b in new light: Evidence of nitrogen chemistry, patchy clouds and sub-solar water. *Monthly Notices of the Royal Astronomical Society*, *469*(2), 1979–1996. https://doi.org/10.1093/mnras/stx804
MacDonald, R. J., Marley, M. S., Fortney, J. J., & Lewis, N. K. (2018). Exploring H_2O prominence in reflection spectra of cool giant planets. *The Astrophysical Journal*, *858*(2), 69. https://doi.org/10.3847/1538-4357/aabb05
Macintosh, B., Graham, J. R., Barman, T., De Rosa, R. J., Konopacky, Q., Marley, M. S., et al. (2015). Discovery and spectroscopy of the young Jovian planet 51 Eri b with the Gemini Planet Imager. *Science*, *350*(6256), 64–67. https://doi.org/10.1126/science.aac5891
Mahapatra, G., Helling, C., & Miguel, Y. (2017). Cloud formation in metal-rich atmospheres of hot super-Earths like 55 Cnc e and CoRoT7b. *Monthly Notices of the Royal Astronomical Society*, *472*(1), 447–464. https://doi.org/10.1093/mnras/stx1666
Mai, C., & Line, M. R. (2019). Exploring exoplanet cloud assumptions in JWST transmission spectra. *The Astrophysical Journal*, *883*(2), 144. https://doi.org/10.3847/1538-4357/ab3e6d
Majeau, C., Agol, E., & Cowan, N. B. (2012). A two-dimensional infrared map of the extrasolar planet HD 189733b. *The Astrophysical Journal Letters*, *747*(2), L20. https://doi.org/10.1088/2041-8205/747/2/L20
Mallonn, M., Köhler, J., Alexoudi, X., von Essen, C., Granzer, T., Poppenhaeger, K., & Strassmeier, K. G. (2019). Low albedos of hot to ultra-hot Jupiters in the optical to near-infrared transition regime. *Astronomy & Astrophysics*, *624*, A62. https://doi.org/10.1051/0004-6361/201935079
Manjavacas, E., Apai, D., Lew, B. W. P., Zhou, Y., Schneider, G., Burgasser, A. J., et al. (2019). Cloud Atlas: Rotational Spectral Modulations and Potential Sulfide Clouds in the Planetary-mass, Late T-type Companion Ross 458C. *The Astrophysical Journal Letters*, *875*(2), L15. https://doi.org/10.3847/2041-8213/ab13b9
Manjavacas, E., Apai, D., Zhou, Y., Karalidi, T., Lew, B. W. P., Schneider, G., et al. (2018). Cloud Atlas: Discovery of Rotational Spectral Modulations in a Low-mass, L-type Brown Dwarf Companion to a Star. *The Astronomical Journal*, *155*(1), 11. https://doi.org/10.3847/1538-3881/aa984f
Marley, M. S., Ackerman, A. S., Cuzzi, J. N., & Kitzmann, D. (2013). Clouds and hazes in exoplanet atmospheres. In S. J. Mackwell, A. A. Simon-Miller, J. W. Harder, M. A.Bullock (Eds.), *Comparative climatology of terrestrial planets* (pp. 367–391). Phoenix: University of Arizona Press. https://doi.org/10.2458/azu_uapress_9780816530595-ch015
Marley, M. S., Gelino, C., Stephens, D., Lunine, J. I., & Freedman, R. (1999). Reflected spectra and albedos of extrasolar giant planets. I. Clear and cloudy atmospheres. *The Astrophysical Journal*, *513*(2), 879–893. https://doi.org/10.1086/306881
Marley, M. S., Saumon, D., Cushing, M., Ackerman, A. S., Fortney, J. J., & Freedman, R. (2012). Masses, radii, and cloud properties of the HR 8799 planets. *The Astrophysical Journal*, *754*(2), 135. https://doi.org/10.1088/0004-637X/754/2/135
Marley, M. S., Saumon, D., & Goldblatt, C. (2010). A patchy cloud model for the L to T dwarf transition. *The Astrophysical Journal Letters*, *723*(1), L117–L121. https://doi.org/10.1088/2041-8205/723/1/L117
Marley, M. S., Saumon, D., Guillot, T., Freedman, R. S., Hubbard, W. B., Burrows, A., & Lunine, J. I. (1996). Atmospheric, evolutionary, and spectral models of the brown dwarf Gliese 229 B. *Science*, *272*(5270), 1919–1921. https://doi.org/10.1126/science.272.5270.1919
Marley, M. S., Seager, S., Saumon, D., Lodders, K., Ackerman, A. S., Freedman, R. S., & Fan, X. (2002). Clouds and chemistry: Ultracool dwarf atmospheric properties from optical and infrared colors. *The Astrophysical Journal*, *568*(1), 335–342. https://doi.org/10.1086/338800
Marley, M. S., & Sengupta, S. (2011). Probing the physical properties of directly imaged gas giant exoplanets through polarization. *Monthly Notices of the Royal Astronomical Society*, *417*(4), 2874–2881. https://doi.org/10.1111/j.1365-2966.2011.19448.x
Marois, C., Macintosh, B., Barman, T., Zuckerman, B., Song, I., Patience, J., et al. (2008). Direct imaging of multiple planets orbiting the star HR 8799. *Science*, *322*(5906), 1348. https://doi.org/10.1126/science.1166585
Martínez, G. M., Newman, C. N., De Vicente-Retortillo, A., Fischer, E., Renno, N. O., Richardson, M. I., et al. (2017). The modern near-surface Martian climate: A review of in-situ meteorological data from Viking to Curiosity. *Space Science Reviews*, *212*(1–2), 295–338. https://doi.org/10.1007/s11214-017-0360-x
Masuda, K. (2014). Very low density planets around Kepler-51 revealed with transit timing variations and an anomaly similar to a planet-planet eclipse event. *The Astrophysical Journal*, *783*(1), 53. https://doi.org/10.1088/0004-637X/783/1/53
May, E. M., Gardner, T., Rauscher, E., & Monnier, J. D. (2020). MOPSS. II. Extreme optical scattering slope for the inflated super-Neptune HATS-8b. *The Astronomical Journal*, *159*(1), 7. https://doi.org/10.3847/1538-3881/ab5361
Mayorga, L. C., Batalha, N. E., Lewis, N. K., & Marley, M. S. (2019). Reflected light phase curves in the TESS era. *The Astronomical Journal*, *158*(2), 66. https://doi.org/10.3847/1538-3881/ab29fa
Mayorga, L. C., Jackiewicz, J., Rages, K., West, R. A., Knowles, B., Lewis, N., & Marley, M. S. (2016). Jupiter's phase variations from Cassini: A testbed for future direct-imaging missions. *The Astronomical Journal*, *152*(6), 209. https://doi.org/10.3847/0004-6256/152/6/209
Mbarek, R., & Kempton, E. M. R. (2016). Clouds in super-Earth atmospheres: Chemical equilibrium calculations. *The Astrophysical Journal*, *827*(2), 121. https://doi.org/10.3847/0004-637X/827/2/121
McGruder, C. D., López-Morales, M., Espinoza, N., Rackham, B. V., Apai, D., Jordán, A., et al. (2020). ACCESS: Confirmation of no potassium in the atmosphere of WASP-31b. *The Astronomical Journal*, *160*(5), 230. https://doi.org/10.3847/1538-3881/abb806
McKay, C. P., Pollack, J. B., & Courtin, R. (1989). The thermal structure of Titan's atmosphere. *Icarus*, *80*(1), 23–53. https://doi.org/10.1016/0019-1035(89)90160-7

Mendonça, J. M., Tsai, S.-M., Malik, M., Grimm, S. L., & Heng, K. (2018). Three-dimensional circulation driving chemical disequilibrium in WASP-43b. *The Astrophysical Journal*, *869*(2), 107. https://doi.org/10.3847/1538-4357/aaed23
Menou, K. (2019). Turbulent vertical mixing in hot exoplanet atmospheres. *Monthly Notices of the Royal Astronomical Society*, *485*(1), L98–L103. https://doi.org/10.1093/mnrasl/slz041
Metchev, S. A., Heinze, A., Apai, D., Flateau, D., Radigan, J., Burgasser, A., et al. (2015). Weather on other worlds. II. Survey results: Spots are ubiquitous on L and T dwarfs. *The Astrophysical Journal*, *799*(2), 154. https://doi.org/10.1088/0004-637X/799/2/154
Miguel, Y., Kaltenegger, L., Fegley, B., & Schaefer, L. (2011). Compositions of hot super-Earth atmospheres: Exploring Kepler candidates. *The Astrophysical Journal Letters*, *742*(2), L19. https://doi.org/10.1088/2041-8205/742/2/L19
Mikal-Evans, T., Sing, D. K., Goyal, J. M., Drummond, B., Carter, A. L., Henry, G. W., et al. (2019). An emission spectrum for WASP-121b measured across the 0.8–1.1 μm wavelength range using the Hubble Space Telescope. *Monthly Notices of the Royal Astronomical Society*, *488*(2), 2222–2234. https://doi.org/10.1093/mnras/stz1753
Miles-Páez, P. A., Metchev, S., Apai, D., Zhou, Y., Manjavacas, E., Karalidi, T., et al. (2019). Cloud atlas: Variability in and out of the water band in the planetary-mass HD 203030B points to cloud sedimentation in low-gravity L dwarfs. *The Astrophysical Journal*, *883*(2), 181. https://doi.org/10.3847/1538-4357/ab3d25
Millar-Blanchaer, M. A., Girard, J. H., Karalidi, T., Marley, M. S., van Holstein, R. G., Sengupta, S., et al. (2020). Detection of polarization due to cloud bands in the nearby Luhman 16 brown dwarf binary. *The Astrophysical Journal*, *894*(1), 42. https://doi.org/10.3847/1538-4357/ab6ef2
Mills, F. P., Esposito, L. W., & Yung, Y. L. (2007). Atmospheric composition, chemistry, and clouds. In L. W. Esposito, E. R. Stofan, & T. E. Cravens (Eds.), *Exploring Venus as a terrestrial planet* (pp. 73–100). Washington, DC, USA: American Geophysical Union.
Misra, A., Krissansen-Totton, J., Koehler, M. C., & Sholes, S. (2015). Transient sulfate aerosols as a signature of exoplanet volcanism. *Astrobiology*, *15*(6), 462–477. https://doi.org/10.1089/ast.2014.1204
Močnik, T., Hellier, C., & Southworth, J. (2018). WASP-104b is darker than charcoal. *The Astronomical Journal*, *156*(2), 44. https://doi.org/10.3847/1538-3881/aacb26
Mollière, P., Stolker, T., Lacour, S., Otten, G. P. P. L., Shangguan, J., Charnay, B., et al. (2020). *Retrieving scattering clouds and disequilibrium chemistry in the atmosphere of HR 8799e*. arXiv e-prints, arXiv:2006.09394.
Mollière, P., Wardenier, J. P., van Boekel, R., Henning, T., Molaverdikhani, K., & Snellen, I. A. G. (2019). petitRADTRANS. A Python radiative transfer package for exoplanet characterization and retrieval. *Astronomy & Astrophysics*, *627*, A67. https://doi.org/10.1051/0004-6361/201935470
Montmessin, F., Gondet, B., Bibring, J.-P., Langevin, Y., Drossart, P., Forget, F., & Fouchet, T. (2007). Hyperspectral imaging of convective CO_2 ice clouds in the equatorial mesosphere of Mars. *Journal of Geophysical Research*, *112*(E11). https://doi.org/10.1029/2007JE002944
Moran, S. E., Hörst, S. M., Batalha, N. E., Lewis, N. K., & Wakeford, H. R. (2018). Limits on clouds and hazes for the TRAPPIST-1 planets. *The Astronomical Journal*, *156*(6), 252. https://doi.org/10.3847/1538-3881/aae83a
Moran, S. E., Hörst, S. M., Vuitton, V., He, C., Lewis, N. K., Flandinet, L., et al. (2020). Chemistry of temperate super-Earth and mini-Neptune atmospheric hazes from laboratory experiments. *The Planetary Science Journal*, *1*(1), 17. https://doi.org/10.3847/PSJ/ab8eae
Morley, C. V., Fortney, J. J., Kempton, E. M. R., Marley, M. S., Visscher, C., & Zahnle, K. (2013). Quantitatively assessing the role of clouds in the transmission spectrum of GJ 1214b. *The Astrophysical Journal*, *775*(1), 33. https://doi.org/10.1088/0004-637X/775/1/33
Morley, C. V., Fortney, J. J., Marley, M. S., Visscher, C., Saumon, D., & Leggett, S. K. (2012). Neglected clouds in T and Y dwarf atmospheres. *The Astrophysical Journal*, *756*(2), 172. https://doi.org/10.1088/0004-637X/756/2/172
Morley, C. V., Fortney, J. J., Marley, M. S., Zahnle, K., Line, M., Kempton, E., et al. (2015). Thermal emission and reflected light spectra of super Earths with flat transmission spectra. *The Astrophysical Journal*, *815*(2), 110. https://doi.org/10.1088/0004-637X/815/2/110
Morley, C. V., Marley, M. S., Fortney, J. J., & Lupu, R. (2014a). Spectral variability from the patchy atmospheres of T and Y dwarfs. *The Astrophysical Journal Letters*, *789*(1), L14. https://doi.org/10.1088/2041-8205/789/1/L14
Morley, C. V., Marley, M. S., Fortney, J. J., Lupu, R., Saumon, D., Greene, T., & Lodders, K. (2014b). Water clouds in Y dwarfs and exoplanets. *The Astrophysical Journal*, *787*(1), 78. https://doi.org/10.1088/0004-637X/787/1/78
Morley, C. V., Skemer, A. J., Allers, K. N., Marley, M. S., Faherty, J. K., Visscher, C., et al. (2018). An L band spectrum of the coldest brown dwarf. *The Astrophysical Journal*, *858*(2), 97. https://doi.org/10.3847/1538-4357/aabe8b
Moses, J. I., Line, M. R., Visscher, C., Richardson, M. R., Nettelmann, N., Fortney, J. J., et al. (2013). Compositional diversity in the atmospheres of hot Neptunes, with application to GJ 436b. *The Astrophysical Journal*, *777*(1), 34. https://doi.org/10.1088/0004-637X/777/1/34
Moses, J. I., Marley, M. S., Zahnle, K., Line, M. R., Fortney, J. J., Barman, T. S., et al. (2016). On the composition of young, directly imaged giant planets. *The Astrophysical Journal*, *829*(2), 66. https://doi.org/10.3847/0004-637X/829/2/66
Moses, J. I., & Poppe, A. R. (2017). Dust ablation on the giant planets: Consequences for stratospheric photochemistry. *Icarus*, *297*, 33–58. https://doi.org/10.1016/j.icarus.2017.06.002
Müller, A., Keppler, M., Henning, T., Samland, M., Chauvin, G., Beust, H., et al. (2018). Orbital and atmospheric characterization of the planet within the gap of the PDS 70 transition disk. *Astronomy & Astrophysics*, *617*, L2. https://doi.org/10.1051/0004-6361/201833584
Niraula, P., Redfield, S., de Wit, J., Dai, F., Mireles, I., Serindag, D., & Shporer, A. (2018). *Discovery of six optical phase curves with K2*. arXiv e-prints, arXiv:1812.09227.
Nugroho, S. K., Gibson, N. P., de Mooij, E. J. W., Watson, C. A., Kawahara, H., & Merritt, S. (2020). *Searching for thermal inversion agents in the transmission spectrum of MASCARA-2b/KELT-20b: Detection of neutral iron and ionised calcium H&K lines*. arXiv e-prints, arXiv:2003.04856.
Ohno, K., & Kawashima, Y. (2020). Super-Rayleigh slopes in transmission spectra of exoplanets generated by photochemical haze. *The Astrophysical Journal Letters*, *895*(2), L47. https://doi.org/10.3847/2041-8213/ab93d7
Ohno, K., & Okuzumi, S. (2017). A condensation-coalescence cloud model for exoplanetary atmospheres: Formulation and test applications to terrestrial and Jovian clouds. *The Astrophysical Journal*, *835*(2), 261. https://doi.org/10.3847/1538-4357/835/2/261
Ohno, K., & Okuzumi, S. (2018). Microphysical modeling of mineral clouds in GJ1214 b and GJ436 b: Predicting upper limits on the cloud-top height. *The Astrophysical Journal*, *859*(1), 34. https://doi.org/10.3847/1538-4357/aabee3
Ohno, K., Okuzumi, S., & Tazaki, R. (2020a). Clouds of fluffy aggregates: How they form in exoplanetary atmospheres and influence transmission spectra. *The Astrophysical Journal*, *891*(2), 131. https://doi.org/10.3847/1538-4357/ab44bd
Ohno, K., Zhang, X., Tazaki, R., & Okuzumi, S. (2020b). *Haze formation on Triton*. arXiv e-prints, arXiv:2012.11932.
Ormel, C. W., & Min, M. (2019). ARCiS framework for exoplanet atmospheres. The cloud transport model. *Astronomy & Astrophysics*, *622*, A121. https://doi.org/10.1051/0004-6361/201833678
Oxtoby, D. W. (1992). Homogeneous nucleation: Theory and experiment. *Journal of Physics: Condensed Matter*, *4*(38), 7627–7650. https://doi.org/10.1088/0953-8984/4/38/001

Parisi, A. V., & Downs, N. (2004). Variation of the enhanced biologically damaging solar UV due to clouds. *Photochemical and Photobiological Sciences*, *3*(7), 643–647. https://doi.org/10.1039/B402035A

Parmentier, V., & Crossfield, I. J. M. (2018). Exoplanet phase curves: Observations and theory. In H. J. Deeg& J. A.Belmonte (Eds.), *Handbook of exoplanets* (pp. 1419–1440). Cham: Springer International Publishing. Retrieved from https://doi.org/10.1007/978-3-319-55333-7_116

Parmentier, V., Fortney, J. J., Showman, A. P., Morley, C., & Marley, M. S. (2016). Transitions in the cloud composition of hot Jupiters. *The Astrophysical Journal*, *828*(1), 22. https://doi.org/10.3847/0004-637X/828/1/22

Parmentier, V., & Guillot, T. (2014). A non-grey analytical model for irradiated atmospheres. I. Derivation. *Astronomy & Astrophysics*, *562*, A133. https://doi.org/10.1051/0004-6361/201322342

Parmentier, V., Line, M. R., Bean, J. L., Mansfield, M., Kreidberg, L., Lupu, R., et al. (2018). From thermal dissociation to condensation in the atmospheres of ultra hot Jupiters: WASP-121b in context. *Astronomy & Astrophysics*, *617*, A110. https://doi.org/10.1051/0004-6361/201833059

Parmentier, V., Showman, A. P., & Fortney, J. J. (2021). The cloudy shape of hot Jupiter thermal phase curves. *Monthly Notices of the Royal Astronomical Society*, *501*(1), 78–108. https://doi.org/10.1093/mnras/staa3418

Parmentier, V., Showman, A. P., & Lian, Y. (2013). 3D mixing in hot Jupiters atmospheres. I. Application to the day/night cold trap in HD 209458b. *Astronomy &Astrophysics*, *558*, A91. https://doi.org/10.1051/0004-6361/201321132

Pavlov, A. A., Brown, L. L., & Kasting, J. F. (2001). UV shielding of NH_3 and O_2 by organic hazes in the Archean atmosphere. *Journal of Geophysical Research*, *106*(E10), 23267–23288. https://doi.org/10.1029/2000JE001448

Pinhas, A., & Madhusudhan, N. (2017). On signatures of clouds in exoplanetary transit spectra. *Monthly Notices of the Royal Astronomical Society*, *471*(4), 4355–4373. https://doi.org/10.1093/mnras/stx1849

Pinhas, A., Madhusudhan, N., Gandhi, S., & MacDonald, R. (2019). H_2O abundances and cloud properties in ten hot giant exoplanets. *Monthly Notices of the Royal Astronomical Society*, *482*(2), 1485–1498. https://doi.org/10.1093/mnras/sty2544

Pino, L., Ehrenreich, D., Allart, R., Lovis, C., Brogi, M., Malik, M., et al. (2018). Diagnosing aerosols in extrasolar giant planets with cross-correlation function of water bands. *Astronomy & Astrophysics*, *619*, A3. https://doi.org/10.1051/0004-6361/201832986

Piskorz, D., Benneke, B., Crockett, N. R., Lockwood, A. C., Blake, G. A., Barman, T. S., et al. (2016). Evidence for the direct detection of the thermal spectrum of the non-transiting hot gas giant HD 88133 b. *The Astrophysical Journal*, *832*(2), 131. https://doi.org/10.3847/0004-637X/832/2/131

Piskorz, D., Benneke, B., Crockett, N. R., Lockwood, A. C., Blake, G. A., Barman, T. S., et al. (2017). Detection of water vapor in the thermal spectrum of the non-transiting hot Jupiter Upsilon Andromedae b. *The Astronomical Journal*, *154*(2), 78. https://doi.org/10.3847/1538-3881/aa7dd8

Pont, F., Knutson, H., Gilliland, R. L., Moutou, C., & Charbonneau, D. (2008). Detection of atmospheric haze on an extrasolar planet: The 0.55–1.05 μm transmission spectrum of HD 189733b with the Hubble Space Telescope. *Monthly Notices of the Royal Astronomical Society*, *385*(1), 109–118. https://doi.org/10.1111/j.1365-2966.2008.12852.x

Pont, F., Sing, D. K., Gibson, N. P., Aigrain, S., Henry, G., & Husnoo, N. (2013). The prevalence of dust on the exoplanet HD 189733b from Hubble and Spitzer observations. *Monthly Notices of the Royal Astronomical Society*, *432*(4), 2917–2944. https://doi.org/10.1093/mnras/stt651

Posch, T., Kerschbaum, F., Fabian, D., Mutschke, H., Dorschner, J., Tamanai, A., & Henning, T. (2003). Infrared properties of solid titanium oxides: Exploring potential primary dust condensates. *The Astrophysical Journal Supplement Series*, *149*(2), 437–445. https://doi.org/10.1086/379167

Powell, D., Louden, T., Kreidberg, L., Zhang, X., Gao, P., & Parmentier, V. (2019). Transit signatures of inhomogeneous clouds on hot Jupiters: Insights from microphysical cloud modeling. *The Astrophysical Journal*, *887*(2), 170. https://doi.org/10.3847/1538-4357/ab55d9

Powell, D., Zhang, X., Gao, P., & Parmentier, V. (2018). *Formation of silicate and titanium clouds on hot Jupiters*. ArXiv e-prints.

Pruppacher, H. R., & Klett, J. D. (1978). *Microphysics of clouds and precipitation*. Dordrecht, Holland: D. Reidel Publishing Company.

Querry, M. R. (1987). *Optical constants of minerals and other materials from the millimeter to the ultraviolet*. Dover, New Jersey, USA: U.S. Army Armament, Munitions Chemical Research.

Radigan, J. (2014). An independent analysis of the brown dwarf atmosphere monitoring (BAM) data: Large-amplitude variability is rare outside the L/T transition. *The Astrophysical Journal*, *797*(2), 120. https://doi.org/10.1088/0004-637X/797/2/120

Radigan, J., Jayawardhana, R., Lafrenière, D., Artigau É., Marley, M., & Saumon, D. (2012). Large-amplitude variations of an L/T transition brown dwarf: Multi-wavelength observations of patchy, high-contrast cloud features. *The Astrophysical Journal*, *750*(2), 105. https://doi.org/10.1088/0004-637X/750/2/105

Radigan, J., Lafrenière, D., Jayawardhana, R., & Artigau, E. (2014). Strong brightness variations signal cloudy-to-clear transition of brown dwarfs. *The Astrophysical Journal*, *793*(2), 75. https://doi.org/10.1088/0004-637X/793/2/75

Rages, K., & Pollack, J. B. (1992). Voyager imaging of Triton's clouds and hazes. *Icarus*, *99*(2), 289–301. https://doi.org/10.1016/0019-1035(92)90147-Y

Rajan, A., Patience, J., Wilson, P. A., Bulger, J., De Rosa, R. J., Ward-Duong, K., et al. (2015). The brown dwarf atmosphere monitoring (BAM) project - II. Multi-epoch monitoring of extremely cool brown dwarfs. *Monthly Notices of the Royal Astronomical Society*, *448*(4), 3775–3783. https://doi.org/10.1093/mnras/stv181

Rajan, A., Rameau, J., De Rosa, R. J., Marley, M. S., Graham, J. R., Macintosh, B., et al. (2017). Characterizing 51 ERI b from 1 to 5 μm: A partly cloudy exoplanet. *The Astronomical Journal*, *154*(1), 10. https://doi.org/10.3847/1538-3881/aa74db

Reed, N. W., Browne, E. C., & Tolbert, M. A. (2020). Impact of hydrogen sulfide on photochemical haze formation in methane/nitrogen atmospheres. *ACS Earth and Space Chemistry*, *4*(6), 897–904. https://doi.org/10.1021/acsearthspacechem.0c00086

Ribas, I., Tuomi, M., Reiners, A., Butler, R. P., Morales, J. C., Perger, M., et al. (2018). A candidate super-Earth planet orbiting near the snow line of Barnard's star. *Nature*, *563*(7731), 365–368. https://doi.org/10.1038/s41586-018-0677-y

Robinson, T. D., Maltagliati, L., Marley, M. S., & Fortney, J. J. (2014). Titan solar occultation observations reveal transit spectra of a hazy world. *Proceedings of the National Academy of Science*, *111*(25), 9042–9047. https://doi.org/10.1073/pnas.1403473111

Rogers, T. M. (2017). Constraints on the magnetic field strength of HAT-P-7 b and other hot giant exoplanets. *Nature Astronomy*, *1*, 0131. https://doi.org/10.1038/s41550-017-0131

Rogers, T. M., & Komacek, T. D. (2014). Magnetic effects in hot Jupiter atmospheres. *The Astrophysical Journal*, *794*(2), 132. https://doi.org/10.1088/0004-637X/794/2/132

Roman, M., & Rauscher, E. (2017). Modeling the effects of inhomogeneous aerosols on the hot Jupiter Kepler-7b's atmospheric circulation. *The Astrophysical Journal*, *850*(1), 17. https://doi.org/10.3847/1538-4357/aa8ee4

Roman, M., & Rauscher, E. (2019). Modeled temperature-dependent clouds with radiative feedback in hot Jupiter atmospheres. *The Astrophysical Journal*, *872*(1), 1. https://doi.org/10.3847/1538-4357/aafdb5

Roman, M. T., Kempton, E. M. R., Rauscher, E., Harada, C. K., Bean, J. L., & Stevenson, K. B. (2020). *Clouds in three-dimensional models of hot Jupiters over a wide range of temperatures I: Thermal structures and broadband phase curve predictions*. arXiv e-prints, arXiv:2010.06936.

Romani, P., & Atreya, S. (1988). Methane photochemistry and haze production on neptune. *Icarus*, *74*(3), 424–445. https://doi.org/10.1016/0019-1035(88)90113-3

Rosenfeld, D., Andreae, M. O., Asmi, A., Chin, M., de Leeuw, G., Donovan, D. P., et al. (2014). Global observations of aerosol-cloud-precipitation-climate interactions. *Reviews of Geophysics*, *52*(4), 750–808. https://doi.org/10.1002/2013RG000441

Rossow, W. B. (1978). Cloud microphysics: Analysis of the clouds of Earth, Venus, Mars, and Jupiter. *Icarus*, *36*(3), 1–50.

Rowe, J. F., Matthews, J. M., Seager, S., Miller-Ricci, E., Sasselov, D., Kuschnig, R., et al. (2008). The very low albedo of an extrasolar planet: MOST space-based photometry of HD 209458. *The Astrophysical Journal*, *689*(2), 1345–1353. https://doi.org/10.1086/591835

Sagan, C., Thompson, W. R., & Khare, B. N. (1992). Titan: A laboratory for prebiological organic chemistry. *Accounts of Chemical Research*, *25*(7), 286–292. https://doi.org/10.1021/ar00019a003

Samland, M., Mollière, P., Bonnefoy, M., Maire, A. L., Cantalloube, F., Cheetham, A. C., et al. (2017). Spectral and atmospheric characterization of 51 Eridani b using VLT/SPHERE. *Astronomy & Astrophysics*, *603*, A57. https://doi.org/10.1051/0004-6361/201629767

Samra, D., Helling, C., & Min, M. (2020). *Mineral snowflakes on exoplanets and brown dwarfs: Effects of micro-porosity, size distributions, and particle shape*. arXiv e-prints, arXiv:2004.13502.

Sánchez-López, A., López-Puertas, M., Snellen, I. A. G., Nagel, E., Bauer, F. F., Pallé, E., et al. (2020). Discriminating between hazy and clear hot-Jupiter atmospheres with CARMENES. *Astronomy & Astrophysics*, *643*, A24. https://doi.org/10.1051/0004-6361/202038629

Sanghavi, S., & Shporer, A. (2018). Photopolarimetric characteristics of brown dwarfs. I. uniform cloud decks. *The Astrophysical Journal*, *866*(1), 28. https://doi.org/10.3847/1538-4357/aadf94

Saumon, D., Hubbard, W. B., Burrows, A., Guillot, T., Lunine, J. I., & Chabrier, G. (1996). A theory of extrasolar giant planets. *The Astrophysical Journal*, *460*, 993. https://doi.org/10.1086/177027

Saumon, D., & Marley, M. S. (2008). The evolution of L and T dwarfs in color–magnitude diagrams. *The Astrophysical Journal*, *689*(2), 1327–1344. https://doi.org/10.1086/592734

Schaefer, L., & Fegley, B. (2009). Chemistry of silicate atmospheres of evaporating super-Earths. *The Astrophysical Journal Letters*, *703*(2), L113–L117. https://doi.org/10.1088/0004-637X/703/2/L113

Schaefer, L., Lodders, K., & Fegley, B. (2012). Vaporization of the Earth: Application to exoplanet atmospheres. *The Astrophysical Journal*, *755*(1), 41. https://doi.org/10.1088/0004-637X/755/1/41

Schlawin, E., Burgasser, A. J., Karalidi, T., Gizis, J. E., & Teske, J. (2017). Spectral variability of two rapidly rotating brown dwarfs: 2MASS J08354256-0819237 and 2MASS J18212815+1414010. *The Astrophysical Journal*, *849*(2), 163. https://doi.org/10.3847/1538-4357/aa90b8

Seager, S., & Sasselov, D. D. (1998). Extrasolar giant planets under strong stellar irradiation. *The Astrophysical Journal Letters*, *502*(2), L157–L161. https://doi.org/10.1086/311498

Seager, S., & Sasselov, D. D. (2000). Theoretical transmission spectra during extrasolar giant planet transits. *The Astrophysical Journal*, *537*(2), 916–921. https://doi.org/10.1086/309088

Seager, S., Whitney, B. A., & Sasselov, D. D. (2000). Photometric light curves and polarization of close-in extrasolar giant planets. *The Astrophysical Journal*, *540*(1), 504–520. https://doi.org/10.1086/309292

Sedaghati, E., Boffin, H. M. J., MacDonald, R. J., Gandhi, S., Madhusudhan, N., Gibson, N. P., et al. (2017). Detection of titanium oxide in the atmosphere of a hot Jupiter. *Nature*, *549*(7671), 238–241. https://doi.org/10.1038/nature23651

Seidel, J. V., Lendl, M., Bourrier, V., Ehrenreich, D., Allart, R., Sousa, S. G., et al. (2020). Hot Exoplanet Atmospheres Resolved with Transit Spectroscopy (HEARTS). VI. Non-detection of sodium with HARPS on the bloated super-Neptune WASP-127b. *Astronomy & Astrophysics*, *643*, A45. https://doi.org/10.1051/0004-6361/202039058

Sengupta, S., & Krishan, V. (2001). Probing dust in the atmosphere of brown dwarfs through polarization. *The Astrophysical Journal Letters*, *561*(1), L123–L126. https://doi.org/10.1086/324559

Sheets, H. A., & Deming, D. (2014). Statistical eclipses of close-in Kepler sub-Saturns. *The Astrophysical Journal*, *794*(2), 133. https://doi.org/10.1088/0004-637X/794/2/133

Sheets, H. A., & Deming, D. (2017). Average albedos of close-in super-Earths and super-Neptunes from statistical analysis of long-cadence Kepler secondary eclipse data. *The Astronomical Journal*, *154*(4), 160. https://doi.org/10.3847/1538-3881/aa88b9

Showman, A. P., & Kaspi, Y. (2013). Atmospheric dynamics of brown dwarfs and directly imaged giant planets. *The Astrophysical Journal*, *776*(2), 85. https://doi.org/10.1088/0004-637X/776/2/85

Showman, A. P., Tan, X., & Parmentier, V. (2020). Atmospheric dynamics of hot giant planets and brown dwarfs. *Space Science Reviews*, *216*(8), 139. https://doi.org/10.1007/s11214-020-00758-8

Shporer, A. (2017). The astrophysics of visible-light orbital phase curves in the space age. *Publications of the Astronomical Society of the Pacific*, *129*(977), 072001. https://doi.org/10.1088/1538-3873/aa7112

Shporer, A., & Hu, R. (2015). Studying atmosphere-dominated hot Jupiter Kepler phase curves: Evidence that inhomogeneous atmospheric reflection is common. *The Astronomical Journal*, *150*(4), 112. https://doi.org/10.1088/0004-6256/150/4/112

Shporer, A., O'Rourke, J. G., Knutson, H. A., Szabó, G. M., Zhao, M., Burrows, A., et al. (2014). Atmospheric characterization of the hot Jupiter Kepler-13Ab. *The Astrophysical Journal*, *788*(1), 92. https://doi.org/10.1088/0004-637X/788/1/92

Shporer, A., Wong, I., Huang, C. X., Line, M. R., Stassun, K. G., Fetherolf, T., et al. (2019). TESS full orbital phase curve of the WASP-18b system. *The Astronomical Journal*, *157*(5), 178. https://doi.org/10.3847/1538-3881/ab0f96

Simon, A. A., Rowe, J. F., Gaulme, P., Hammel, H. B., Casewell, S. L., Fortney, J. J., et al. (2016). Neptune's dynamic atmosphere from Kepler K2 observations: Implications for brown dwarf light curve analyses. *The Astrophysical Journal*, *817*(2), 162. https://doi.org/10.3847/0004-637X/817/2/162

Sing, D. K., Désert, J. M., Fortney, J. J., Lecavelier Des Etangs, A., Ballester, G. E., Cepa, J., et al. (2011). Gran Telescopio Canarias OSIRIS transiting exoplanet atmospheric survey: Detection of potassium in XO-2b from narrowband spectrophotometry. *Astronomy & Astrophysics*, *527*, A73. https://doi.org/10.1051/0004-6361/201015579

Sing, D. K., Fortney, J. J., Nikolov, N., Wakeford, H. R., Kataria, T., Evans, T. M., et al. (2016). A continuum from clear to cloudy hot-Jupiter exoplanets without primordial water depletion. *Nature*, *529*, 59–62.

Sing, D. K., Lavvas, P., Ballester, G. E., Lecavelier des Etangs, A., Marley, M. S., Nikolov, N., et al. (2019). The Hubble Space Telescope PanCET Program: Exospheric Mg II and Fe II in the Near-ultraviolet Transmission Spectrum of WASP-121b Using Jitter Decorrelation. *The Astronomical Journal*, *158*(2), 91. https://doi.org/10.3847/1538-3881/ab2986

Sing, D. K., Lecavelier des Etangs, A., Fortney, J. J., Burrows, A. S., Pont, F., Wakeford, H. R., et al. (2013). HST hot-Jupiter transmission spectral survey: Evidence for aerosols and lack of TiO in the atmosphere of WASP-12b. *Monthly Notices of the Royal Astronomical Society*, *436*, 2956–2973.

Sing, D. K., Wakeford, H. R., Showman, A. P., Nikolov, N., Fortney, J. J., Burrows, A. S., et al. (2015). HST hot-Jupiter transmission spectral survey: Detection of potassium in WASP-31b along with a cloud deck and Rayleigh scattering. *Monthly Notices of the Royal Astronomical Society*, *446*(3), 2428–2443. https://doi.org/10.1093/mnras/stu2279

Skemer, A. J., Hinz, P. M., Esposito, S., Burrows, A., Leisenring, J., Skrutskie, M., et al. (2012). First light LBT AO images of HR 8799 bcde at 1.6 and 3.3 μm: New discrepancies between young planets and old brown dwarfs. *The Astrophysical Journal*, *753*(1), 14. https://doi.org/10.1088/0004-637X/753/1/14

Skemer, A. J., Marley, M. S., Hinz, P. M., Morzinski, K. M., Skrutskie, M. F., Leisenring, J. M., et al. (2014). Directly imaged L-T transition exoplanets in the mid-infrared. *The Astrophysical Journal*, *792*(1), 17. https://doi.org/10.1088/0004-637X/792/1/17

Snellen, I. A. G., de Mooij, E. J. W., & Albrecht, S. (2009). The changing phases of extrasolar planet CoRoT-1b. *Nature*, *459*(7246), 543–545. https://doi.org/10.1038/nature08045

Southworth, J., Mancini, L., Madhusudhan, N., Mollière, P., Ciceri, S., & Henning, T. (2017). Detection of the atmosphere of the 1.6 $M_{\oplus}$ exoplanet GJ 1132 b. *The Astronomical Journal*, *153*(4), 191. https://doi.org/10.3847/1538-3881/aa6477

Sromovsky, L., Fry, P., & Kim, J. (2011). Methane on Uranus: The case for a compact CH_4 cloud layer at low latitudes and a severe CH_4 depletion at high-latitudes based on re-analysis of voyager occultation measurements and stis spectroscopy. *Icarus*, *215*(1), 292–312. https://doi.org/10.1016/j.icarus.2011.06.024

Steinrueck, M. E., Parmentier, V., Showman, A. P., Lothringer, J. D., & Lupu, R. E. (2019). The effect of 3D transport-induced disequilibrium carbon chemistry on the atmospheric structure, phase curves, and emission spectra of hot Jupiter HD 189733b. *The Astrophysical Journal*, *880*(1), 14. https://doi.org/10.3847/1538-4357/ab2598

Stephens, D. C., Leggett, S. K., Cushing, M. C., Marley, M. S., Saumon, D., Geballe, T. R., et al. (2009). The 0.8–14.5 μm spectra of mid-L to mid-T dwarfs: Diagnostics of effective temperature, grain sedimentation, gas transport, and surface gravity. *The Astrophysical Journal*, *702*(1), 154–170. https://doi.org/10.1088/0004-637X/702/1/154

Stevenson, K. B. (2016). Quantifying and predicting the presence of clouds in exoplanet atmospheres. *The Astrophysical Journal Letters*, *817*(2), L16. https://doi.org/10.3847/2041-8205/817/2/L16

Stevenson, K. B., Désert, J.-M., Line, M. R., Bean, J. L., Fortney, J. J., Showman, A. P., et al. (2014). Thermal structure of an exoplanet atmosphere from phase-resolved emission spectroscopy. *Science*, *346*(6211), 838–841. https://doi.org/10.1126/science.1256758

Stevenson, K. B., Harrington, J., Nymeyer, S., Madhusudhan, N., Seager, S., Bowman, W. C., et al. (2010). Possible thermochemical disequilibrium in the atmosphere of the exoplanet GJ 436b. *Nature*, *464*(7292), 1161–1164. https://doi.org/10.1038/nature09013

Stolker, T., Min, M., Stam, D. M., Mollière, P., Dominik, C., & Waters, L. B. F. M. (2017). Polarized scattered light from self-luminous exoplanets. Three-dimensional scattering radiative transfer with ARTES. *Astronomy & Astrophysics*, *607*, A42. https://doi.org/10.1051/0004-6361/201730780

Stone, J. M., Barman, T., Skemer, A. J., Briesemeister, Z. W., Brock, L. S., Hinz, P. M., et al. (2020). High-contrast Thermal Infrared Spectroscopy with ALES: The 3–4 μm Spectrum of κ Andromedae b. *The Astronomical Journal*, *160*(6), 262. https://doi.org/10.3847/1538-3881/abbef3

Sudarsky, D., Burrows, A., & Hubeny, I. (2003). Theoretical spectra and atmospheres of extrasolar giant planets. *The Astrophysical Journal*, *588*(2), 1121–1148. https://doi.org/10.1086/374331

Sudarsky, D., Burrows, A., & Pinto, P. (2000). Albedo and reflection spectra of extrasolar giant planets. *The Astrophysical Journal*, *538*(2), 885–903. https://doi.org/10.1086/309160

Suissa, G., Mandell, A. M., Wolf, E. T., Villanueva, G. L., Fauchez, T., & Kopparapu, R. k. (2020). Dim prospects for transmission spectra of ocean Earths around M stars. *The Astrophysical Journal*, *891*(1), 58. https://doi.org/10.3847/1538-4357/ab72f9

Swain, M., Deroo, P., Tinetti, G., Hollis, M., Tessenyi, M., Line, M., et al. (2013). Probing the extreme planetary atmosphere of WASP-12b. *Icarus*, *225*(1), 432–445. https://doi.org/10.1016/j.icarus.2013.04.003

Tan, X., & Showman, A. P. (2017). Effects of latent heating on atmospheres of brown dwarfs and directly imaged planets. *The Astrophysical Journal*, *835*(2), 186. https://doi.org/10.3847/1538-4357/835/2/186

Tan, X., & Showman, A. P. (2019). Atmospheric variability driven by radiative cloud feedback in brown dwarfs and directly imaged extrasolar giant planets. *The Astrophysical Journal*, *874*(2), 111. https://doi.org/10.3847/1538-4357/ab0c07

Tan, X., & Showman, A. P. (2020). *Atmospheric circulation of brown dwarfs and directly imaged exoplanets driven by cloud radiative feedback: Effects of rotation*. arXiv e-prints, arXiv:2005.12152.

Tan, X., & Showman, A. P. (2021). *Atmospheric circulation of brown dwarfs and directly imaged exoplanets driven by cloud radiative feedback: Global and equatorial dynamics*. Monthly Notices of the Royal Astronomical Society. https://doi.org/10.1093/mnras/stab097

Taylor, J., Parmentier, V., Irwin, P. G. J., Aigrain, S., Lee, G. K. H., & Krissansen-Totton, J. (2020a). Understanding and mitigating biases when studying inhomogeneous emission spectra with JWST. *Monthly Notices of the Royal Astronomical Society*, *493*(3), 4342–4354. https://doi.org/10.1093/mnras/staa552

Taylor, J., Parmentier, V., Line, M. R., Lee, G. K. H., Irwin, P. G. J., & Aigrain, S. (2020b). *How does thermal scattering shape the infrared spectra of cloudy exoplanets? A theoretical framework and consequences for atmospheric retrievals in the JWST era*. arXiv e-prints, arXiv:2009.12411.

Thao, P. C., Mann, A. W., Johnson, M. C., Newton, E. R., Guo, X., Kain, I. J., et al. (2020). Zodiacal exoplanets in time (ZEIT). IX. A flat transmission spectrum and a highly eccentric orbit for the young Neptune K2-25b as revealed by Spitzer. *The Astronomical Journal*, *159*(1), 32. https://doi.org/10.3847/1538-3881/ab579b

Thorngren, D., Gao, P., & Fortney, J. J. (2019). The intrinsic temperature and radiative-convective boundary depth in the atmospheres of hot Jupiters. *The Astrophysical Journal Letters*, *884*(1), L6. https://doi.org/10.3847/2041-8213/ab43d0

Tinetti, G., Vidal-Madjar, A., Liang, M.-C., Beaulieu, J.-P., Yung, Y., Carey, S., et al. (2007). Water vapour in the atmosphere of a transiting extrasolar planet. *Nature*, *448*(7150), 169–171. https://doi.org/10.1038/nature06002

Toon, O. B., Turco, R. P., Hamill, P., Kiang, C. S., & Whitten, R. C. (1979). A one-dimensional model describing aerosol formation and evolution in the stratosphere: II. Sensitivity studies and comparison with observations. *Journal of the Atmospheric Sciences*, *36*(4), 718–736.

Trainer, M. G., Pavlov, A. A., Curtis, D. B., McKay, C. P., Worsnop, D. R., Delia, A. E., et al. (2004). Haze aerosols in the atmosphere of early Earth: Manna from heaven. *Astrobiology*, *4*(4), 409–419. https://doi.org/10.1089/ast.2004.4.409

Trainer, M. G., Pavlov, A. A., Dewitt, H. L., Jimenez, J. L., McKay, C. P., Toon, O. B., & Tolbert, M. A. (2006). Inaugural article: Organic haze on Titan and the early Earth. *Proceedings of the National Academy of Science*, *103*(48), 18035–18042. https://doi.org/10.1073/pnas.0608561103

Trainer, M. G., Sebree, J. A., Yoon, Y. H., & Tolbert, M. A. (2013). The influence of benzene as a trace reactant in Titan aerosol analogs. *The Astrophysical Journal Letters*, *766*(1), L4. https://doi.org/10.1088/2041-8205/766/1/L4

Tremblin, P., Amundsen, D. S., Chabrier, G., Baraffe, I., Drummond, B., Hinkley, S., et al. (2016). Cloudless atmospheres for L/T dwarfs and extrasolar giant planets. *The Astrophysical Journal Letters*, *817*(2), L19. https://doi.org/10.3847/2041-8205/817/2/L19

Tsiaras, A., Waldmann, I. P., Tinetti, G., Tennyson, J., & Yurchenko, S. N. (2019). Water vapour in the atmosphere of the habitable-zone eight-Earth-mass planet K2-18 b. *Nature Astronomy*, *3*(12), 1086–1091. https://doi.org/10.1038/s41550-019-0878-9

Tsiaras, A., Waldmann, I. P., Zingales, T., Rocchetto, M., Morello, G., Damiano, M., et al. (2018). A population study of gaseous exoplanets. *The Astronomical Journal*, *155*(4), 156. https://doi.org/10.3847/1538-3881/aaaf75

Tsuji, T. (2002). Dust in the photospheric environment: Unified cloudy models of M, L, and T dwarfs. *The Astrophysical Journal*, *575*(1), 264–290. https://doi.org/10.1086/341262

Tsuji, T., & Nakajima, T. (2003). Transition from L to T dwarfs on the color-magnitude diagram. *The Astrophysical Journal Letters*, *585*(2), L151–L154. https://doi.org/10.1086/374388

Tsuji, T., Ohnaka, K., & Aoki, W. (1999). Warm dust in the cool brown dwarf Gliese 229B and spectroscopic diagnosis of dusty photospheres. *The Astrophysical Journal Letters*, *520*(2), L119–L122. https://doi.org/10.1086/312161

Turco, R. P., Hamill, P., Toon, O. B., Whitten, R. C., & Kiang, C. S. (1979). A one-dimensional model describing aerosol formation and evolution in the stratosphere: I. Physical processes and mathematical analogs. *Journal of the Atmospheric Sciences*, *36*(4), 699–717.

Ugelow, M. S., De Haan, D. O., Hörst, S. M., & Tolbert, M. A. (2018). The effect of oxygen on organic haze properties. *The Astrophysical Journal Letters*, *859*(1), L2. https://doi.org/10.3847/2041-8213/aac2c7

Vanderburg, A., Rappaport, S. A., Xu, S., Crossfield, I. J. M., Becker, J. C., Gary, B., et al. (2020). A giant planet candidate transiting a white dwarf. *Nature*, *585*(7825), 363–367. https://doi.org/10.1038/s41586-020-2713-y

Vidal-Madjar, A., Huitson, C. M., Bourrier, V., Désert, J. M., Ballester, G., Lecavelier des Etangs, A., et al. (2013). Magnesium in the atmosphere of the planet HD 209458 b: Observations of the thermosphere-exosphere transition region. *Astronomy & Astrophysics*, *560*, A54. https://doi.org/10.1051/0004-6361/201322234

Visscher, C., Lodders, K., & Fegley, B., Jr. (2006). Atmospheric chemistry in giant planets, brown dwarfs, and low-mass dwarf stars. II. Sulfur and phosphorus. *The Astrophysical Journal*, *648*(2), 1181–1195. https://doi.org/10.1086/506245

Visscher, C., Lodders, K., & Fegley, J., Bruce.(2010). Atmospheric chemistry in giant planets, brown dwarfs, and low-mass dwarf stars. III. Iron, magnesium, and silicon. *The Astrophysical Journal*, *716*(2), 1060–1075. https://doi.org/10.1088/0004-637X/716/2/1060

von Essen, C., Mallonn, M., Cowan, N. B., Piette, A., Madhusudhan, N., Agol, E., et al. (2020). *TESS unveils the optical phase curve of KELT-1b. Thermal emission and ellipsoidal variation from the brown dwarf companion, and activity from the star*. arXiv e-prints, arXiv:2006.09750.

von Essen, C., Mallonn, M., Welbanks, L., Madhusudhan, N., Pinhas, A., Bouy, H., & Weis Hansen, P. (2019). An optical transmission spectrum of the ultra-hot Jupiter WASP-33 b. First indication of aluminum oxide in an exoplanet. *Astronomy & Astrophysics*, *622*, A71. https://doi.org/10.1051/0004-6361/201833837

von Paris, P., Gratier, P., Bordé, P., Leconte, J., & Selsis, F. (2016). Inferring asymmetric limb cloudiness on exoplanets from transit light curves. *Astronomy & Astrophysics*, *589*, A52. https://doi.org/10.1051/0004-6361/201527894

Vos, J. M., Allers, K. N., & Biller, B. A. (2017). The viewing geometry of brown dwarfs influences their observed colors and variability amplitudes. *The Astrophysical Journal*, *842*(2), 78. https://doi.org/10.3847/1538-4357/aa73cf

Vos, J. M., Biller, B. A., Allers, K. N., Faherty, J. K., Liu, M. C., Metchev, S., et al. (2020). Spitzer variability properties of low-gravity L dwarfs. *The Astronomical Journal*, *160*(1), 38. https://doi.org/10.3847/1538-3881/ab9642

Vos, J. M., Biller, B. A., Bonavita, M., Eriksson, S., Liu, M. C., Best, W. M. J., et al. (2019). A search for variability in exoplanet analogues and low-gravity brown dwarfs. *Monthly Notices of the Royal Astronomical Society*, *483*(1), 480–502. https://doi.org/10.1093/mnras/sty3123

Vuitton, V., Moran, S. E., He, C., Wolters, C., Flandinet, L., Orthous-Daunay, F.-R., et al. (2021). H_2SO_4 and organosulfur compounds in laboratory analogue aerosols of warm high-metallicity exoplanet atmospheres. *The Planetary Science Journal*, *2*(1), 2. https://doi.org/10.3847/psj/abc558

Wakeford, H. R., Lewis, N. K., Fowler, J., Bruno, G., Wilson, T. J., Moran, S. E., et al. (2019a). Disentangling the planet from the star in late-type M dwarfs: A case study of TRAPPIST-1g. *The Astronomical Journal*, *157*(1), 11. https://doi.org/10.3847/1538-3881/aaf04d

Wakeford, H. R., & Sing, D. K. (2015). Transmission spectral properties of clouds for hot Jupiter exoplanets. *Astronomy & Astrophysics*, *573*, A122. https://doi.org/10.1051/0004-6361/201424207

Wakeford, H. R., Sing, D. K., Deming, D., Lewis, N. K., Goyal, J., Wilson, T. J., et al. (2018). The complete transmission spectrum of WASP-39b with a precise water constraint. *The Astronomical Journal*, *155*(1), 29. https://doi.org/10.3847/1538-3881/aa9e4e

Wakeford, H. R., Sing, D. K., Stevenson, K. B., Lewis, N. K., Pirzkal, N., Wilson, T. J., et al. (2020). Into the UV: A precise transmission spectrum of HAT-P-41b using Hubble's WFC3/UVIS G280 grism. *The Astronomical Journal*, *159*(5), 204. https://doi.org/10.3847/1538-3881/ab7b78

Wakeford, H. R., Stevenson, K. B., Lewis, N. K., Sing, D. K., López-Morales, M., Marley, M., et al. (2017a). HST PanCET program: A cloudy atmosphere for the promising JWST target WASP-101b. *The Astrophysical Journal Letters*, *835*(1), L12. https://doi.org/10.3847/2041-8213/835/1/L12

Wakeford, H. R., Visscher, C., Lewis, N. K., Kataria, T., Marley, M. S., Fortney, J. J., & Mandell, A. M. (2017b). High-temperature condensate clouds in super-hot Jupiter atmospheres. *Monthly Notices of the Royal Astronomical Society*, *464*, 4247–4254. https://doi.org/10.1093/mnras/stw2639

Wakeford, H. R., Wilson, T. J., Stevenson, K. B., & Lewis, N. K. (2019b). Exoplanet atmosphere forecast: Observers should expect spectroscopic transmission features to be muted to 33%. *Research Notes of the American Astronomical Society*, *3*(1), 7. https://doi.org/10.3847/2515-5172/aafc63

Wallack, N. L., Knutson, H. A., Morley, C. V., Moses, J. I., Thomas, N. H., Thorngren, D. P., et al. (2019). Investigating trends in atmospheric compositions of cool gas giant planets using Spitzer secondary eclipses. *The Astronomical Journal*, *158*(6), 217. https://doi.org/10.3847/1538-3881/ab2a05

Wang, J. J., Ginzburg, S., Ren, B., Wallack, N., Gao, P., Mawet, D., et al. (2020). Keck/NIRC2 L'-band imaging of Jovian-mass accreting protoplanets around PDS 70. *The Astronomical Journal*, *159*(6), 263. https://doi.org/10.3847/1538-3881/ab8aef

Wang, L., & Dai, F. (2019). Dusty outflows in planetary atmospheres: Understanding "super-puffs" and transmission spectra of sub-Neptunes. *The Astrophysical Journal Letters*, *873*(1), L1. https://doi.org/10.3847/2041-8213/ab0653

Wang, Y., Abe, Y., Matsuura, Y., Miyagi, M., & Uyama, H. (1998). Refractive indices and extinction coefficients of polymers for the mid-infrared region. *Applied Optics*, *37*(30), 7091–7095. https://doi.org/10.1364/AO.37.007091

Way, M. J., Del Genio, A. D., Aleinov, I., Clune, T. L., Kelley, M., & Kiang, N. Y. (2018). Climates of warm Earth-like planets. I. 3D Model simulations. *The Astrophysical Journal Supplement Series*, *239*(2), 24. https://doi.org/10.3847/1538-4365/aae9e1

Webb, R. K., Brogi, M., Gandhi, S., Line, M. R., Birkby, J. L., Chubb, K. L., et al. (2020). A weak spectral signature of water vapour in the atmosphere of HD 179949 b at high spectral resolution in the L band. *Monthly Notices of the Royal Astronomical Society*, *494*(1), 108–119. https://doi.org/10.1093/mnras/staa715

Webber, M. W., Lewis, N. K., Marley, M., Morley, C., Fortney, J. J., & Cahoy, K. (2015). Effect of longitude-dependent cloud coverage on exoplanet visible wavelength reflected-light phase curves. *The Astrophysical Journal*, *804*(2), 94. https://doi.org/10.1088/0004-637X/804/2/94

Welbanks, L., Madhusudhan, N., Allard, N. F., Hubeny, I., Spiegelman, F., & Leininger, T. (2019). Mass-metallicity trends in transiting exoplanets from atmospheric abundances of H_2O, Na, and K. *The Astrophysical Journal Letters*, *887*(1), L20. https://doi.org/10.3847/2041-8213/ab5a89

Wiktorowicz, S. J., Nofi, L. A., Jontof-Hutter, D., Kopparla, P., Laughlin, G. P., Hermis, N., et al. (2015). A ground-based albedo upper limit for HD 189733b from polarimetry. *The Astrophysical Journal*, *813*(1), 48. https://doi.org/10.1088/0004-637X/813/1/48

Wilson, P. A., Rajan, A., & Patience, J. (2014). The brown dwarf atmosphere monitoring (BAM) project. I. The largest near-IR monitoring survey of L and T dwarfs. *Astronomy & Astrophysics*, *566*, A111. https://doi.org/10.1051/0004-6361/201322995

Woitke, P., & Helling, C. (2003). Dust in brown dwarfs. II. The coupled problem of dust formation and sedimentation. *Astronomy & Astrophysics*, *399*(1), 297–313. https://doi.org/10.1051/0004-6361:20021734

Woitke, P., & Helling, C. (2004). Dust in brown dwarfs. III. Formation and structure of quasi-static cloud layers. *Astronomy & Astrophysics*, *414*(1), 335–350. https://doi.org/10.1051/0004-6361:20031605

Woitke, P., Helling, C., & Gunn, O. (2020). Dust in brown dwarfs and extra-solar planets. VII. Cloud formation in diffusive atmospheres. *Astronomy & Astrophysics*, *634*, A23. https://doi.org/10.1051/0004-6361/201936281

Wolf, E. T., & Toon, O. B. (2010). Fractal organic hazes provided an ultraviolet shield for early Earth. *Science*, *328*(5983), 1266. https://doi.org/10.1126/science.1183260

Wong, I., Benneke, B., Gao, P., Knutson, H. A., Chachan, Y., Henry, G. W., et al. (2020a). Optical to near-infrared transmission spectrum of the warm sub-Saturn HAT-P-12b. *The Astronomical Journal*, *159*(5), 234. https://doi.org/10.3847/1538-3881/ab880d

Wong, I., Knutson, H. A., Kataria, T., Lewis, N. K., Burrows, A., Fortney, J. J., et al. (2016). 3.6 and 4.5 μm Spitzer phase curves of the highly irradiated hot Jupiters WASP-19b and HAT-P-7b. *The Astrophysical Journal*, *823*(2), 122. https://doi.org/10.3847/0004-637X/823/2/122

Wong, I., Knutson, H. A., Lewis, N. K., Kataria, T., Burrows, A., Fortney, J. J., et al. (2015a). 3.6 and 4.5 μm phase curves of the highly irradiated eccentric hot Jupiter WASP-14b. *The Astrophysical Journal*, *811*(2), 122. https://doi.org/10.1088/0004-637X/811/2/122

Wong, I., Shporer, A., Daylan, T., Benneke, B., Fetherolf, T., Kane, S. R., et al. (2020b). Systematic Phase Curve Study of Known Transiting Systems from Year One of the TESS Mission. *The Astronomical Journal*, *160*(4), 155. https://doi.org/10.3847/1538-3881/ababad

Wong, M. H., Atreya, S. K., Kuhn, W. R., Romani, P. N., & Mihalka, K. M. (2015b). Fresh clouds: A parameterized updraft method for calculating cloud densities in one-dimensional models. *Icarus*, *245*, 273–281. https://doi.org/10.1016/j.icarus.2014.09.042

Wong, M. L., Fan, S., Gao, P., Liang, M.-C., Shia, R.-L., Yung, Y. L., et al. (2017). The photochemistry of Pluto's atmosphere as illuminated by New Horizons. *Icarus*, *287*, 110–115. https://doi.org/10.1016/j.icarus.2016.09.028

Wood, P. L., Maxted, P. F. L., Smalley, B., & Iro, N. (2011). Transmission spectroscopy of the sodium 'D' doublet in WASP-17b with the VLT. *Monthly Notices of the Royal Astronomical Society*, *412*(4), 2376–2382. https://doi.org/10.1111/j.1365-2966.2010.18061.x

Yan, F., Casasayas-Barris, N., Molaverdikhani, K., Alonso-Floriano, F. J., Reiners, A., Pallé, E., et al. (2019). Ionized calcium in the atmospheres of two ultra-hot exoplanets WASP-33b and KELT-9b. *Astronomy & Astrophysics*, *632*, A69. https://doi.org/10.1051/0004-6361/201936396

Yang, H., Apai, D., Marley, M. S., Karalidi, T., Flateau, D., Showman, A. P., et al. (2016). Extrasolar storms: Pressure-dependent changes in light-curve phase in brown dwarfs from simultaneous HST and Spitzer Observations. *The Astrophysical Journal*, *826*(1), 8. https://doi.org/10.3847/0004-637X/826/1/8

Yang, H., Apai, D., Marley, M. S., Saumon, D., Morley, C. V., Buenzli, E., et al. (2015). HST rotational spectral mapping of two L-type brown dwarfs: Variability in and out of water bands indicates high-altitude haze layers. *The Astrophysical Journal Letters*, *798*(1), L13. https://doi.org/10.1088/2041-8205/798/1/L13

Yang, J., Boué, G., Fabrycky, D. C., & Abbot, D. S. (2014). Strong dependence of the inner edge of the habitable zone on planetary rotation rate. *The Astrophysical Journal Letters*, *787*(1), L2. https://doi.org/10.1088/2041-8205/787/1/L2

Yang, J., Cowan, N. B., & Abbot, D. S. (2013). Stabilizing cloud feedback dramatically expands the habitable zone of tidally locked planets. *The Astrophysical Journal Letters*, *771*(2), L45. https://doi.org/10.1088/2041-8205/771/2/L45

Yoon, Y. H., Hörst, S. M., Hicks, R. K., Li, R., de Gouw, J. A., & Tolbert, M. A. (2014). The role of benzene photolysis in Titan haze formation. *Icarus*, *233*, 233–241. https://doi.org/10.1016/j.icarus.2014.02.006

Zahnle, K., Marley, M. S., Morley, C. V., & Moses, J. I. (2016). Photolytic hazes in the atmosphere of 51 Eri B. *The Astrophysical Journal*, *824*(2), 137. https://doi.org/10.3847/0004-637X/824/2/137

Zalesky, J. A., Line, M. R., Schneider, A. C., & Patience, J. (2019). A uniform retrieval analysis of ultra-cool dwarfs. III. Properties of Y dwarfs. *The Astrophysical Journal*, *877*(1), 24. https://doi.org/10.3847/1538-4357/ab16db

Zeidler, S., Posch, T., Mutschke, H., Richter, H., & Wehrhan, O. (2011). Near-infrared absorption properties of oxygen-rich stardust analogs. The influence of coloring metal ions. *Astronomy & Astrophysics*, *526*, A68. https://doi.org/10.1051/0004-6361/201015219

Zellem, R. T., Lewis, N. K., Knutson, H. A., Griffith, C. A., Showman, A. P., Fortney, J. J., et al. (2014). The 4.5 μm full-orbit phase curve of the hot Jupiter HD 209458b. *The Astrophysical Journal*, *790*(1), 53. https://doi.org/10.1088/0004-637X/790/1/53

Zhang, M., Chachan, Y., Kempton, E. M. R., & Knutson, H. A. (2019). Forward modeling and retrievals with PLATON, a fast open-source tool. *Publications of the Astronomical Society of the Pacific*, *131*(997), 034501. https://doi.org/10.1088/1538-3873/aaf5ad

Zhang, X., & Showman, A. P. (2018a). Global-mean vertical tracer mixing in planetary atmospheres. II. Tidally locked planets. *The Astrophysical Journal*, *866*(1), 2. https://doi.org/10.3847/1538-4357/aada7c

Zhang, X., & Showman, A. P. (2018b). Global-mean vertical tracer mixing in planetary atmospheres. I. Theory and fast-rotating planets. *The Astrophysical Journal*, *866*(1), 1. https://doi.org/10.3847/1538-4357/aada85

Zhang, X., Strobel, D. F., & Imanaka, H. (2017). Haze heats Pluto's atmosphere yet explains its cold temperature. *Nature*, *551*(7680), 352–355. https://doi.org/10.1038/nature24465

Zhang, Z., Zhou, Y., Rackham, B. V., & Apai, D. (2018). The Near-infrared Transmission Spectra of TRAPPIST-1 Planets b, c, d, e, f, and g and Stellar Contamination in Multi-epoch Transit Spectra. *The Astronomical Journal*, *156*(4), 178. https://doi.org/10.3847/1538-3881/aade4f

Zhou, Y., Apai, D., Metchev, S., Lew, B. W. P., Schneider, G., Marley, M. S., et al. (2018). Cloud atlas: Rotational modulations in the L/T transition brown dwarf companion HN Peg B. *The Astronomical Journal*, *155*(3), 132. https://doi.org/10.3847/1538-3881/aaabbd

Zhou, Y., Apai, D., Schneider, G. H., Marley, M. S., & Showman, A. P. (2016). Discovery of rotational modulations in the planetary-mass companion 2M1207b: Intermediate rotation period and heterogeneous clouds in a low gravity atmosphere. *The Astrophysical Journal*, *818*(2), 176. https://doi.org/10.3847/0004-637X/818/2/176

Zhou, Y., Bowler, B. P., Morley, C. V., Apai, D., Kataria, T., Bryan, M. L., & Benneke, B. (2020). Spectral Variability of VHS J1256-1257b from 1 to 5 μm. *The Astronomical Journal*, *160*(2), 77. https://doi.org/10.3847/1538-3881/ab9e04